

REPORT NO. CCEER-86-1

A SIMPLE HYSTERETIC ELEMENT FOR
BIAXIAL BENDING OF R/C COLUMNS AND
IMPLEMENTATION IN NEABS-86

by

George E. Ghusn
Mehdi Saiidi

A Report to the
National Science Foundation
Research Grant CEE-8317477

Civil Engineering Department
University of Nevada Reno

July 1986

ABSTRACT

A new nonlinear biaxial bending element for reinforced concrete columns was developed. The new element represents the column as a group of five translational springs, each representing the properties of the concrete and reinforcement. The element was implemented in a nonlinear static analysis program. Results using the five-spring element compared favorably with experimental results producing a better match than either the bilinear biaxial yield surface model or the trilinear degrading yield surface model.

The new element was added to an existing nonlinear dynamic analysis program (program NEABS). Three bridge structures, the Rose Creek Interchange, the Meloland Overpass, and the Flamingo Road Overpass, were modeled for dynamic analysis. Each bridge structure was modeled using both the elasto-plastic yield surface element and the five-spring element. Comparisons of the dynamic responses showed that the new element provided a more realistic stiffness degradation, a higher amplitude acceleration response, and a lower amplitude displacement response than the elasto-plastic yield surface element. The analyses using the elasto-plastic yield surface element generally required much longer execution times to produce stable results.

Nonlinear dynamic analyses using the five-spring element execute faster, do not become unstable, and provide for a more realistic response for reinforced concrete columns subjected to biaxial bending.

ACKNOWLEDGEMENTS

The study presented in this report was part of a continuing investigation at the University of Nevada, Reno (UNR) on the seismic response of highway bridges. The project was funded by Grant CEE-8317477 from the National Science Foundation (NSF). The statements in this report, however, are those of the authors and do not necessarily present the views of NSF.

The authors are indebted to Mr. Shing Lai, a former graduate student at the University of Toronto, and to Professor George Will of the University of Toronto for providing information about their model.

Dr. Jack Scalzi, the NSF program manager for the project, is especially thanked for his support and encouragement throughout the project. The authors are also thankful to Dr. Bruce Douglas, the director of the Center for Civil Engineering Earthquake Research at UNR, for his advice.

Miss T. "Jeanie" Pratt and Chris Archer of the Civil Engineering Department are appreciated for their careful typing of this report.

The CYBER 830 computer system at UNR was used for all the computations and computer graphics work.

This report is primarily based on a master of science thesis by G.E. Ghusn directed by M. Saidi.

TABLE OF CONTENTS

<u>CHAPTER</u>	<u>PAGE</u>
1	INTRODUCTION
1.1	Introduction..... 1
1.2	Reveiw of Previous Work..... 1
1.2.1	The yield surface models 2
1.2.1a	The bilinear biaxial model..... 3
1.2.1b	The trilinear degrading model..... 3
1.2.2	The finite element method..... 5
1.2.3	The multiple spring model..... 5
1.3	Object and Scope..... 6
2	FORMULATION OF THE MODIFIED NINE-SPRING ELEMENT
2.1	Introduction..... 8
2.2	Nonlinear Model Element Description..... 9
2.2.1	The steel spring..... 10
2.2.2	The concrete spring..... 12
2.2.3	Inelastic Element stiffness matrix..... 15
2.3	Hysteresis Models..... 18
2.3.1	Hysteresis model for steel springs..... 18
2.3.2	Hysteresis model for concrete springs..... 20
3	FORMULATION OF THE FIVE-SPRING ELEMENT
3.1	Introduction..... 22
3.2	Element Description..... 22
3.2.1	The composite spring..... 23
3.3	Hysteresis Model for Composite Spring..... 24
4	COMPARISON OF ANALYTICAL AND EXPERIMENTAL RESULTS
4.1	Introduction..... 27
4.2	Description of the Cantilever Structure..... 27
4.3	Evaluation of the Modified Nine-Spring Element..... 29
4.4	Evaluation of the Five-Spring Element..... 32
4.5	Comments and Conclusions..... 35
5	IMPLEMENTATION IN A NONLINEAR BRIDGE ANALYSIS MCDL
5.1	Introduction..... 37
5.2	Description of Program NEABS..... 37
5.3	Modifications to Program NEABS..... 38
5.3.1	Subroutines SMOD, TEAMOD, NEWMOD, and SPRING.. 39
5.3.2	Subroutines STMCD and NMCD..... 39
5.3.3	Subroutines AQHYST and CHYST..... 40
5.4	Evaluation of Modified NEABS..... 40
5.5	Comments and Conclusions..... 41

6	CASE STUDIES	
6.1	Introduction.....	43
6.2	Structure Modeling.....	43
6.3	The Meloland Overpass.....	44
6.3.1	Description of the structure.....	44
6.3.2	Modeling of the structure.....	45
6.3.3	Results of dynamic analyses.....	45
6.4	The Rose Creek Interchange.....	47
6.4.1	Description of the structure.....	47
6.4.2	Modeling of the structure.....	47
6.4.3	Results of dynamic analyses.....	48
6.5	The Flamingo Road Overpass.....	49
6.5.1	Description of the structure.....	49
6.5.2	Modeling of the structure.....	49
6.5.3	Results of dynamic analyses.....	50
6.6	Comments and Conclusions.....	51
7	SUMMARY AND CONCLUSIONS	
7.1	Summary.....	52
7.2	Observations and Conclusions.....	54
	REFERENCES.....	56
	APPENDICES	
	Appendix A	
	User guide to NEABS-86.....	155
	Appendix B	
	Notations.....	157
	Appendix C	
	List of CCEER publications.....	159

LIST OF TABLES

<u>TABLE</u>		<u>PAGE</u>
6.1	Meloland Overpass Section Data.....	59
6.2	Rose Creek Interchange Section Data.....	60
6.3	Flamingo Road Overpass Section Data.....	61

LIST OF FIGURES

<u>FIGURE</u>		<u>PAGE</u>
2.1	The Multiple Spring Biaxial Bending Model.....	62
2.2	The Multispring Biaxial Bending Element at the Balanced Condition.....	63
2.3	Idealized Stress-Strain Relationship for Concrete Spring.....	64
2.4	Spring Displacements in a Diagonal Section.....	65
2.5	The QHYST Hysteresis Model.....	66
2.6	The GHYST Hysteresis Model.....	67
3.1	The Five-Spring Element.....	68
3.2	Primary Curve for the Composite Springs.....	69
3.3	The AQHYST Hysteresis Model for Composite Steel-Concrete Springs.....	70
4.1	Configuration of Specimens SP-7 and SP-8.....	71
4.2	Loading History for Otani's Specimen SP-7.....	72
4.3	Loading History for Otani's Specimen SP-8.....	73
4.4	Elevation of the Idealized Cantilever Column Model.....	74
4.5	Degrees of Freedom in the Cantilever Model.....	75
4.6	Flowchart for Program APPDIS.....	76
4.7	Force-Deflection Curve for SP-7 - BTO = 0.5.....	77
4.8	Force-Deflection Curve for SP-7 - ETO = 0.5.....	78
4.9	Force-Deflection Curve for SP-7 - BTO = 0.2.....	79
4.10	Force-Deflection Curve for SP-7 - ETO = 0.2.....	80
4.11	Force-Deflection Curve for SP-8 - BTO = 0.2.....	81
4.12	Force-Deflection Curve for SP-8 - ETO = 0.2.....	82
4.13	Force-Deflection Curve for SP-7.....	83
4.14	Force-Deflection Curve for SP-7.....	84

4.15	Illustration of Spring Force "Overshoot".....	85
4.16	Force-Deflection Curve for SP-7 Using the Bilinear Yield Surface Model.....	86
4.17	Force-Deflection Curve for SP-7 Using 5-Spring Element - BTO = 0.2.....	87
4.18	Force-Deflection Curve for SP-7 Using 5-Spring Element - BTO = 0.2.....	88
4.19	Force-Deflection Curve for SP-8 Using 5-Spring Element - BTO = BT1 = 0.2.....	89
4.20	Force-Deflection Curve for SP-8 Using 5-Spring Element - BTO = BT1 = 0.2.....	90
4.21	Force-Deflection Curve for SP-7 Using 5-Spring Element - BTO = BT1 = 0.4.....	91
4.22	Force-Deflection Curve for SP-7 Using 5-Spring Element - BTO = BT1 = 0.4.....	92
4.23	Force-Deflection Curve for SP-7 Using 5-Spring Element - BTO = 0.4, BT1 = 0.7.....	93
4.24	Force-Deflection Curve for SP-7 Using 5-Spring Element - BTO = 0.4, BT1 = 0.7.....	94
4.25	Force-Deflection Curve for SP-7 Using 5-Spring Element - BTO = 0.4, BT1 = 0.3.....	95
4.26	Force-Deflection Curve for SP-7 Using 5-Spring Element - BTO = 0.4, BT1 = 0.3.....	96
4.27	Force-Deflection Curve for SP-7 Using 5-Spring Element - $K_Y = 5\% K_{se}$	97
4.28	Force-Deflection Curve for SP-7 Using 5-Spring Element - $K_Y = 5\% K_{se}$	98
4.29	Force-Deflection Curve for SP-7 Using 5-Spring Element - $K_Y = 0.2\% K_{se}$	99
4.30	Force-Deflection Curve for SP-7 Using 5-Spring Element - $K_Y = 0.2\% K_{se}$	100
5.1	Subroutine Organization of NEABS and NEABS-86.....	101
5.2	Flowchart for Subroutines SMOD and TEAMOD.....	102
5.3	Flowcharts for Subroutines SPRING, NEWMOD, and STMOD.....	103

5.4	Flowchart for Subroutine NMOD.....	104
6.1	Elevation and Model of the Meloland Overpass.....	105
6.2	Elevation of Meloland Overpass.....	106
6.3	Pier Cross Section for the Rectangular Column Model.....	106
6.4	The 1979 Imperial Valley Earthquake.....	107
6.5	The 1979 Imperial Valley Earthquake.....	108
6.6	Meloland Overpass Model Response - Imperial Valley Earthquake *1.0 (round column).....	109
6.7	Meloland Overpass Model Response - Imperial Valley Earthquake *1.0 (round column).....	110
6.8	1940 El Centro Earthquake E-W.....	111
6.9	1940 El Centro Earthquake N-S.....	112
6.10	Meloland Overpass Model Response Using El Centro Earthquake *2.0 (round column).....	113
6.11	Meloland Overpass Model Response Using El Centro Earthquake *2.0 (round column).....	114
6.12	Meloland Overpass Model Response Using El Centro Earthquake *2.0 (rectangular column).....	115
6.13	Meloland Overpass Model Response Using El Centro Earthquake *2.0 (rectangular column).....	116
6.14	Rose Creek Interchange Plan and Elevation.....	117
6.15	Elevation of Rose Creek Interchange Pier and Column Cross Section.....	118
6.16	Model of the Rose Creek Interchange.....	119
6.17	Rose Creek Interchange Model Response (El Centro *1.0).....	120
6.18	Rose Creek Interchange Model Response (El Centro *1.0).....	121
6.19	Rose Creek Interchange Model Response (El Centro *1.0).....	122
6.20	Rose Creek Interchange Model Response (El Centro *1.0).....	123

6.21	Rose Creek Interchange Model Response (El Centro *1.0).....	124
6.22	Rose Creek Interchange Model Response (El Centro *1.0).....	125
6.23	Rose Creek Interchange Model Response (El Centro *1.0).....	126
6.24	Rose Creek Interchange Model Response (El Centro *1.0).....	127
6.25	Diagram of the Flamingo Road Overpass.....	128
6.26	Idealized Pier Elevation for Flamingo Road Overpass.....	129
6.27	Flamingo Road Overpass Model.....	130
6.28	Flamingo Road Overpass Model Response Using El Centro *1.0.....	131
6.29	Flamingo Road Overpass Model Response Using El Centro *1.0.....	132
6.30	Flamingo Road Overpass Model Response Using El Centro *1.0.....	133
6.31	Flamingo Road Overpass Model Response Using El Centro *1.0.....	134
6.32	Flamingo Road Overpass Model Response Using El Centro *1.0.....	135
6.33	Flamingo Road Overpass Model Response Using El Centro *1.0.....	136
6.34	Flamingo Road Overpass Model Response Using El Centro *1.0.....	137
6.35	Flamingo Road Overpass Model Response Using El Centro *1.0.....	138
6.36	Flamingo Road Overpass Model Response Using El Centro *1.5 (Unstable Elasto-Plastic Response).....	139
6.37	Flamingo Road Overpass Model Response Using El Centro *1.5 (Unstable Elasto-Plastic Response).....	140
6.38	Flamingo Road Overpass Model Response Using El Centro *1.5 (Unstable Elasto-Plastic Response).....	141

6.39	Flamingo Road Overpass Model Response Using El Centro *1.5 (Unstable Elasto-Plastic Response).....	142
6.40	Flamingo Road Overpass Model Response Using El Centro *1.5 (Unstable Elasto-Plastic Response).....	143
6.41	Flamingo Road Overpass Model Response Using El Centro *1.5 (Unstable Elasto-Plastic Response).....	144
6.42	Flamingo Road Overpass Model Response Using El Centro *1.5 (Unstable Elasto-Plastic Response).....	145
6.43	Flamingo Road Overpass Model Response Using El Centro *1.5 (Unstable Elasto-Plastic Response).....	146
6.44	Flamingo Road Overpass Model Response Using El Centro *1.5 (Unstable Elasto-Plastic Response).....	147
6.45	Flamingo Road Overpass Model Response Using El Centro *1.5 (Unstable Elasto-Plastic Response).....	148
6.46	Flamingo Road Overpass Model Response Using El Centro *1.5 (Unstable Elasto-Plastic Response).....	149
6.47	Flamingo Road Overpass Model Response Using El Centro *1.5 (Unstable Elasto-Plastic Response).....	150
6.48	Flamingo Road Overpass Model Response Using El Centro *1.5 (Unstable Elasto-Plastic Response).....	151
6.49	Flamingo Road Overpass Model Response Using El Centro *1.5 (Unstable Elasto-Plastic Response).....	152
6.50	Flamingo Road Overpass Model Response Using El Centro *1.5 (Unstable Elasto-Plastic Response).....	153
6.51	Flamingo Road Overpass Model Response Using El Centro *1.5 (Unstable Elasto-Plastic Response).....	154

CHAPTER 1

INTRODUCTION

1.1 Introduction

Many reinforced concrete column failures are caused by a combination of biaxial bending and axial load as a result of earthquake loadings. Several researchers, (10,16,26,30) have confirmed that biaxial bending is more critical than uniaxial bending when structures are subjected to bidirectional horizontal earthquake motions.

To evaluate the inelastic dynamic response of reinforced concrete structures subjected to strong bidirectional ground motions, a three-dimensional analysis using a hysteresis model for the biaxial bending of columns is required. Because earthquakes generally produce variations in the axial forces, the model must define the interaction of axial load and the two bending moment components for elastic and inelastic deformations. Modeling biaxial behavior is crucial for the accurate and realistic prediction of inelastic dynamic response of reinforced concrete structures.

The modeling of biaxial behavior in reinforced concrete columns is complex and involves many assumptions. This study reviews existing models and introduces a simple hysteresis model to predict the interaction of axial load and biaxial bending. The effect of the hysteretic modeling is demonstrated through the analysis of three highway bridges.

1.2 Review of Previous Work

Many models have been proposed that predict the hysteretic response of reinforced concrete members subjected to earthquake

loadings in only one direction (3,6,23,29,31). However, few models consider the interaction between bending in two orthogonal directions. The models that consider the interaction may be grouped into three categories: (1) the yield surface models, (2) the finite element models, and (3) the multispring models.

1.2.1 The Yield Surface Models: A yield surface describes the relationship between interaction diagrams calculated for axial load and bending about each principal axis. As developed by Bressler (5), the mathematical relationship is given by:

$$(M_x/M_{ox})^a + (M_y/M_{oy})^a = 1 \quad (1.1)$$

where

M_x and M_y = moments acting about the x and y axis, respectively;
and

M_{ox} and M_{oy} = the yield moments about the x and y axis, respectively. This relationship was found to correlate well with experimental results involving monotonic loadings (5) and is one of the methods used in designing reinforced concrete columns for combined biaxial and axial loadings (34). The parameter a is generally recognized to lie between 1.0 and 2.0 and depends on the axial load applied and on the bar arrangement in the column. For the models examined herein, $a = 2.0$ is assumed for typical columns with small aspect ratios and for mathematical simplicity. The yield surface is used as a general limit surface based on which the yield point in different hysteresis models is computed. The assumptions about the variation of stiffness for pre- and postyielding stages vary depending on the hysteresis model.

1.2.1.a The Bilinear Biaxial Model: The simplest model using the yield surface is the bilinear biaxial model. The basic formulation (17,30,32) is based on plasticity theory with the elastic-perfectly plastic (elasto-plastic) model being a special case.

The column is assumed to be perfectly elastic until the combination of applied moments at a fixed axial load value intersects the yield surface. The cracking point in the force-deformation relationship is ignored. Once the yield surface is reached, the column stiffness is reduced to zero (elasto-plastic) or to small postyielding stiffness value. The yield surface is then allowed to translate in moment space but does not change shape as the column yields. Upon unloading, the original elastic stiffness is assumed to apply. Hence, this model does not allow for degradation of the stiffness of the element. Lai (11) compared the analytical results based on this model with experimental results obtained by Otani (16) for a cantilever column subjected to bidirectional lateral deformations and found that the bilinear biaxial model produced poor correlations with respect to the force-displacement history of the test specimens. Although the elasto-plastic model is not realistic, it has been used or evaluated by many researchers (8,17,19,26,32) because the addition of degradation effects has been considered too cumbersome to consider.

1.2.1.b The Trilinear Degrading Model: The trilinear degrading model, developed by Takizawa and Aoyama (30), improves upon the biaxial bilinear model by including the stiffness degradation of the column. This model, as used by Takizawa and Aoyama, is not capable of accounting for variations in axial load. No attempt was made to

include variations in axial load because of the increase in the complexity of the analysis that variable axial load would introduce.

The trilinear model is based on two "yield" surfaces, one within the other. The outer one represents the yielding of the column and is comparable to the yield surface explained in the previous section. The inner surface represents the cracking of the column. The size of each surface is determined from a trilinear skeleton curve that relates moment to end rotation.

The column is perfectly elastic until the cracking surface is reached. Once the cracking surface is reached, the stiffness is modified and the cracking surface is allowed to translate in moment space without changing shape. Once the yielding surface is reached, the yield surface and the cracking surface are allowed to expand along the direction of yielding. Beyond the yield surface, the stiffness is further reduced to an assigned postyielding stiffness.

Upon unloading, the stiffness is multiplied by degradation factors that are based on the maximum displacements achieved in each coordinate direction. This technique accounts for permanent deformations in the column and leads to a more realistic response because it accounts for the stiffness degradation of the element.

The mathematical equations that define the rules for movement and for the lengthening of the surfaces are quite complex and require a considerable amount of calculations. The additional complexity improves the results; Lai (11) found a better correlation using analytical results from the trilinear degrading model than from the bilinear model for Otani's (16) experimental data. Still, Lai found

the correlation between experimental and trilinear degrading model analytical results to be poor and unacceptable.

The trilinear degrading model is probably as sophisticated as yield surface techniques will become. The extra complexity of any additional refinements to the technique will not overcome the many approximations that are inherent in yield surface models.

1.2.2 The Finite Element Method: Another approach for determining the biaxial behavior of reinforced concrete models is the finite element method. A few researchers are reported to have used this technique (11,20,28) to model the columns as a mesh of nodes. The disadvantages of this method are the enormous amount of computation required even for simple structures and that the microscopic interaction of concrete and steel (such as bond slip) are not modeled well. As a result, this technique does not appear to be promising for large structural analyses.

1.2.3 The Multiple Spring Model: A major step toward accuracy and simplification in modeling the biaxial bending was recently taken by Lai (11). The model developed by Lai does not depend on the formulation of a yield surface; hence, the complexities and approximations that plagued the other models are eliminated. According to Lai's method, the column in the vicinity of the probable yielding region is represented by a special configuration of several springs representing concrete and steel. Two hysteresis models are used to idealize the behavior of the springs. The multiple spring is far simpler and gives better correlations with experimental results (11) than either of the yield surface techniques. The multispring model

developed as part of the study reported herein uses the same basic philosophy. Therefore, the detailed descriptions of the components of Lai's model are provided in Chapter 2.

1.3 Object and Scope

The modeling of biaxial bending in reinforced concrete columns subjected to two-dimensional earthquake loads has been investigated by many reserachers, and its importance in accurately predicting seismic structural performance has been confirmed. Yield surface techniques used in the analysis of biaxial bending behavior are both complicated and unrealistic. The finite element technique requires too much computation to be considered for the analysis of typical structures. The only technique to date that provides for a relatively simple and accurate prediction of the inelastic biaxial bending behavior of reinforced concrete structures is a multiple spring type model.

The multispring model introduced by Lai is a considerable improvement over existing techniques but still requires substantial "bookkeeping" in computer memory to store the parameters for each spring. The first object of this study was to develop a multispring model with a considerably reduced amount of computation and bookkeeping without sacrificing the accuracy of the results. To evaluate the model, analytical results were compared with the available experimental data. Parametric studies were used to determine the important factors affecting the amplitudes and shape of the hysteresis loops.

The second goal of this study was the implementation of the new model into an existing inelastic dynamic analysis program for highway bridges. This modified program was used to assess the effects of the

model to overall bridge structural performance under bidirectional dynamic loadings.

The program chosen for implementation was NEABS, Nonlinear Earthquake Analysis of Bridge Systems. This program originally used the bilinear elasto-plastic model for inelastic beam and column elements.

CHAPTER 2

THE FORMULATION OF THE MODIFIED NINE-SPRING ELEMENT

2.1 Introduction

A simple accurate model for the biaxial behavior of reinforced concrete columns under bidirectional dynamic loadings is essential for the economical and realistic prediction of the response of structures subjected to strong earthquakes. Simplicity reduces computational effort and expense, which is an important factor in three-dimensional analyses. Even the simplest of yield surface techniques, the biaxial bilinear model, requires considerable computation to define the yield surface and its movement through moment space. The trilinear degrading model requires more calculations but still does not produce good correlations with experimental results (11).

The multiple spring (nine-spring) model developed by Lai (11) does not require the calculation of a yield surface or skeleton curves. The spring parameters are calculated from cross section and material properties. The interaction effects of biaxial bending and axial load are accounted for directly from the relationship between the spring stiffnesses and the rotational and axial degrees of freedom.

Two shortcomings can be identified in the nine-spring model in its original form: (1) To calculate the rotational stiffness of the element, the center of rotation is assumed to be at the centroid of the section; and (2) a relatively complex hysteresis model is used for the steel springs. The former results in the coupling of axial force

and bending moment as soon as the extent of nonlinearity in different springs is nonuniform. This problem is described in detail in section 2.2.3. The latter problem, namely, the complexity of the hysteresis model, requires a considerable amount of bookkeeping during the computation. This chapter describes the components of the Lai model and the solutions to the problems outlined above.

2.2 Nonlinear Model Element Description

In developing the Lai model, it is assumed that the hysteretic behavior of a reinforced concrete column can be approximated by a zero length nonlinear model element between the column and the joint. The model is formulated assuming that torsional and shear deformations are negligible. This assumption is reasonable for reinforced concrete columns with a sufficient number of ties to prevent an inelastic shear response. Because recent seismic design codes indeed require such details, the model is applicable to relatively recent structures. Another assumption incorporated into the Lai model is that the column has a symmetric cross section and steel.

The nonlinear model element developed by Lai (11) consists of nine springs: four representing reinforcing steel and five representing concrete. The springs are allowed to deform only in the axial direction. The nine springs are located in five positions: one steel and one concrete spring at each corner and a concrete spring in the center (Fig. 2.1). The two springs at each corner are assumed to be concentric. All nine springs are assumed to be nonlinear. The hysteresis models used for these springs are discussed at the end of this chapter.

The deformations of different springs are related by compatibility equations. The compatibility equations are derived assuming that plane sections remain plane. The column axial force is related to the spring forces. Thus, the model is capable of accounting for axial load variations during biaxial bending, a feature not easily accomplished with yield surface techniques.

In the following sections, a brief description of the nine-spring model is presented. The material is included in this report to facilitate the description of the background for the model which was developed in the present study (see Ch. 3).

2.2.1 The Steel Spring: Each steel spring represents the behavior of one-quarter of the steel in the cross section. The properties of this spring incorporate the slippage of the reinforcing bars. Lai (11) assumed that bond strength is uniform and can be approximated by

$$u = 14 \sqrt{f'_c} \quad (2.1)$$

in which

u = the bond strength in psi and

f'_c = the compressive strength of concrete in psi.

The applicable bond strength expression specified in the 1963 ACI code (1) for tensile bars ranged from $6 \sqrt{f'_c}$ to $9.5 \sqrt{f'_c}/d_b$ and for compressive bars was $13 \sqrt{f'_c}$. Emori and Schorobrich (7) studied the test data on #6 bars obtained by Wight and Sozen (35) and concluded that Eq. 2.1 leads to a good correlation with experimental data. The ACI equation results in $12.7 \sqrt{f'_c}$ for #6 bars. Given the degree of scatter in experimental data and all the approximations that will be

discussed in the following sections, Eq. 2.1 was considered to be reasonable for both tensile and compressive bars. The bond strength can be used to determine the development length of the bar at yield stress:

$$l_d = A_b f_y / (\pi * d_b * u) \quad (2.2)$$

in which

l_d = development length,

A_b = area of a single bar,

f_y = yield stress of the bar, and

d_b = diameter of a single bar.

Assuming a uniform bond stress distribution and a triangular strain distribution along the development length, the concentrated bar displacement at the joint due to slippage is

$$d = f_y l_d (2 * E_s) \quad (2.3)$$

in which

E_s = Young's modulus for steel bar.

Using these simple relationships, the initial elastic stiffness, k_{se} of the steel spring is calculated from

$$k_{se} = A_s f_y / d \quad (2.4)$$

which simplifies to

$$k_{se} = 2A_s E_s / l_d \quad (2.5)$$

in which

A_s = one-fourth of the total area of longitudinal steel.

The initial stiffness is assumed to be the same in both tension and compression. Reasonable results have been obtained using this equation as will be demonstrated in Ch. 3.

The yield displacement, d_y , for the spring is given by

$$d_Y = A_s f_Y / k_{se} \quad (2.6)$$

This yield displacement is used in the hysteresis rules and other relationships described in the following sections.

The postyielding stiffness of the steel spring depends on the strain-hardening of the bars, the amount of confining steel, and the thickness of the concrete cover. Lai assumed that the steel springs representing a column element have zero postyielding stiffness. However, test data from reinforced concrete columns subjected to bidirectional lateral loads (16) have revealed a small postyielding stiffness. In Chapter 3, it will be demonstrated that a postyielding stiffness value of two percent of the initial elastic stiffness leads to reasonable results.

2.2.2 The Concrete Spring: The concrete spring simulates the behavior of concrete in a reinforced concrete member. The properties of these springs are determined by the compressive strength of concrete and the moment and axial load at the balanced condition of the section.

The yielding force level in each concrete spring is determined from

$$P_{CY} = 0.85 f'_C A_C \quad (2.7)$$

in which

P_{CY} = yield level in the concrete spring,

A_C = area of concrete represented by the corner or center spring, and

f'_C = compressive strength of concrete.

The area represented by each of the corner concrete springs is the

same because of symmetry. The areas are determined from the balanced condition defined by conventional flexural theory (2,34). The area for the center spring is the remaining area of concrete not represented by the corner springs.

The balanced condition occurs when the outermost reinforcement layer yields in tension as the outermost fiber of concrete crushes in compression. The crushing strain for concrete is assumed to be 0.003, which is the value used by ACI (2).

In establishing the area of concrete springs, two simplifying assumptions are made: (1) the compressive steel springs yield under the balanced conditions, and (2) the neutral axis is located such that the force in the central concrete spring is zero. Based on these assumptions and given the symmetry of the column section, the area for the corner concrete springs is found from Eq. 2.8.

$$A_{\text{corner}} = P_b / (2 * 0.85 f'_c) \quad (2.8)$$

in which

P_b = balanced axial load for the section.

An average P_b is used for rectangular sections with different balanced loads in each orthogonal direction. The center spring area becomes

$$A_{\text{center}} = A_{\text{gross}} - 4 * A_{\text{corner}} - A_{\text{st}} \quad (2.9)$$

in which

A_{gross} = gross area of the cross section and

A_{st} = total area of steel in the cross section.

The initial elastic stiffness for the corner springs is

$$k_{ce} = 0.85 A_{\text{corner}} f'_c / d_y \quad (2.10)$$

and for the center spring is

$$k_{cce} = 0.85 A_{center} f'_c / d_y \quad (2.11)$$

Both of these stiffnesses are found under the assumption that the yield displacement for the concrete springs is the same as that for the steel springs.

The above stiffnesses are valid only for compression. The springs have no contribution in tension because the section is assumed to be initially cracked. This is not an unreasonable assumption because the initial cracking strength of concrete does not make a significant contribution to response. The primary curve for concrete springs is represented by an elasto-plastic relationship with no postyielding stiffness assumed (Fig. 2.3).

The locations of the springs are also determined based on the balanced condition. The moment at the yielding of opposing spring sets is assumed to be equal to the balanced moment in the corresponding direction (Fig. 2.2). The springs are assumed to be located in a symmetric pattern. The distance between the springs in direction i is

$$d_{si} = 2M_{bi} / (A_{st} f_y + 2 * 0.85 A_{corner} f'_c) \quad (2.12)$$

where

M_{bi} = the balanced moment computed from flexural theory and

i = either the x or y coordinate direction.

Note that d_{sx} is the distance perpendicular to the x axis and so on.

The above relationships describe the characteristics of the components of the element. The balanced moments and axial loads are the only values that need to be calculated for the actual section in order to formulate the element.

2.2.3 Inelastic Element Stiffness Matrix: The nine springs described in sections 2.2.1 and 2.2.2 form an element with three degrees of freedom: one axial and two rotational. The element stiffness matrix translates the axial stiffnesses of the component springs into joint rotational and axial stiffnesses. Shear and torsion deformations are neglected, and the stiffnesses in these degrees-of-freedom are assumed to be infinite. The derivation of the stiffness matrix is based on the equilibrium of forces and planar strain compatibility.

Lai (11) constructed the element stiffness matrix with the center of rotation always at the center of the section. When inelastic deformations are developed in the springs, this assumption generally leads to a coupling between axial load and rotation (i.e., an axial force is generated from pure bending) as described below. This problem is not addressed in Ref. 11.

Suppose the column shown in Fig. 2.1 has undergone a load history that has caused yielding of the springs at location 1 but no yielding in other springs. The instantaneous stiffness in location 1 is considerably less than that of the other springs. With the neutral axis fixed at the center and assuming plane sections remain plane, any rotation (say, about the x axis) should produce equal displacements in the upper (locations 1 and 2) and lower (locations 3 and 4) springs. Because the stiffness at location 1 is lower than that of other locations, the force in this spring is smaller. As a result, the total forces at the upper springs will be smaller than the forces at the lower springs. This, of course, leads to a lack of equilibrium in the axial direction.

Elimination of the coupling effect requires the neutral axis to translate in response to the changing stiffnesses of the springs. Using displacement compatibility relationships, the joint deformations can be written as

$$\begin{Bmatrix} \Delta p \\ \theta_x \\ \theta_y \end{Bmatrix} = \begin{bmatrix} 1/2 & 1/2 & 0 \\ 1/d_{sx} & 0 & -1/d_{sx} \\ 0 & -1/d_{sy} & -1/d_{sy} \end{bmatrix} \begin{Bmatrix} d_1 \\ d_3 \\ d_4 \end{Bmatrix} \quad (2.13)$$

where

d_{sx} , d_{sy} = distances between the spring locations as shown in Fig. 2.1,

d_i = displacement in the i th spring location as shown in Fig. 2.1,

Δp = axial displacement at the center of the section (at spring 5), and

θ_x , θ_y = rotations about the x and y coordinate axes, respectively.

Note that the displacements at spring locations 2 and 5 do not enter into Eq. 2.13. This is because the displacements at only three of the spring locations are sufficient to define the plane of deformation. The displacements at the other two locations can be determined based on the location of this plane.

Equation 2.13 relates the displacements in the springs to rotational and axial degrees-of-freedom without forcing rotation about the centroid.

The moments and axial force at the column section can be related to the spring forces as follows. As it was pointed out in previous

sections, the displacements at only three of the spring locations are independent variables. The three locations chosen for formulating the multispring element stiffness were 1, 3, and 4. The displacement at the center spring is found from

$$d_5 = (d_1 + d_3)/2$$

Referring to Fig. 2.4, the displacement at location 2 will be

$$d_2 = (d_1 + d_3)/2 + [(d_1 + d_3)/2 - d_4]$$

or

$$d_2 = d_1 + d_3 - d_4$$

The axial force and moments about the two orthogonal axes can be written in terms of spring forces as follows.

$$P = \sum_{i=1}^5 K_i d_i$$

$$M_x = \left(\sum_{i=1}^4 K_i d_i \right) (d_{sx}/2)$$

$$M_y = \left(\sum_{i=1}^4 K_i d_i \right) (d_{sy}/2)$$

Substituting the expressions for d_2 and d_5 in the expressions for forces and writing the equations in matrix form will lead to

$$\begin{Bmatrix} P \\ M_x \\ M_y \end{Bmatrix} = 1/2 \begin{bmatrix} 2(K_5/2+K_1+K_2) & 2(K_5/2+K_3+K_2) & 2(K_4-K_2) \\ (K_1+K_2)d_{sx} & (K_2-K_3)d_{sx} & (-K_4-K_2)d_{sx} \\ (K_1-K_2)d_{sy} & (-K_2-K_3)d_{sy} & (K_2+K_4)d_{sy} \end{bmatrix} \begin{Bmatrix} d_1 \\ d_3 \\ d_4 \end{Bmatrix} \quad (2.14)$$

where

k_i = stiffness at the i th spring location (Fig. 2.1).

The moments are calculated about the centroid of the section, but the neutral axis can be at any location.

Summarizing Eqs. 2.13 and 2.14

$$\{\theta\} = [T_1]\{d\} \quad (2.15)$$

and

$$\{P\} = [T_2]\{d\} \quad (2.16)$$

where $[T_1]$ and $[T_2]$ are the 3 x 3 coefficient matrices presented in Eqs. 2.13 and 2.14 respectively.

Substituting and rearranging results in

$$\{P\} = [T_1][T_2]^{-1}\{\theta\} \quad (2.17)$$

which can be rewritten as

$$\{P\} = [K]\{\theta\} \quad (2.18)$$

where $[K]$ is the element stiffness matrix.

2.3 Hysteresis Models

In the original nine-spring models, the variation of stiffness as a function of the load/deformation history was represented by the Takeda hysteresis model (29) for the steel springs and by a modified elastic-plastic model (named GHYST in this report) for the concrete springs. Although the hysteretic behavior of steel (as a material) is better idealized by a nondegrading model such as the bilinear or the Ramberg-Osgood model (21) because the steel springs in the multispring element represent the bond slip behavior of the bars as well as the steel behavior, it is appropriate to use a degrading hysteresis model for the steel springs. The Takeda model, however, is overly complicated. A comparison of hysteresis models (23) has shown that the Q-Hyst model (22), which is considerably simpler than the Takeda model, produces comparable results.

2.3.1 Hysteresis model for steel springs: The hysteresis model

for the steel springs is the QHYST model as developed by Saiidi and Sozen (22,23). The QHYST model is a simplified version of the Takeda model (23,29) and is different from the one used by Lai (11). The rules for the QHYST hysteresis model (Fig. 2.5) are as follows.

Rule 1: (operates on branch Y'Y)

1.1 Loading: if $d_i \leq d_y$; $K = K_{se}$; LVL = 1

if $d_i > d_y$; $K = K_y$; LVL = 2

1.2 Unloading: $K = K_{se}$; LVL = 1

1.3 Load reversal: $K = K_{se}$; LVL = 1

Rule 2: (operates on the postyielding branch)

2.1 Loading: $K = K_y$; LVL = 2

2.2 Unloading: $K = S1$; LVL = 3

Rule 3: (operates on $X_{O'U_m}$ or $X_{O'R}$)

3.1 Loading: 1. if last unloading point on YU, go to 3.1.2

if $f_i \leq f_R$ $K = S1$; LVL = 3

if $f_i > f_R$ $K = \text{slope of } X_{O'U_m}$; LVL = 4

2. if $f_i \leq f_{U_m}$ $K = S1$; LVL = 3

if $f_i > f_{U_m}$ $K = K_y$; LVL = 2

3.2 Unloading: $K = S1$; LVL = 3

3.3 Load reversal: $K = \text{slope of } X_{O'U_m}$; LVL = 4

Rule 4: (operates on $X_{O'U_m}$ or $X_{O'U_m}$)

4.1 Loading: if $f_i \leq f_{U_m}$ $K = \text{slope of } X_{O'U_m}$; LVL = 4

if $f_i > f_{U_m}$ $K = K_y$; LVL = 2

4.2 Unloading: unloading point is "R"; $K = S1$; LVL = 3

in which

d_i = the absolute value of the total current displacement in the
ith spring,

f_i = the absolute value of the total current force in the ith
spring,

K_{se} = the elastic stiffness of the spring,

K_y = the postyielding stiffness in the spring,

LVL = the pointer to the next rule,

$sl = K_{se} * (d_y / d_{max})^{bt0}$,

bt0 = a factor between 0 and 1,

d_y = the yield displacement,

d_{max} = the absolute value of the maximum displacement the spring
has experienced in either direction,

f_{U_m} = the absolute value of the force at U_m (or U_m'), and

f_R = the absolute value of the force at the unloading point R.

2.3.2 Hysteresis model for concrete springs: The hysteresis model for the concrete springs is a simple model formulated by Lai (11) for use in the multispring model. It is an extremely simple approximation of the response of concrete. The rules for the hysteresis model for concrete springs, called GHYST in this report, are as follows (Fig. 2.6).

Rule 1

1.1 Loading: if d_i positive (tension) $K = 0$; LVL = 1

if $|d_i| < d_y$; $K = K_{ce}$; LVL = 1

if $|d_i| > d_y$; $K = 0$; LVL = 2

1.1 Unloading: $K = K_{ce}$; LVL = 1

Rule 2

2.1 Loading: $K = 0$; $LVL = 2$

2.2 Unloading: $K = S1 = f_i/d_i$; $d_y = d_i$; $LVL = 3$

Rule 3

3.1 Loading: if $|d_i| \leq d_y$; $K = S1$; $LVL = 3$

if $|d_i| > d_y$; $K = 0$; $LVL = 2$

3.2 Unloading: if $d_i = > 0$; $K = 0$; $LVL = 3$

if $d_i < 0$; $K = S1$; $LVL = 3$

in which

d_i = the total displacement in the i th spring,

f_i = the total force in the i th spring, and

K_{ce} = the initial elastic stiffness for the springs.

A corner concrete spring is assumed to have the same total displacement as the corresponding steel spring. therefore, it is not necessary to use plasticity theory to update the displacement for the concrete spring when its stiffness is zero. Although the model is extremely simplified, in combination with the steel hysteresis steel models, it has produced reasonable results when compared to experimental data for reinforced concrete elements (see Ch. 4).

CHAPTER 3

FORMULATION OF THE FIVE-SPRING ELEMENT

3.1 Introduction

The nine-spring element introduced by Lai and the modified version described in Ch. 2 are both more realistic and simpler than the available yield surface or finite element models. Nonetheless, the fact that the force and displacement of each spring need to be traced throughout the analysis means that, for each column, nine subelements are necessary. For a structure with a relatively large number of columns, the required computer memory and the computation time may be excessive. To reduce the number of the subelements, the modified nine-spring element described in Ch. 2 was further refined and a five-spring model was developed. This model produced results which were of the same or better quality than those obtained from the original and modified nine-spring elements (see Ch. 4). The purpose of this chapter is to describe the five-spring element and the hysteresis models used for the springs within this element.

3.2 Element Description

The five-spring element is shown in Fig. 3.1. The major difference between this element and the nine-spring element is that the concrete and steel springs which were located at each corner of the nine-spring element are replaced by a composite spring. The center concrete spring remains unchanged. The five-spring element requires approximately forty percent less computer memory and execution time.

In subsequent sections, the composite springs and the hysteresis model used to represent their behavior are described. The concrete spring (spring 5 in Fig. 3.1) has the same description as that in sec. 2.2.2, and it utilizes the GHYST hysteresis model presented in sec. 2.3.2.

3.2.1 The Composite Spring: The composite springs (springs 1 through 4) have different characteristics in tension and compression. When in compression, they represent the steel and corner concrete springs discussed in secs. 2.2.1 and 2.2.2. When the composite springs are in tension, however, they represent only the steel springs described in sec. 2.2.1. The derivation of the properties of the composite spring is primarily based on the assumptions presented in Ch. 2. The primary curve for the composite springs (Fig. 3.2) has the following characteristics.

Tension:

$$\text{Initial stiffness, } K_{se} = 2A_s E_s / l_d$$

$$\text{Postyielding stiffness, } K_1 = 0.02 K_{se}$$

$$\text{Yield displacement, } d_y = A_s f_y / K_{se}$$

$$\text{Yield force} = A_s f_y$$

Compression:

$$\text{Initial stiffness, } (K_{se} + K_{ce}) = 2A_s E_s / l_d + 0.85 A_{\text{corner}} f'_c / d_y$$

$$\text{Postyielding stiffness, } K_y = 0.02 K_{se}$$

$$\text{Yield displacement, } d_y = A_s f_y / K_{se}$$

$$\text{Yield force} = A_s f_y + 0.85 f'_c A_{\text{corner}}$$

3.3 Hysteresis Model for Composite Spring

A modified version of QHYST, called AQHYST, was developed to model the response of the composite spring. AQHYST is based on the same four rules as those used in the QHYST model except that the initial stiffnesses for compression and tension are different. The AQHYST model does not incorporate the rules from GHYST (sec. 2.3.2), rather the concrete spring is assumed to "follow" the hysteretic path of the steel spring. The GHYST model for the concrete springs is used only for the center concrete spring.

The absolute value of the yield displacement is the same for both compression and tension. The yield force in tension is the yield force for a steel spring, and the yield force in compression is the sum of the yield forces for a steel spring and a concrete spring. The postyielding stiffness for both compression and tension is that of a steel spring. The properties for each type of spring are calculated as described in Chs. 2 and 3 and then combined to create the composite spring properties.

The rules for the AQHYST model are as follows (Fig. 3.3).

Rule 1:

- 1.1 Loading: if $0 < d_i \leq d_y$; $K = K_{se}$; LVL = 1
if $0 > d_i \geq -d_y$; $K = K_{ce} + K_{se}$; LVL = 1
if $|d_i| > d_y$; $K = K_y$; LVL = 2
- 1.2 Unloading: if $d_i > 0$; $K = K_{se}$; LVL = 1
if $d_i \leq 0$; $K = K_{se} + K_{ce}$; LVL = 1
- 1.3 Load Reversal: if $d_i > 0$; $K = K_{se}$; LVL = 1
if $d_i \leq 0$; $K = K_{se} + K_{ce}$; LVL = 1

Rule 2:

- 2.1 Loading: $K = K_Y$; LVL = 2
- 2.2 Unloading: if $d_i \geq 0$; $K = S1$; LVL = 3
if $d_i < 0$; $K = S2$; LVL = 3

Rule 3:

3.1 Loading: if last unloading point on YU go to 3.1.2.

1. if $|f_i| < |f_R|$; and:
if $f_i < 0$; $K = S2$; LVL = 3
if $f_i > 0$; $K = S1$; LVL = 3
if $|f_i| > |f_R|$; $K = \text{slope of } X_{O'}U_m'$; LVL = 4
2. if $0 < f_i < f_{U_m}$; $K = S1$; LVL = 3
if $0 > f_i \geq f_{U_m}$; $K = S2$; LVL = 3
if $f_i < f_{U_m}$; $K = K_Y$; LVL = 2
if $f_i > f_{U_m}$; $K = K_Y$; LVL = 2

- 3.2 Unloading: if $f_i > 0$; $K = S1$; LVL = 3
if $f_i < 0$; $K = S2$; LVL = 3

3.3 Load reversal: $K = \text{slope of } X_{O'}U_m'$ (or $X_{O'}U_m'$); LVL = 4

Rule 4

- 4.1 Loading: if $0 > f_i > f_{U_m}$; $K = \text{slope of } X_{O'}U_m'$; LVL = 4
if $0 < f_i < f_{U_m}$; $K = \text{slope of } X_{O'}U_m'$; LVL = 4
if $f_i < f_{U_m}$; $K = K_Y$; LVL = 2
if $f_i > f_{U_m}$; $K = K_Y$; LVL = 2

4.2 Unloading: unloading point is "R".

if $f_i > 0$ $K = S1$; LVL = 3

if $f_i < 0$ $K = S2$; LVL = 3

in which

$$S1 = K_{se} * (d_y/d_{max})^{bt0},$$

$$S2 = (K_{se} + K_{ce}) (d_y/d_{max})^{bt1},$$

bt1 = the degradation factor for compression, and

all other variables are the same as for the QHYST model (sec. 2.3.1).

The new hysteresis model provides a smoother transition between tension and compression. The model also degrades the stiffness and allows for permanent deformation of the composite springs. Subroutine AQHYST is used for each corner spring location at every iteration.

CHAPTER 4

COMPARISON OF ANALYTICAL AND EXPERIMENTAL RESULTS

4.1 Introduction

All of the springs that make up the multispring biaxial bending elements are inelastic. Each spring type (concrete, steel, or composite) is governed by a set of hysteresis rules which describe the stiffness of the spring depending on its loading history. The quality of the response calculated, based on the multispring elements described in Chapters 2 and 3, depends on (1) the assumptions made in developing the general form (Figs. 2.1 and 3.1) of the element and (2) the method of idealizing the hysteretic behavior. For the multispring elements presented in previous chapters, both of these appear to be rational. That is, the layouts shown in Figs. 2.1 and 3.1 have the potential of simulating the behavior of a biaxially bent column and the hysteresis models used for the constituent components are acceptable representatives of the behavior of concrete and steel.

To evaluate the multispring elements presented in Chapters 2 and 3, the elements were incorporated in a cantilever column analytical model. The model was used to calculate the response of two biaxially bent columns for which experimental data were available. This chapter presents the cantilever model as well as the analytical and experimental results.

4.2 Description of the Cantilever Structure

Few experimental data concerning the inelastic biaxial behavior in reinforced concrete columns subjected to cyclic loads are available. Some of the available data, such as those from Umehara and Jirsa

(33), are for relatively short specimens in which shear deformations, and not flexural deformations, dominate. Otani (16) presents data for cantilever column specimens subjected to static bidirectional lateral deflections. The specimens were designed to behave dominantly in flexure. These data are used to test the biaxial bending elements described in previous chapters.

The configuration and specifications for two of Otani's test specimens SP-7 and SP-8 are presented in Fig. 4.1. The only difference between SP-7 and SP-8 is the applied deflection history (Figs. 4.2 and 4.3). Neither test specimens had an applied axial load.

The column was modelled as an elastic line element with a biaxial bending multispring element (Chapters 2 and 3) at the base (Fig. 4.4). The stiffness for the elastic line element was based on the gross moment of inertia and the modulus of elasticity for concrete. The parameters for the biaxial bending multispring elements were calculated as described in Chapters 2 and 3. Only flexural and axial degrees-of-freedom were considered as torsion effects were considered negligible. Shear deformations were also ignored.

Figure 4.5 shows the degrees of freedom (DOF's) for the cantilever column model. DOF's five and eight were slaved because the axial deformation of the line element (Fig. 4.4) was ignored. The stiffness matrix for the system was condensed with respect to DOF's one and two to allow for input displacement at these locations. For any set of input displacements at DOF's one and two, the forces and deformations at DOF's six through eight were calculated and used to determine spring displacements and forces in the multispring element.

The cantilever model was implemented in program APPDIS. This

program first calculates the spring properties and then applies the displacement history to the structure in small increments. The displacement histories for SP-7 and SP-8 were divided into 2950 and 2600 increments, respectively. For each incremental displacement an incremental moment is calculated at the location of the multispring element. An incremental axial deformation is calculated for each spring location and the proper hysteresis subroutine is called for each spring. A large stiffness value was assigned to the element for the pre-yielding stage to simulate the elastic behavior of the column. Once the hysteresis routines indicate that one or more of the springs have yielded, then a new stiffness matrix is created for all of the subsequent iterations. The new shear forces at the top of the column are calculated using the updated spring forces returned from the hysteresis subroutines. The new shear force at the top of the cantilever is then plotted against the total column deflection. The APPDIS program was used for parametric studies presented later in this chapter. A flowchart of APPDIS is presented in Fig. 4.6.

4.3 Evaluation of the Modified Nine-Spring Element

Lai (11) has demonstrated that the original nine-spring model will produce results which are in reasonable agreement with experimental data. The purpose of testing the modified nine-spring element was to study the effects of using a new element stiffness matrix and the QHYST hysteresis model. The postyielding stiffness for the steel springs was assumed to be two percent of the initial elastic stiffness. Figures 4.7 and 4.8 are comparisons of the experimental and analytical response for SP-7 in the x and y directions, respectively.

The bt_0 factor (Sec. 2.3.1) used for this case is 0.5. A reasonable value for bt_0 is 0.4 or 0.5 (20,27).

Note that bt_0 controls the width of the hysteresis loops. As the value of bt_0 increases, the area within hysteresis loops will decrease. The value of bt_0 is used in the Takeda hysteresis model as well as the Q-HYST and AQHYST models.

The overall shape of the hysteretic response curves shown in Figs. 4.7 and 4.8 are similar, especially for the inner loops. The calculated outermost loop in the x direction is not well matched with the experimental data because of significant deterioration of column which caused shear deformations to become significant for the last displacement increments (16). The comparisons show that this value of bt_0 does not allow for the hysteretic energy loss experienced by the actual column, as measured by the area within the curves.

Smaller values of bt_0 produce greater energy loss for the element. A bt_0 value of 0.2 was used for the response histories presented in Figs. 4.9 and 4.10. The calculated curves are noticeably wider in the displacement direction, comparing more favorably with the experimental data. This value of bt_0 produced the best fit and is the value used by Lai (11) in his hysteresis model. Responses for SP-8 are shown in Figs. 4.11 and 4.12. Again acceptable results have been obtained using a bt_0 value of 0.2.

Both of the above comparisons show that the modified nine-spring element underestimates the peak strength of the column by ten percent to twenty percent. This is not unreasonable given the variability of concrete and steel properties and the simplified nature of the model.

The analytical results based on the original nine-spring element for SP-7, shown in Figs. 4.13 and 4.14 shows a better peak strength comparison than the response for the modified element, but the shape of the response curve for the y direction is not as good as that produced by the modified element presented here.

A characteristic of this implementation is the "stepping error". A stepping error occurs when a spring stiffness changes abruptly, such as in the transition from compression to tension. These stepping errors cause abrupt changes in the response, such as the "zig-zag" shown in the left part of the outer loop of Fig. 4.12. These zig-zags slightly reduce the amount of energy dissipated by the structure and affect subsequent load-deformation relationships. Stepping errors are minimized by small displacement increments, but cannot be completely eliminated.

Another characteristic of the nine-spring element is the overshoot error. This error affects the axial force balance of the structure and is not evident from the hysteresis curves. The error occurs because the hysteresis routines modify each spring stiffness and spring force without regard to the other springs. The hysteresis routines change the force in the spring to correct for "overshooting", or allowing a force in the spring that is not on the hysteresis curve (Fig. 4.15). Because modifying the force in one spring has no effect on the other springs during an iteration, the axial load (the sum of the spring forces) equilibrium is generally violated. The imbalance is generally too large to be ignored; for the test cases presented here the axial load imbalance in some instances approached 1,000 kips. The moment response of the element is not greatly affected, but modeling

variations in axial load cannot be performed accurately.

Although this implementation has some problems, it still produces better results than the bilinear yield surface model. A representative sample, obtained from Ref. 11, is shown in Fig. 4.16. The bilinear model overestimates the peak forces by approximately forty percent. The hysteretic energy loss is also significantly larger than what is indicated by the experimental data.

4.4 Evaluation of the Five-spring Element

The main difference between the five-spring and the modified nine-spring elements is the smaller computer memory and shorter computation time requirements for the five-spring model, and the hysteresis modeling of the corner springs.

The hysteresis model used in the five-spring element (AQHYST, Sec. 3.3.1) reduces stepping errors by allowing for a smoother transition between compression and tension forces in a spring. However, it does not remove the axial load imbalance caused by force modification within a load interval. Using much smaller displacement increments would reduce the error, but would take far too much computation time. A simple correction scheme was implemented which applies the opposite of the axial load imbalance to the element in the next iteration. A similar approach was used to correct force imbalances in a frame analysis program developed by Otani (14), among others. This method is simple and fast as compared with other methods.

In AQHYST, the slope of unloading branch for the postyielding stage is controlled by parameters bt_0 and bt_1 (Sec. 3.3.1). These parameters control the "fatness" of the hysteresis loops. Because a

value of 0.2 had been used for a comparable parameter in the nine-spring model, this value was also used for bt_0 and bt_1 .

The experimental results from Otani's (16) specimens SP-7 and SP-8 were utilized as the basis of evaluating the five-spring element. Figures 4.17 through 4.20 compare the experimental data to the analytical results. The effects of the smoother transition from compression to tension are evident in smoother curves. The overall shape of the curves remains a good fit in both directions for both specimens. The correlation with experimental data is as good or better than the correlation between the nine-spring element results and the measured data (Figs. 4.9-4.12).

To determine the sensitivity of the calculated response to variation in bt_0 , bt_1 , and postyielding stiffness parameters, specimen SP-7 was analyzed using the five-spring model with different values for these parameters. Figures 4.21 and 4.22 show the effects of using a value of 0.4 for bt_0 and bt_1 . These plots give a slightly better fit for low-amplitude cycles, but are somewhat too narrow.

The values of bt_0 and bt_1 should not necessarily be the same. The bt_0 parameter represents stiffness degradation for a steel spring subjected to tension (Sec. 3.3.1), whereas bt_1 is an index for stiffness degradation of the composite spring which includes the effect of concrete. Note that as bt_1 increases, the permanent displacement will decrease. In the nine-spring model, the concrete springs have no permanent displacement (Fig. 2.6) due to the fact that the branch corresponding to rule 3 is forced to pass through the origin. The slope of this branch could be formulated as follows to obtain a value

of $bt1$ which would produce zero permanent displacement.

$$S_3 = P_{cy}/d_{max} \quad (4.1)$$

In which:

S_3 = slope of branch 3 in Fig. 2.6;

P_{cy} = yield force; and

d_{max} = maximum displacement

writing S_3 in a form comparable to S_1 and S_2 (Sec. 3.3.1.) leads to

$$S_3 = K_{CC} * (d_y/d_{max})^{bt1} \quad (4.2)$$

K_{CC} , the elastic stiffness is found from

$$K_{CC} = P_{cy}/d_y \quad (4.3)$$

substituting S_3 from Eq. 4.1 and K_{CC} from Eq. 4.3 in Eq. 4.2 will lead to $bt1 = 1$ for concrete. The value of $bt1$ used in AQHYST represents both the concrete and steel (the composite spring). Because $bt1 = 0.4$ is reasonable for steel and $bt1 = 1$ simulates the concrete spring model in the nine-spring element, a simple average value of 0.7 may be considered as a representative value for the composite spring. Increasing the $bt1$ factor to 0.7 gives the results presented in Figs. 4.23 and 4.24. These loops do not provide the same amount of energy dissipation as the experimental results indicate. Comparison of these figures with Figs. 4.9 and 4.10 reveals that $bt0 = bt1 = 0.2$ produced better correlation with experimental data.

The analytical results using a $bt0$ value of 0.4 and a $bt1$ value of 0.3 are compared to experimental results in Figs. 4.25 and 4.26. These curves have good correlations with experimental results, although they do slightly underestimate hysteretic energy loss.

The "blunting" of the sharp saw-toothed peaks in the response histories for SP-7 using the five-spring model are in part due to the

correction method used for axial force. The axial force imbalance applied to the springs accelerates the yielding of some of the springs, causing the stiffness to reduce prematurely. While the moment response is reduced, it does force axial equilibrium to be satisfied.

Figures 4.27 and 4.30 illustrate the effects of changing the postyielding stiffness. Figures 4.27 and 4.28 compare the experimental results to analytical results using a postyielding stiffness of five percent of K_{se} (the initial steel spring stiffness). This does increase the peaks, but only in the large-amplitude loops. Using extremely small values of postyielding stiffness can lead to "overloading" of the correction scheme for axial force. Figures 4.29 and 4.30 show what can happen if a value of 0.2 percent of K_{se} is used. The erratic response is caused by drastic changes in the hysteretic path created by large axial force imbalance in a single iteration. The problem can be avoided by using smaller load increments or a larger postyielding stiffness.

4.5 Comments and Conclusions

The first object of this study was to develop a simplified multispring element and to compare its response with experimental data. The completion of this task revealed that the element will produce reasonable hysteretic responses for cantilever columns subjected to bidirectional lateral displacements. Although the biaxial bending element does not produce perfect match and must be used with some care, it is simple and executes quickly.

It is recommended, on the basis of the comparisons presented here, that a postyielding stiffness value in the range of one percent

to five percent be used for typical columns, unless a better approximation is available or a different axial force correction method is used. Values for bt_0 and bt_1 should be between 0.2 and 0.4 for adequate hysteretic energy loss. When additional experimental data become available, more representative general relations for postyielding stiffness, the bt_0 factor, and the bt_1 factor may be possible.

CHAPTER 5

IMPLEMENTATION IN A NONLINEAR BRIDGE MODEL

5.1 Introduction

The multispring biaxial bending element described in Chapter 3 was added to program NEABS (Nonlinear Earthquake Analysis of Bridge Systems) as a new element type. Program NEABS is a FORTRAN IV program written for nonlinear dynamic analysis of highway bridges. The original program used four element types:

- 1) Linear elastic and elasto-plastic straight beam elements;
- 2) Linear elastic circularly curved beam elements;
- 3) Linear elastic foundation spring elements;
- 4) Linear and nonlinear expansion joint elements.

A fifth type of element, the five-spring biaxial bending element, was installed in the program for this study. This chapter describes the operation of NEABS and the modifications made to the program.

5.2 Description of Program NEABS

The subroutine organization of program NEABS is presented in Fig. 5.1. The analysis procedure used in NEABS is similar to that described by Tseng and Penzien (30). This procedure can be summarized as follows:

- 1) The initial static equilibrium equations of the bridge are formed from the input data (Subroutine SETUP).
- 2) The static systems of equations are solved for dead load and static nodal load response (Subroutine STATIC). In this analysis, the structure is assumed to remain elastic. The results are used as the initial conditions for the subsequent nonlinear dynamic

analysis.

- 3) Digitized dynamic load functions applied at nodes or ground accelerations are input for equal or unequal time intervals. Dynamic load vectors are calculated for each time step of integration (Subroutine LOADS).
- 4) Incremental dynamic equilibrium equations are formed and solved for incremental nodal displacements, velocities, accelerations using Newmark's solution technique for the equations of motion (13). Total nodal displacements, velocities, and accelerations are calculated for each time step (Subroutine INTGR).
- 5) The nonlinearity conditions of each nonlinear element are checked within each time interval. If necessary, a new element stiffness matrix and nonlinear force vector are calculated for the element. The bridge stiffness matrix is then recalculated for the next time interval. Equilibrium of the bridge is checked using the linear and nonlinear forces (Subroutine NELSTF).
- 6) The time histories of response results from the step-by-step solution are rearranged for output (Subroutine OUTPUT).

5.3 Modifications to Program NEABS

The subroutines highlighted in Fig. 5.1 were added to NEABS to implement the five-spring biaxial bending element. The subroutines are SMOD, TEAMOD, NEWMOD, SPRING, STMOD, NMOD, AQHYST, and GHYST. Subroutines SMOD, TEAMOD, NEWMOD, and SPRING create the element stiffness matrix. Subroutine STMOD initializes the element hysteresis model after the static loads have been determined by subroutine STATIC. Subroutine NMOD calls the hysteresis models, AQHYST and GHYST,

and creates a new element stiffness matrix if necessary. The operation of the subroutines is outlined below.

5.3.1 Subroutines SMOD, TEAMOD, NEWMOD, and SPRING: Subroutine SMOD initializes parameters and then calls TEAMOD. Subroutine TEAMOD first reads the cross section data and calls subroutine SPRING to calculate the composite concrete-steel and concrete spring stiffnesses. Subroutine TEAMOD reads the coordinate information for each multispring element, calculates the local to global transformation matrix, and calls subroutine NEWMOD. Subroutine NEWMOD calculates the local element stiffness (3 x 3), expands the local element stiffness matrix to 12 X 12, then calculates a 12 X 24 matrix which relates global displacements to local forces, and finally calculates a 24 X 24 global element stiffness matrix. These relatively large matrix sizes were used not because they were necessary for the multispring model but to maintain compatibility with the rest of the program. Flowcharts for subroutines SMOD and TEAMOD are presented in Fig. 5.2. Flowcharts for SPRING and NEWMOD are presented in Fig. 5.3.

5.3.2 Subroutines STMOD and NMOD: Subroutine STMOD is called from subroutine STATIC after solution of static equilibrium forces. Subroutine STMOD initializes the hysteresis pointers and calls subroutine NMOD. Subroutine NMOD is called from two points in the program: from subroutine STMOD and subroutine NELSTF. When called from either subroutine, NMOD finds the incremental forces in the element springs and calls the appropriate hysteresis subroutine. After all of the element springs have been updated, NMOD checks to see if any of

the springs have yielded. If none of the springs have yielded, then control is returned to the calling subroutine. If the element has yielded, then new element stiffness matrices are calculated and control is returned to the calling subroutine. Flowcharts for subroutines STMOD and NMOD are presented in Figs. 5.3 and 5.4, respectively.

5.3.3 Subroutines AQHYST and GHYST: The hysteresis subroutines AQHYST and GHYST are the same as those used for the static model in Chapter 4. The operation and theory of these subroutines are presented in Chapters 2 and 3.

5.4 Evaluation of Modified NEABS

The modified version of program NEABS (program NEABS-86) contains the new multispring biaxial bending element. The implementation was tested for compatibility with the existing element types both statically and dynamically using a simple two span bridge. The results indicated the five-spring element was compatible with all elements both statically and dynamically except the elasto-plastic beam element. The elasto-plastic element may lead to instabilities when used in combination with the five-spring element. This incompatibility is discussed in more detail below.

Implementation of the five-spring element for dynamic analysis required that subroutine ITERN be bypassed for timely execution of the program and to limit memory storage requirements (Fig. 5.1). If the square root of the sum of the squares of the imbalanced forces due to yielding or friction losses becomes larger than RTOLS (relative tolerance of subdivision specified by the user) then subroutine ITERN

reverses the program one time interval. Subroutine ITERN then subdivides the time interval by NSDIV (number of subdivisions specified by the user). Subroutine ITERN prevents instabilities due to large time steps which can create large force imbalances in a single time step. The five-spring element is more stable than the elasto-plastic element because stiffness changes are less severe, hence the force imbalances are less. The bypass of subroutine ITERN is accomplished by setting NSDIV and MAXIT (maximum number of iterations) to zero. It is recommended that the five-spring element and the elasto-plastic element not be used together. Care should be taken to ensure that small time steps are used when using the new element.

5.5 Comments and Conclusions

The new multispring element was successfully implemented in program NEABS-86. Testing revealed that the modifications were compatible with the remainder of the original program for static and dynamic analyses except for the elasto-plastic element. This incompatibility is due to the bypassing of the subroutine ITERN, which was necessary for the timely execution of the program and to reduce memory storage requirements. This bypass will not lead to instabilities unless large time steps or large load intervals are used. Testing of the modified program revealed that the force imbalance produced by the new element will increase for only one time interval after a change in stiffness, then it will decrease to virtually zero within two or three time intervals.

Program execution times using the five-spring element are comparable to those using the elasto-plastic element. Depending on the

number of nonlinear program iterations, the execution times for the new element are generally less than those for the elasto-plastic element. Execution speed increases depending on the values of NSDIV and MAXIT and the number of nonlinear iterations. When the bridge remains elastic, the execution time for the model with the five-spring element is considerably longer than that for the model with the yield surface element. This is because it is necessary to keep track of five sub-elements within the five-spring element even during elastic stages, whereas the yield surface element is a single element. When nonlinear deformations are developed, the yield surface element requires iterations within every time interval and, hence, requires a generally longer execution time.

CHAPTER 6

CASE STUDIES

6.1 Introduction

This chapter compares the dynamic response of three highway bridges modeled using both the elasto-plastic yield surface element and the five-spring column elements (or the multiple-spring elements, MSE) presented in Chapter 3. Three modern bridges, the Rose Creek Interchange in Nevada, the Meloland Overpass in California, and the Flamingo Road Overpass in Nevada, were used as the basis for mathematical models analyzed using program NEABS-86 (Chapter 5). The pier top acceleration and displacement histories are presented and compared for each element.

6.2 Structure Modeling

Two models were prepared for each case study: one using elastic-plastic column elements and another using multiple-spring elements at the base of the columns. The objective of this study was to examine the possible differences in dynamic response created by using different nonlinear column models. Ordinarily, the nonlinear response is affected by the nonlinearity of the foundation, columns, hinges, expansion joints, etc. To isolate the effect of modeling of the columns, however, it was necessary to force all the elements other than the columns to remain elastic. As a result, the bridges were not modeled exactly; rather, their properties were used as the basis for realistic structural geometries and cross section properties. Foundation stiffnesses were considered infinite because yielding of the foundation materials interferes with the yielding of the columns (9).

The connections between the foundation and the columns were assumed to be moment resistant, although the actual connections in two of the bridges were "pinned" connections. Abutments were modeled as pinned or roller elements. Considering the above idealization, the results presented in this chapter represent the dynamic response of fictitious bridge structures with realistic structural properties for comparison of two biaxial bending elements. The results do not represent the actual bridge responses.

The models were subjected to rigid ground excitations (no phased input was used) at the pier bases and at the abutments in the transverse and the longitudinal directions. Response histories were plotted for the pier top displacements and accelerations. For the five-spring elements, the bt_0 and bt_1 factors were set to 0.2 (Chapter 3).

6.3 The Meloland Overpass

6.3.1 Description of the structure: The Meloland Overpass is a 208-foot long, two-span, symmetrical reinforced concrete box girder bridge located within one-quarter mile of the Imperial Fault in southern California. The single round concrete column pier is 20.5 feet high and five feet in diameter and is reinforced with eighteen #18 bars equally distributed around its perimeter. An elevation of the bridge is presented in Fig. 6.1.a, and an elevation of the pier is presented in Fig. 6.2. The bridge was subjected to the magnitude 6.4 Imperial Valley Earthquake in October 1979 and did not experience any visible structural damage (9).

6.3.2 Modeling of the structure: The Meloland Overpass was idealized as shown in Fig. 6.1.b. The abutments were modeled as rollers in order to allow for large deformation and yielding of the column at reasonable acceleration levels. Structural damping was assumed to be five percent for all cases. Structural element parameters were based on actual cross section data and are tabulated in Table 6.1. A rectangular column model was prepared to study the effects of the shape of the column cross section on the dynamic response (Fig. 6.3). The properties of this column were chosen such that its strength and stiffness are comparable to the round column, but the balanced moments are different in the two principal axes.

6.3.3 Results of dynamic analyses: The measured free-field horizontal accelerations from the 1979 Imperial Valley Earthquake were applied to the round column model of the Meloland Overpass. These two acceleration histories, one longitudinal and one transverse (Figs. 6.4 and 6.5), were recorded by an instrument located 200 feet from the centerline of the bridge. The results from the analyses are presented in Figs. 6.6 and 6.7. Only the transverse responses are shown because these responses were representative of the correlation between the results from the two hysteresis models. The solid lines represent the response of the MSE model and the dashed lines represent the elasto-plastic response. Note that the early low amplitude accelerations and displacements at the pier top are identical, indicating that the elastic response is the same for both element models. Upon yielding at approximately four seconds, the responses separate dramatically. The elasto-plastic column has zero stiffness, whereas the stiffness in MSE

reduces gradually. The elasto-plastic acceleration response is less than the MSE response, but the displacement response for the elasto-plastic element are very much larger than the MSE response. The responses also show phase differences due to the different effective stiffnesses reflected in the effective period of vibration.

The Meloland model was subjected to the 1940 El Centro Earthquake with the input acceleration doubled (Figs. 6.8 and 6.9). The El Centro east-west history was applied transversely and the El centro north-south history was applied in the longitudinal direction. The results using the double El Centro Earthquake are presented in Figs. 6.10 and 6.11. The displacement and acceleration response for the MSE analysis differs from the elasto-plastic response in both phase and amplitude. These differences are due to the changing of stiffness in the MSE as element springs move from one hysteresis rule to another. The change in stiffness leads to different effective periods for the structure and can lead to a greater response than the softer elasto-plastic model.

A rectangular column was designed with properties similar to those of the actual round column to study the sensitivity of the response when a rectangular column is used in the bridge model. The Meloland model was subjected to the same El Centro Earthquake accelerations with the same peak ground acceleration as that used for the round column model. The responses (Figs. 6.12 and 6.13) are similar to those for the round column model. The major differences between the round column response and the rectangular column response are the displacements after three seconds. The rectangular column models yield earlier during the earthquake than the round column models do. As a

result, the MSE and elasto-plastic responses differ more significantly in the case of the rectangular column (Fig. 6.13). The last five seconds of the rectangular elasto-plastic history show a shift in the oscillation axis. This can be attributed to the drastic stiffness loss in the elasto-plastic model. The MSE histories for both the round and rectangular column models appear similar in amplitude but not in phase.

6.4 The Rose Creek Interchange

6.4.1 Description of the structure: The Rose Creek Interchange is a 400-foot long, five-span, symmetrical reinforced concrete box girder bridge (Fig. 6.14). The bridge crosses I-80 ten miles southwest of Winnemucca, Nevada. The bridge deck is continuous over its entire length and is supported by four, 21-foot high single column piers. The piers are connected to the pile caps at the base using a single transverse line of steel bars to produce a pinned connection in the longitudinal direction of the bridge. The elevation of a typical pier and cross-section of a column is presented in Fig. 6.15. The bridge has been extensively tested statically and dynamically using hydraulic rams to provide lateral loads and free vibration upon release.

6.4.2 Modeling of the structure: The model of the Rose Creek Interchange is shown in Fig. 6.16. The pinned column-pile cap connections were assumed to be fixed to allow for testing of the biaxial bending models. The abutments were modeled as pinned connections. Each of the columns was allowed to become inelastic. Structural element properties were based on the actual cross sections and are shown in

Table 6.2. Structural damping ratio was assumed to be five percent.

6.4.3 Results of dynamic analyses: The Rose Creek Interchange model was subjected to the El Centro Earthquake with the north-south component applied in the longitudinal direction and the east-west component applied in the transverse direction. The results are presented in Figs. 6.17 through 6.24. Because of the symmetry of the structure and the motions, the responses for only piers 1 and 2 are shown. Figures 6.17 through 6.18 present the transverse acceleration responses at the pier tops. The MSE response (solid lines) is generally of higher amplitude than the elasto-plastic response (dashed lines). This reflects the larger effective stiffness modeled by the MSE. The responses are completely out of phase at the top of pier 2. In sharp contrast to the transverse direction, the longitudinal acceleration responses obtained from the two models (Figs. 6.19 and 6.20) are nearly identical. This indicates that the response in the longitudinal direction is insensitive to the hysteresis model used for the piers. It should be noted that, because the abutments are modeled as pins and because of the relatively large axial stiffness of the bridge deck, the response is dominated by the input motion at the abutments and is insensitive to the yielding characteristics of pier bases. The displacements in the longitudinal direction (Figs. 6.23 and 6.24) are also virtually identical. Figures 6.21 and 6.22 present the transverse displacement responses. The effective period for the elasto-plastic model is very long because the columns yielded and reduced the stiffness dramatically. The MSE model produces relatively low amplitude displacements by comparison because of its greater and

more realistic effective stiffness. The displacement histories produced by the elasto-plastic model predict substantial damage to the bridge for an earthquake similar to the 1940 El Centro Earthquake. The MSE model predicts moderate displacements and little damage to the structure.

6.5 The Flamingo Road Overpass

6.5.1 Description of the structure: The Flamingo Road Overpass is actually two bridges side by side (Fig. 6.25). The actual structure spans 270 feet in five unequal slightly curved spans. The decks are continuous reinforced concrete box girders, one wider than the other. Each deck has one intermediate hinge/expansion joint in the middle span. Each pier is supported by two columns 3'-3" in diameter and reinforced with eleven #11 bars. The connection between the columns and pile caps is pinned in both transverse and longitudinal directions by using a small group of five #11 bars positioned near the center. An idealized pier elevation is shown in Fig. 6.26.

6.5.2 Modeling of the structure: The Flamingo Road model bears little resemblance to the actual structure. The model considers only the narrower of the two bridges. For simplicity, the model is straight and flat (Fig. 6.27). The intermediate hinge/expansion joint was modeled as a true hinge with the global Z direction moment released. The piers were assumed to be identical as illustrated in Fig. 6.26. The abutments were assumed to be rollers and the column connections were assumed to be rigid at both ends. Due to a restriction in the available software for computing the ultimate column properties, the reinforcement in each column was assumed to be twelve #11 bars equally

distributed about the perimeter of the column. The structural properties of the rest of the model are based on the actual cross section properties and are summarized in Table 6.3. Structural damping ratio was initially assumed to be five percent of critical damping.

6.5.3 Results of dynamic analyses: The Flamingo Road model is a very strong and rigid structure, as the dynamic results show. The 1940 El Centro north-south component was applied in the longitudinal direction and the east-west component in the transverse direction. The results of the analyses are presented in Figs. 6.28 through 6.51. The longitudinal responses were so small as to be insignificant; therefore, only the transverse responses are presented here. The bridge experienced only minor yielding, hence the large acceleration response and the small amplitude displacements. The MSE and the elasto-plastic responses are very similar, because the MSE stiffness degradation was not large and the elasto-plastic element did not yield. Although the MSE did yield, it did not change the response significantly because the extent of yielding was limited. Instead of producing a dramatically large displacement, the MSE model's response changes only slightly as would be expected of the actual structure.

Because the yield moments in the Flamingo Road model were relatively large, the applied acceleration histories were multiplied by 1.5 and the damping was reduced to three percent. The results indicate that the elasto-plastic model, upon yielding, caused the response to become unstable in the transverse direction (Figs. 6.45-6.51). Attempts to alleviate the problem, such as using time steps of integration four times smaller or more equilibrium iterations, failed

to improve the results. Subsequent analyses with much shorter iteration times showed that the elasto-plastic model requires an enormous number of iterations to produce stable results.

6.6 Comments and Conclusions

In the absence of experimental or empirical data, the best test of the five-spring element is to compare its response to that of another element, in this case the commonly used elasto-plastic yield surface element. The MSE models examined here show that the postyielding strength of concrete is far more significant than the elasto-plastic element would predict. The elasto-plastic element is also subject to instabilities caused by the severe stiffness variation during yielding and after yielding. The program execution times on the CYBER 830 at the University of Nevada ranged from 16 CP seconds for an elastic analysis of the Meloland model to over 1300 CP seconds for the unstable Flamingo Road analysis. Elastic program execution times are three times longer using models with MSE's. Nonlinear analyses are generally faster using the MSE than using the elasto-plastic element, depending on the number of equilibrium iterations required. The Flamingo Road analysis for 1.5 times the El Centro Earthquake ran in 314 CP seconds, four times faster than the unstable elasto-plastic analysis.

CHAPTER 7

SUMMARY AND CONCLUSIONS

7.1 Summary

A new biaxial bending element for the cyclic analysis of non-linear biaxial bending of reinforced concrete columns was developed. The new element incorporates the idea of representing the column section by several springs. This approach was first introduced by Lai (11) who used nine springs to idealize the column. The new element, namely the five-spring element also referred to as MSE in this report, consists of five springs representing steel and concrete within a cross section. The MSE was first implemented in a step-by-step static analysis displacement-controlled program (program APPDIS). Results obtained using the MSE compared favorably to experimental data. The MSE provided for a similar amount of energy loss and reproduced displacement-force response well. The test results indicated that the MSE provides approximately ten percent less peak strength than the experimental data suggest. The MSE results are superior to results obtained using the biaxial bilinear yield surface model or the tri-linear degrading yield surface model (11).

The new five-spring element was added to program NEABS, a program for the nonlinear analysis of bridge systems. The original program used only an elasto-plastic yield surface model. Testing of the modified program, NEABS-86, revealed only one incompatibility. In order to conserve computer memory requirements and reduce program execution times, the MSE does not use the force equilibrium iteration subroutine ITERN. The elasto-plastic element must use this routine to

avoid instabilities caused by large nonlinear force losses. Because forces change gradually in the new element, this routine was not needed. It is therefore necessary that the MSE and the elasto-plastic element are not used together in the same structural model.

Dynamic analyses of three bridge structures were performed using NEABS-86. The structures modeled were the Meloland Overpass, the Rose Creek Interchange, and the Flamingo Road Overpass. The models were idealizations of the structures not intended to represent the actual bridges but to provide realistic geometries and cross sections. The main difference between the models and the real systems was in the idealizations of the boundary elements. These elements were treated either as fixed or free to allow the nonlinear column elements to dominate the response. Results from models using the MSE and the elasto-plastic element were compared. The results reveal dramatic differences in the predicted seismic response of the structures. The elasto-plastic models generally predicted smaller amplitude acceleration response and larger displacement response at the pier tops than did the MSE models. The less severe stiffness changes produced by the MSE model account for the smaller displacement response. The severe changes in stiffness produced by the elasto-plastic model resulted in an unstable displacement history for the Flamingo Road model. Throughout the testing of NEABS-86, the MSE models did not display any sign of instabilities.

Program execution times using the MSE are generally faster for nonlinear analyses. Elastic analyses using the MSE run three times longer than those without the MSE. This is because each MSE is actually five elements which have to be monitored during the motion,

while the elasto-plastic element has but one component. When the elasto-plastic model yields, it requires many more iterations of the program to produce stable results thus making the analysis slow. Nonlinear analyses can run up to four times faster using the MSE instead of the elasto-plastic element depending on the number of equilibrium iterations specified by the user. Program execution times on the CYBER 830 at the University of Nevada ranged from 16 CP seconds for 800 elastic iterations of the Meloland elasto-plastic model to over 1300 CP seconds for the unstable Flamingo Road elasto-plastic model analysis. The Flamingo Road model with the MSE produced stable results and ran in 314 CP seconds.

7.2 Observations and Conclusions

A new nonlinear biaxial bending element for the cyclic analysis of reinforced concrete columns was developed and produced excellent correlations with experimental data for two statically applied force-displacement specimens. The accuracy of the MSE's dynamic response is inferred from these few data. There is little doubt that this new element produces more realistic results than the elasto-plastic element for biaxial bending of reinforced concrete columns. It has been demonstrated that reinforced concrete is not elasto-plastic. However, researchers in this field have used the elasto-plastic model not because it was accurate but because it is simple and convenient. Accuracy of the MSE for dynamic analyses of reinforced concrete columns in bridge structures can only be determined from experimental data. When measured data from either destructive testing of a full-scale bridge or from a well instrumented bridge that undergoes

structural nonlinearities becomes available, then refinements and improvements to the MSE can be made.

Nonlinear analyses using the new five-spring element execute faster, do not become unstable, and provide for a more realistic dynamic response for reinforced concrete columns subjected to biaxial bending. The analyses of models using the MSE can offer insight into the performance of a reinforced concrete structure subjected to biaxial bending due to bidirectional earthquake loadings.

REFERENCES

1. ACI Committee 318-63, Building Code Requirements for Reinforced Concrete, American Concrete Institute, Detroit, Michigan, 1963.
2. ACI Committee 318-83, Building Code Requirements for Reinforced Concrete, American Concrete Institute, Detroit, 1983.
3. Anderson, J.C., and W.H. Townsend, "Models for RC Frames with Degrading Stiffness," Journal of the Structural Division, ASCE, Vol. 103, No. ST12, Dec., 1977, pp. 2361-2376.
4. Arnold, C., "Architectural Implications," Reconnaissance Report Imperial County, California, Earthquake, Earthquake Engineering Institute, Berkeley, February 1980, pp. 111-138.
5. Bressler, B., "Design Criteria for Reinforced Concrete Columns under Axial Load and Biaxial Bending," American Concrete Institute Journal, No. 57, November 1960, pp. 481-490.
6. Clough, R.W. and S.B. Johnston, "Effect of Stiffness Degradation on Earthquake Ductility Requirements," Proceedings, Japan Earthquake Engineering Symposium, Tokyo, Japan, Oct., 1966, pp. 195-198.
7. Emori, K. and W.C. Schnobrich, "Analysis of Reinforced Concrete Frame-Wall Structures for Strong Motion Earthquakes," Civil Engineering Studies, SRS No. 457, University of Illinois at Urbana-Champaign, December 1978.
8. Giberson, M.F., "The Response of Nonlinear Multi-Storey Structures Subjected to Earthquake Excitation," California Institute of Technology, Earthquake Engineering Research Laboratory, 1967.
9. Hart, J.D., "Nonlinear Modeling of Short Highway Bridges Subjected to Earthquake Loading," a thesis submitted in partial fulfillment of the requirements for the Master of Science degree in Civil Engineering, University of Nevada, Reno, May 1984.
10. Hill, R. The Mathematical Theory of Plasticity, London, Oxford University Press, 1950.
11. Lai, S.-S., "Inelastic Analysis of Reinforced Concrete Space Frame under Biaxial Earthquake Motions," a dissertation submitted in partial fulfillment of the requirements for the degree of Doctor of Philosophy in Civil Engineering, University of Toronto, 1984.
12. Moss, P.J., A.J. Carr, and G.C. Pardeon, "Inelastic Analysis of the Imperial County Services Building," Bulletin of the New Zealand National Society for Earthquake Engineering, Vol. 16, No. 2, June 1983.

13. Newmark, N.M., "A Method of Computation for Structural Dynamics," ASCE Journal of the Mechanics Division, July 1959, pp. 67-94.
14. Otani, S., "SAKE-A Computer Program for Inelastic Response of R/C Frames to Earthquake," Civil Engineering Studies, SRS No. 413, University of Illinois, Urbana-Champaign, November 1975.
15. Otani, S., "Hysteresis Models of Reinforced Concrete for Earthquake Response Analysis," Journal of the Faculty of Engineering, University of Tokyo, Vol XXXVI, No. 2, 1981, pp. 125-159.
16. Otani, S. and V.W.-T. Cheung, "Behavior of Reinforced Concrete Columns Subjected to Biaxial Lateral Load Reversals," Publication 81-02, Department of Civil Engineering, University of Toronto, February 1981.
17. Padilla-Mora, R. and W.C. Schnobrich, "Nonlinear Response of Framed Structures Subjected to Two-Dimensional Earthquake Motion," Civil Engineering Studies, SRS No. 408, University of Illinois at Urbana-Champaign, July 1974.
18. Park, R., and Paulay, T., Reinforced Concrete Structures, John Wiley and Sons, 1975.
19. Pecknold, D.A., "Inelastic Structural Response to 2D Ground Motion," ASCE Journal of the Engineering Mechanics Division, Vol. 100, No. EM5, October 1974, pp. 949-963.
20. Penzien, J., R. Imbsen, and W.D. Liu, "NEABS: Nonlinear Earthquake Analysis of Bridge Systems (Users Manual)," NISSEE/Computer Applications, Earthquake Engineering Research Center, University of California at Berkeley, May 1981.
21. Ramberg, W. and W.T. Osgood, "Description of Stress-Strain Curves by Three Parameters," NACA Technical Note No. 902, 1943.
22. Saiidi, M. and M.A. Sozen, "Simple and Complex Models for Non-linear Seismic Response of Reinforced Concrete Structures," Civil Engineering Studies, SRS No. 465, University of Illinois at Urbana-Champaign, August 1979.
23. Saiidi, M., "Hysteresis Models for Reinforced Concrete," ASCE Journal of the Structural Division, Vol. 108, No. ST5, May 1982, pp. 1077-1087.
24. Saiidi, M. and B.M. Douglas, "Effect of Design Seismic Loads on a Highway Bridge," ASCE Journal of Structural Engineering, Vol. 110, No. 11, November 1984, p. 2723-2737.
25. Saiidi, M., Hart, J.D., and Douglas, B.M., "Inelastic Static and Dynamic Analysis of Short R/C Bridges Subjected to Lateral Loads," Civil Engineering Department, Report No. CCEER-84-03, University of Nevada, Reno, July 1984.

26. Shepherd, R. and A.W. Plunkett, "Damage Analysis of Imperial County Services Building," ASCE Journal of Structural Engineering, Vol. 109, No. 7, July 1983, pp. 1711-1726.
27. Sozen, M.A., "Hysteresis in Structural Elements," Applied Mechanics in Earthquake Engineering, ASME, MMD, Vol. 8, November 1974, p. 63-98.
28. Suharwardy, M.I.H. and D.A. Pecknold, "Inelastic Response of Reinforced Concrete Columns Subjected to Two-Dimensional Earthquake Motions," Civil Engineering Studies, SRS No. 455, University of Illinois at Urbana-Champaign, October 1978.
29. Takeda, T., M.A. Sozen, and N.N. Nielsen, "Reinforced Concrete Response to Simulated Earthquakes," ASCE Journal of the Structural Division, Vol. 96, No. ST12, December 1970, pp. 2557-2573.
30. Takizawa, H. and H. Aoyama, "Biaxial Effects in Modeling Earthquake response of R/C Structures," Earthquake Engineering and Structural Dynamics, Vol. 4, 1976, pp. 523-552.
31. Thomas, C.W., I.G. Buckle, and R.C. Fenwick, "The Effects of Inelastic Shear on the Seismic Response of Structures," Report No. 347, Department of Civil Engineering, University of Auckland, New Zealand, March 1983.
32. Tseng, W.S. and J. Penzien, "Analytic Investigations of the Seismic Response of Long Multiple Span Highway Bridges," Report No. EERC 73-12, Earthquake Engineering Research Center, University of California, Berkeley, June 1973.
33. Umehara, H. and J.O. Jirsa, "Shear Strength and Deterioration of Short Reinforced Concrete Columns under Cyclic Deformations," PMFSEL Report No. 82-3, Department of Civil Engineering, University of Texas at Austin, July 1982.
34. Wang, C.-K. and C.G. Salmon, Reinforced Concrete Design, Fourth Edition, Harper & Row, 1985.
35. Wight, J.K. and M.A. Sozen, "Strength Decay of RC Columns under Shear Reversals," ASCE Journal of the Structural Division, Vol. 101, No. 5, May 1975, pp. 1053-1065.
36. Wosser, T.D., D. Campi, M. Fovinci, and W.H. Smith, "On the Earthquake Induced Failure of the Imperial County Services Building," Reconnaissance Report Imperial County, California, Earthquake, Earthquake Engineering Institute, Berkeley, February 1980, pp. 159-184.



TABLE 6.1

Meloland Overpass Data

(a) Section Properties:

Element	Iy	Iz	J	Area
Deck	272.3	4562.0	616.0	27.74
Column (round)	30.68	30.68	61.4	19.64
Column (rect.)	48.52	19.65	61.4	19.25

(b) Five-spring Element Properties:

Element	P (bal)	My (bal)	Mz (bal)
Column (round)	2500.0	8600.0	8600.0
Column (rect.)	3390.8	10904.2	7911.0

(c) Elasto-plastic Element Properties:

Element	P (comp)	Myo	Mzo	Pt/Pc
Column (round)	11112.0	7350.0	7350.0	0.3888
Column (rect.)	10976.0	9550.8	6566.1	0.3936

Element	a1	a2	a3	b1	b2	b3
Column (round)	-1.375	-2.884	-0.508	-1.375	-2.884	-0.509
Column (rect.)	-1.315	-2.887	-0.572	-1.461	-2.664	-0.290

Units: Kips and ft.

TABLE 6.2

Rose Creek Interchange Data

(a) Section Properties:

Element	Iy	Iz	J	Area
Deck	131.3	3533.0	410.6	56.00
Columns	39.1	148.5	117.2	30.00

(b) Five-spring Element Properties:

Element	P (bal)	My (bal)	Mz (bal)
Piers 1 & 4	7474.0	14560.0	22833.5
Piers 2 & 3	7251.2	11887.2	18662.2

(c) Elasto-plastic Element Properties:

Element	P (comp.)	Myo	Mzo	Pt/Po
Piers 1 & 4	19710.3	18406.0	10069.0	0.2880
Piers 2 & 3	17500.0	12367.0	6402.0	0.1920

Element	a1	a2	b3	b1	b2	b3
Piers 1 & 4	-2.152	-4.278	-1.126	-2.505	-3.405	0.100
Piers 2 & 3	-3.798	-6.919	-2.120	-4.219	-5.150	0.069

Units: Kips and ft.

TABLE 6.3

Flamingo Road Overpass

(a) Section Properties:

Element	Iy	Iz	J	Area
Deck	119.6	2188.2	400.0	36.80
Pier Cap	21.3	21.3	36.0	16.00
Columns	5.5	5.5	10.9	8.30

(b) Five-spring Element Properties:

Element	P (bal)	My (bal)	Mz (bal)
Columns	1520.0	1745.9	1745.9

(c) Elasto-plastic Element Properties:

Element	P (comp.)	Myo	Mzo	Pt/Po
Columns	3747.3	1119.2	1119.2	0.200

Element	a1	a2	a3	b1	b2	b3
Columns	-3.671	-6.311	-1.642	-3.671	-3.314	-1.642

Units: Kips and ft.

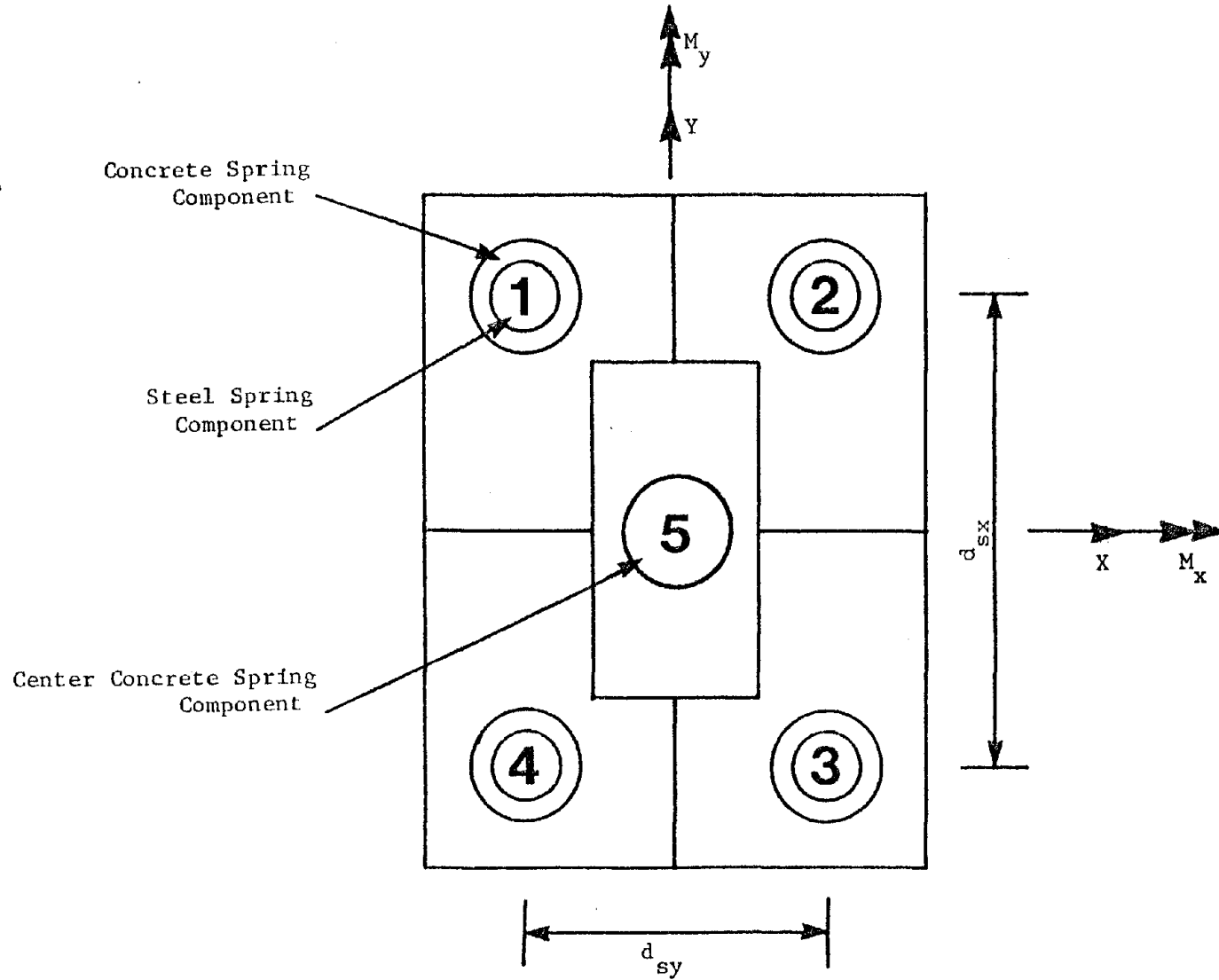


Fig. 2.1. The Multiple Spring Biaxial Bending Model.

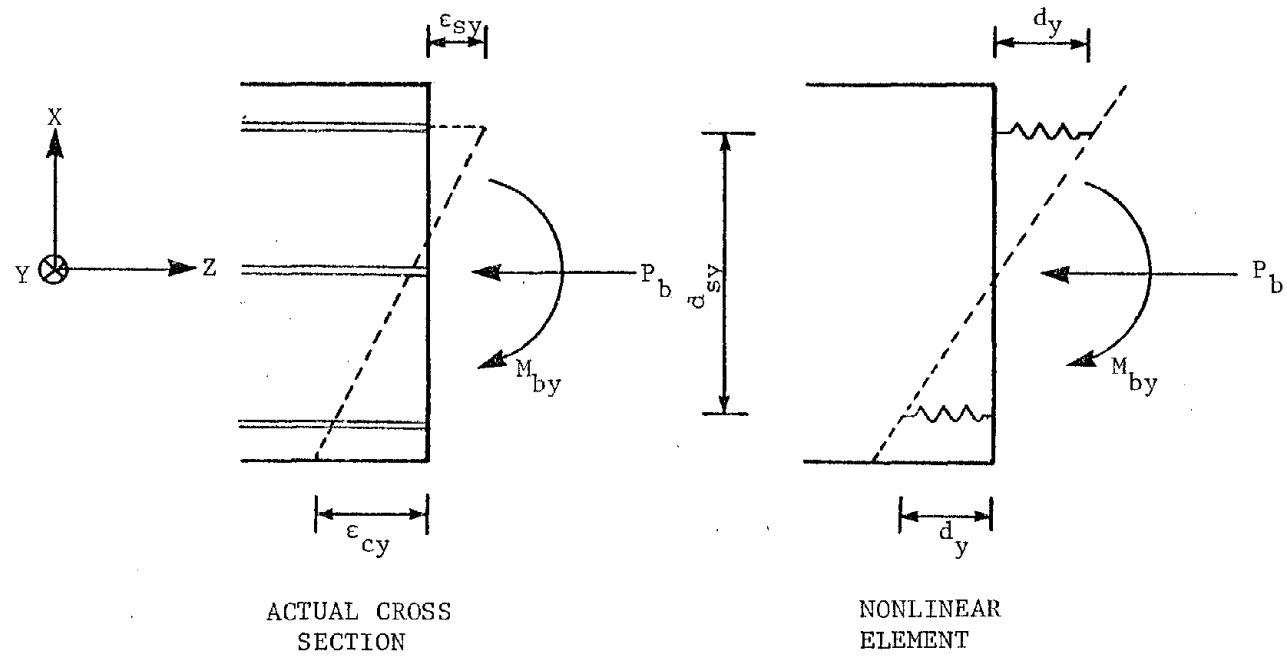


Fig. 2.2. The Multispring Biaxial Bending Element at the Balanced Condition.

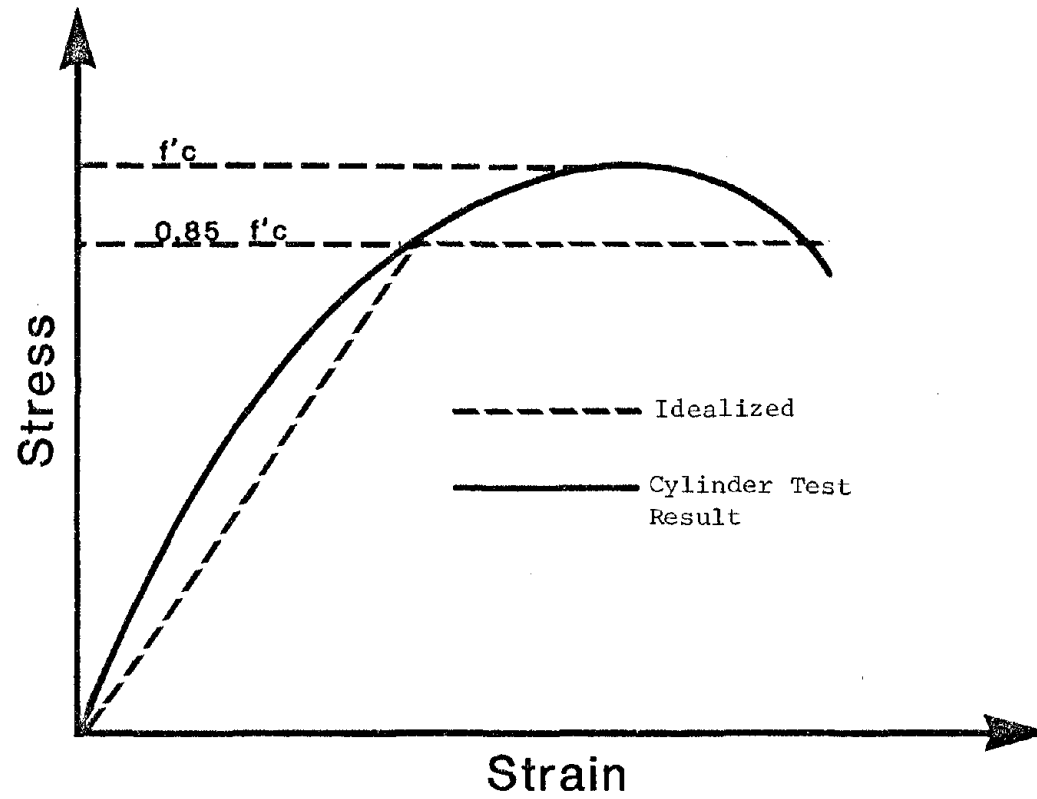


Fig. 2.3. Idealized Stress-Strain Relationship for Concrete Spring.

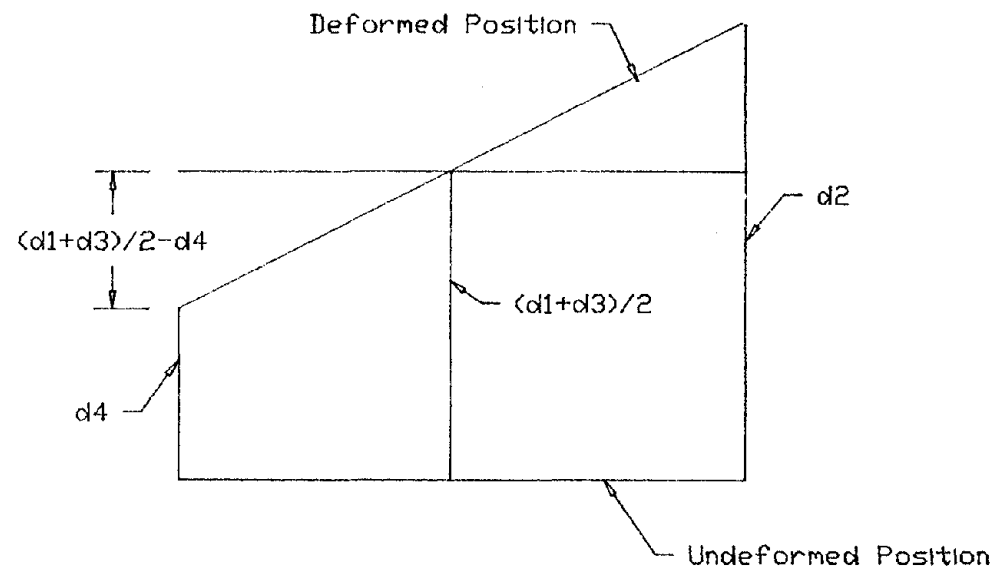
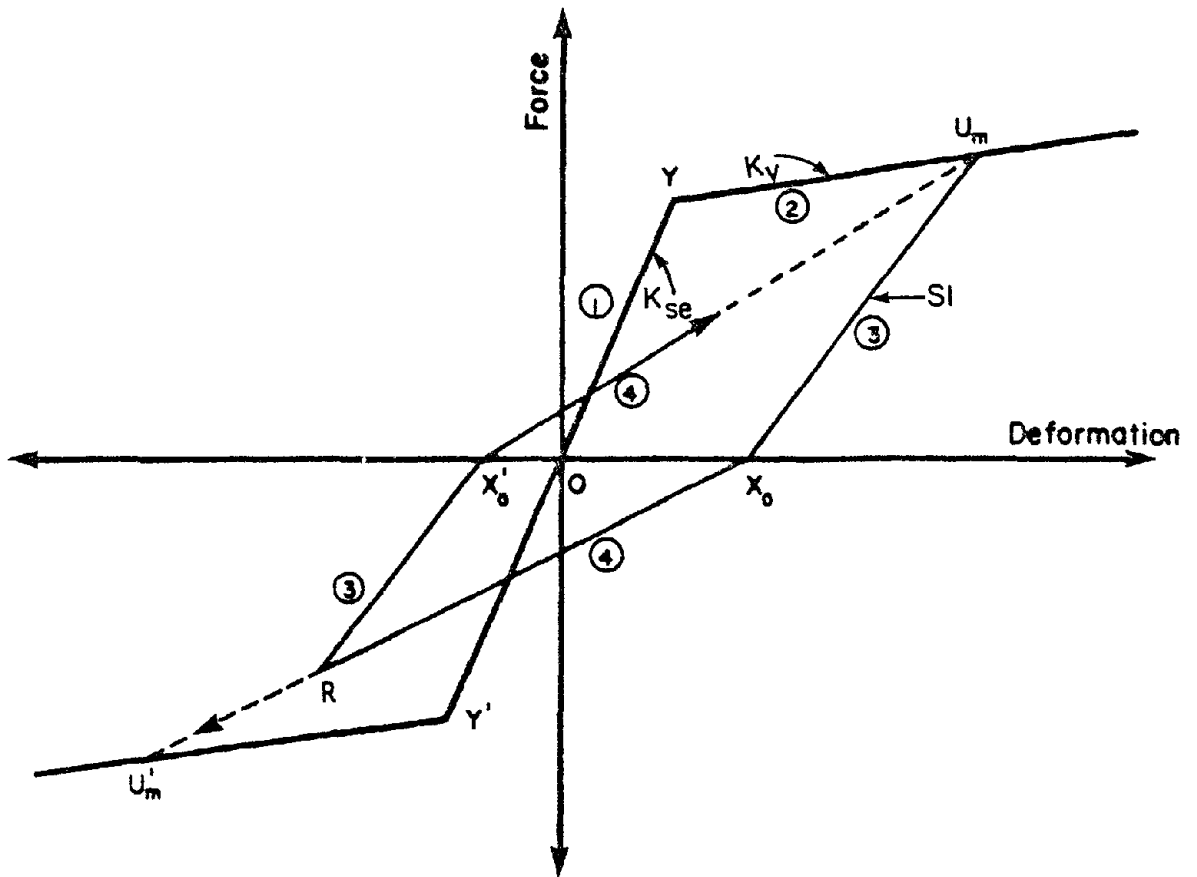


Fig. 2.4. Spring Displacements in a Diagonal Section.



- ① Rule 1
- ② Rule 2
- ③ Rule 3
- ④ Rule 4

Fig. 2.5. The QHYST Hysteresis Model.

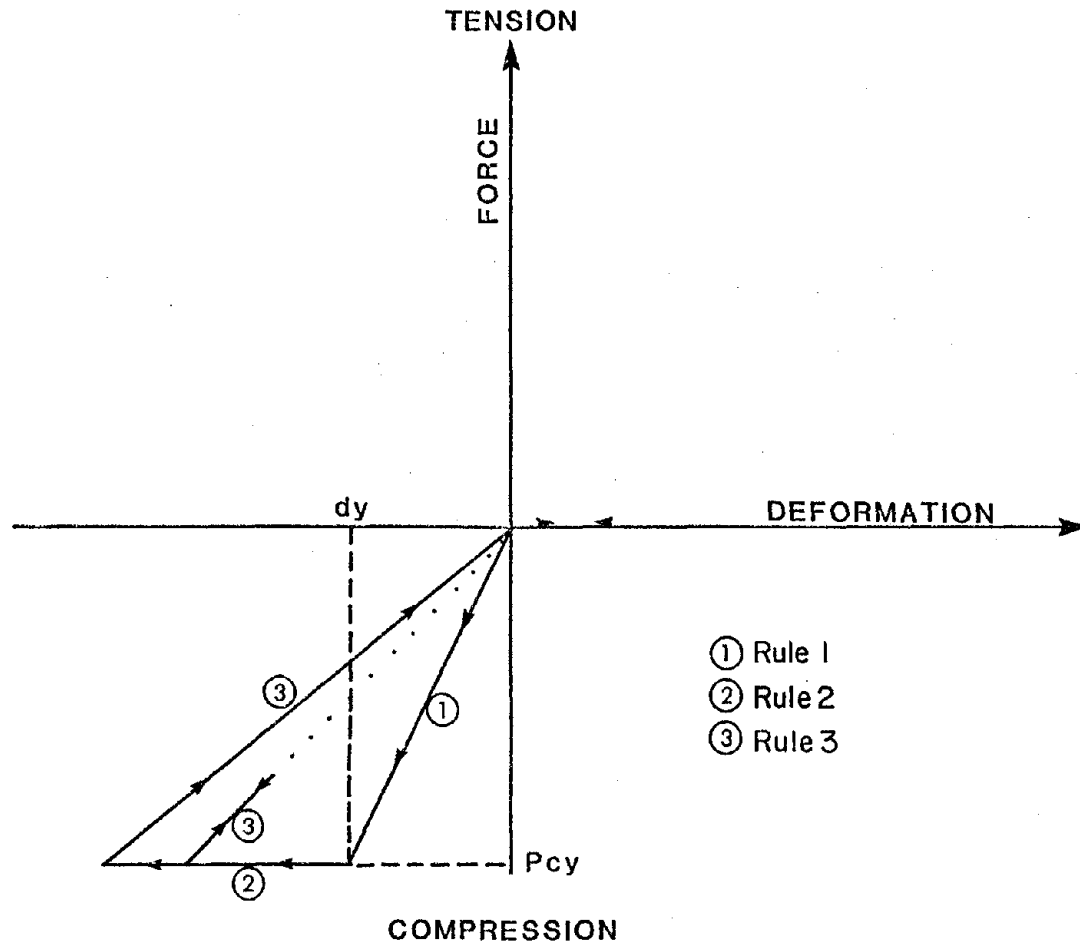


Fig. 2.6. The GHYST Hysteresis Model.

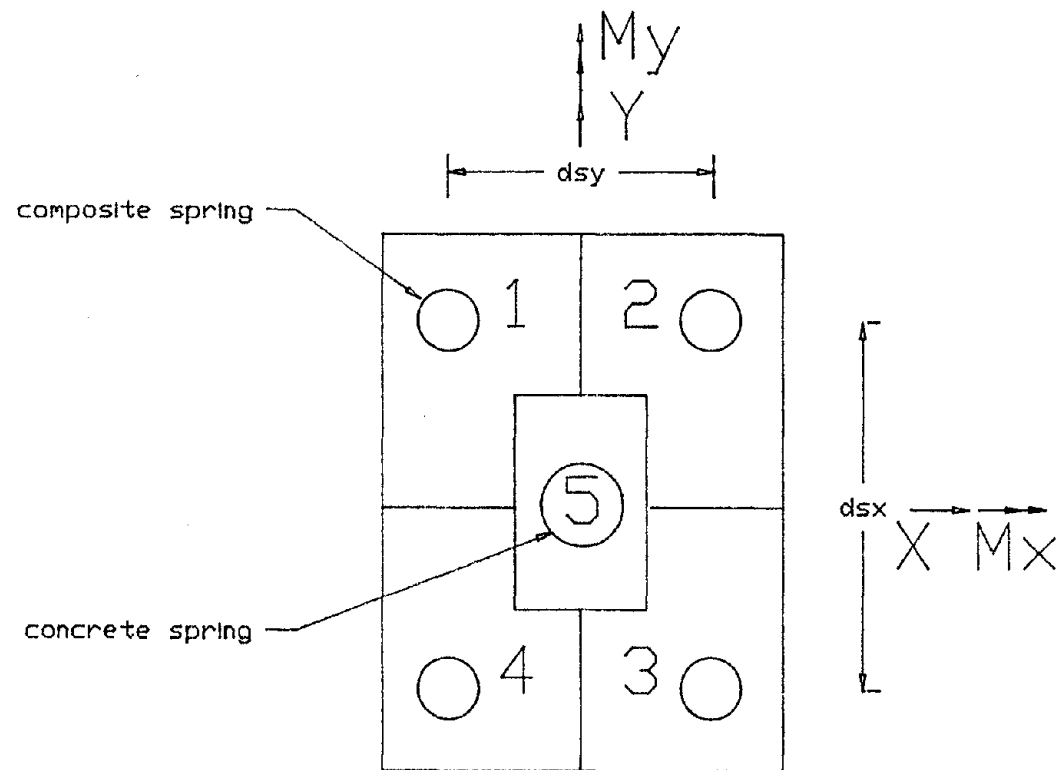


Fig. 3.1. The Five-Spring Element.

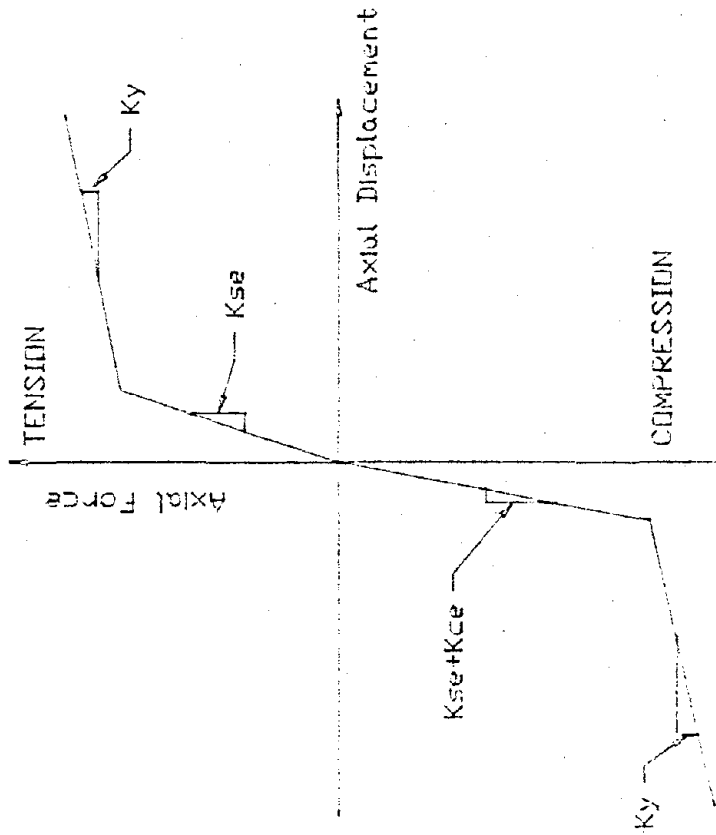


Fig. 3.2. Primary Curve for the Composite Springs.

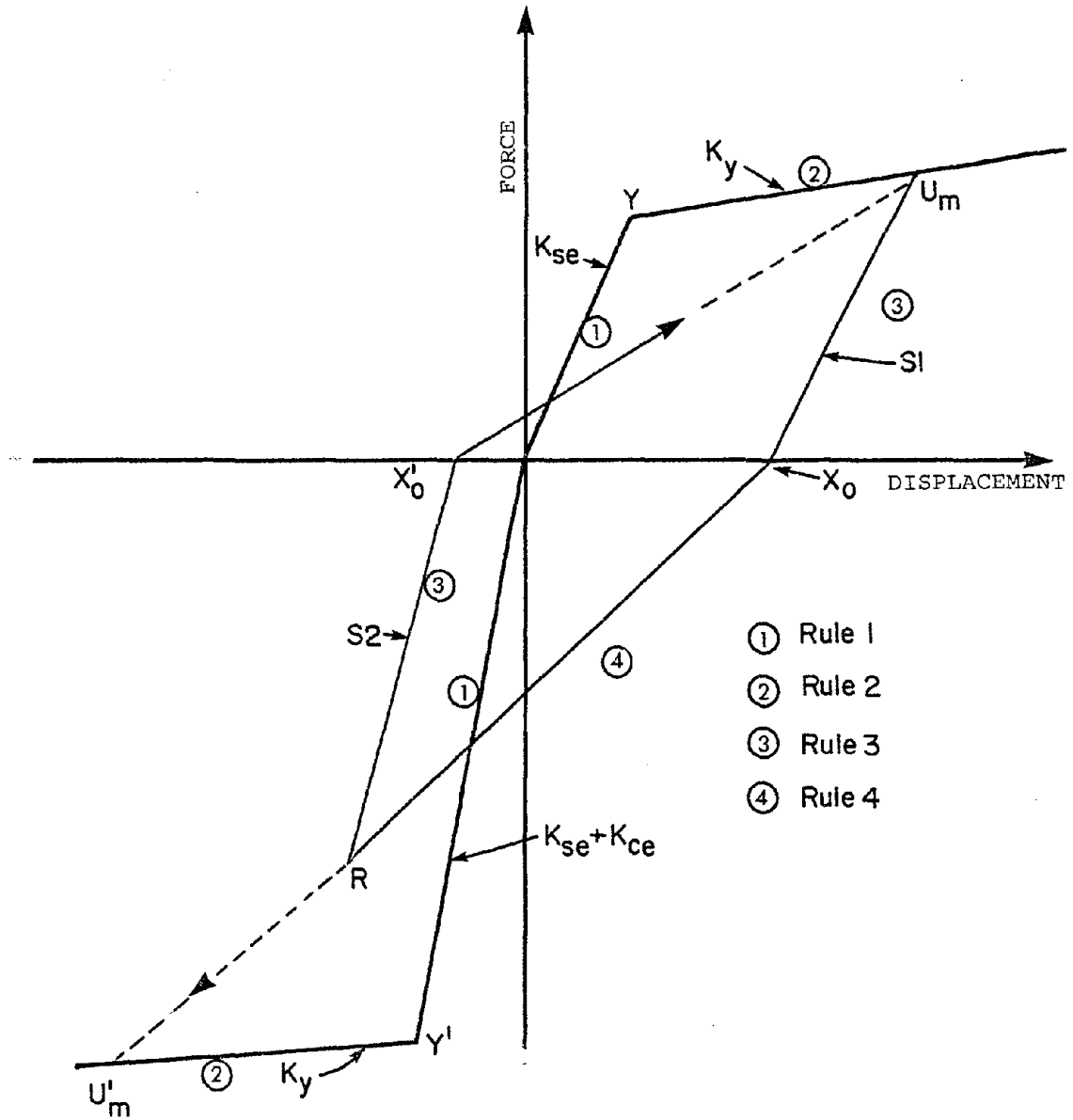


Fig. 3.3. The AQHYST Hysteresis Model for Composite Steel-Concrete Springs.

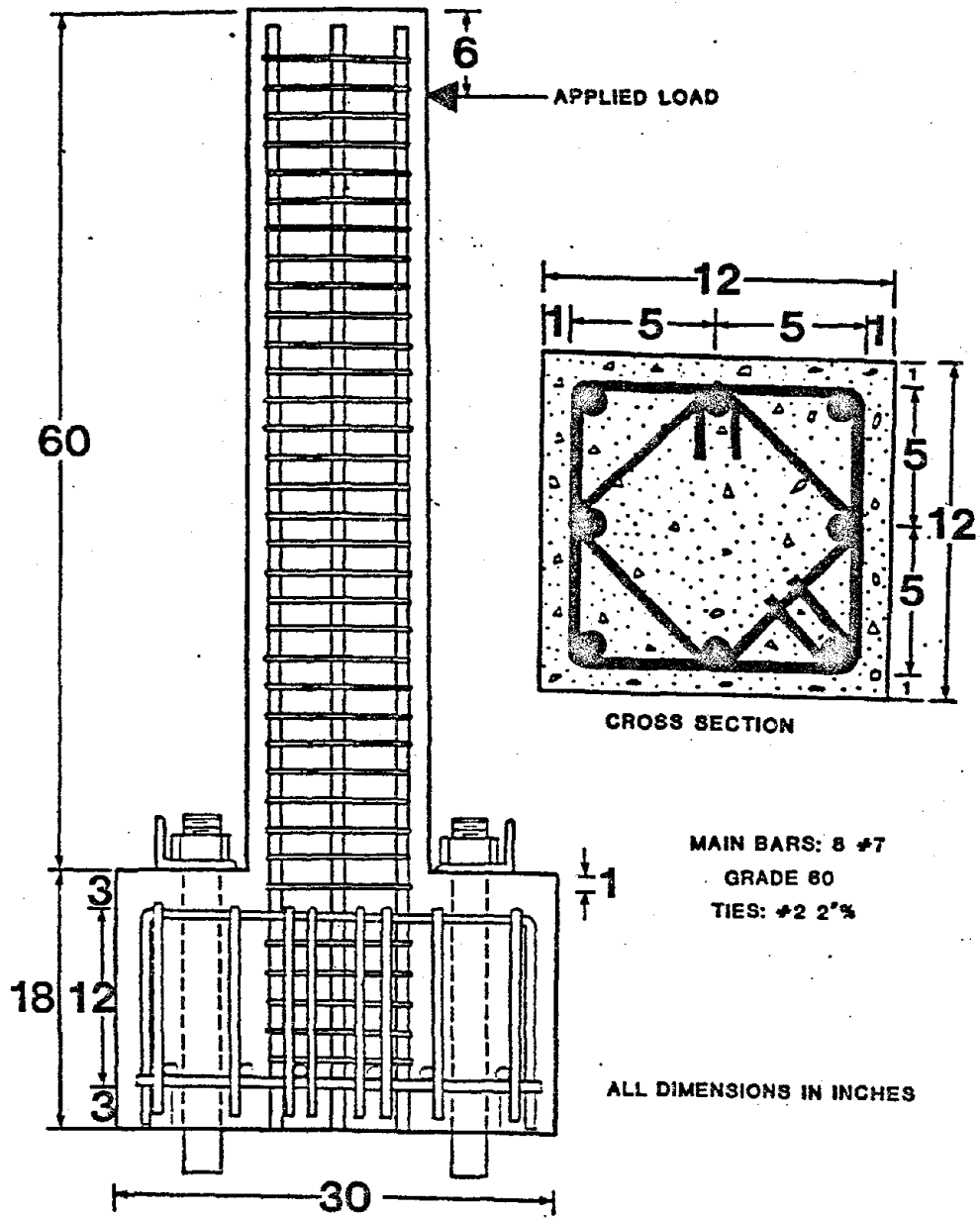


Fig. 4.1. Configuration of Specimens SP-7 and SP-8.

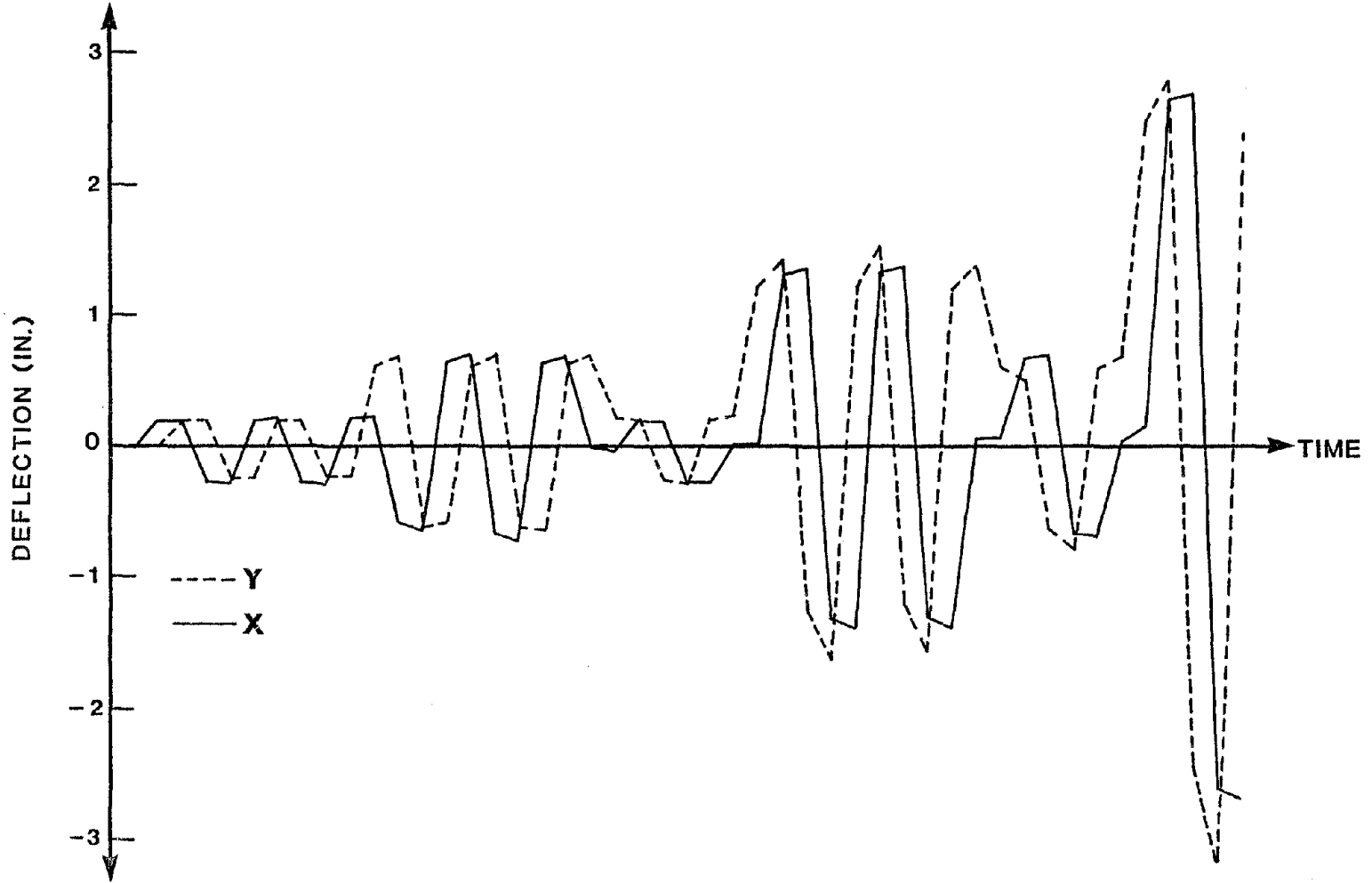


Fig. 4.2. Loading History for Otani's Specimen SP-7.

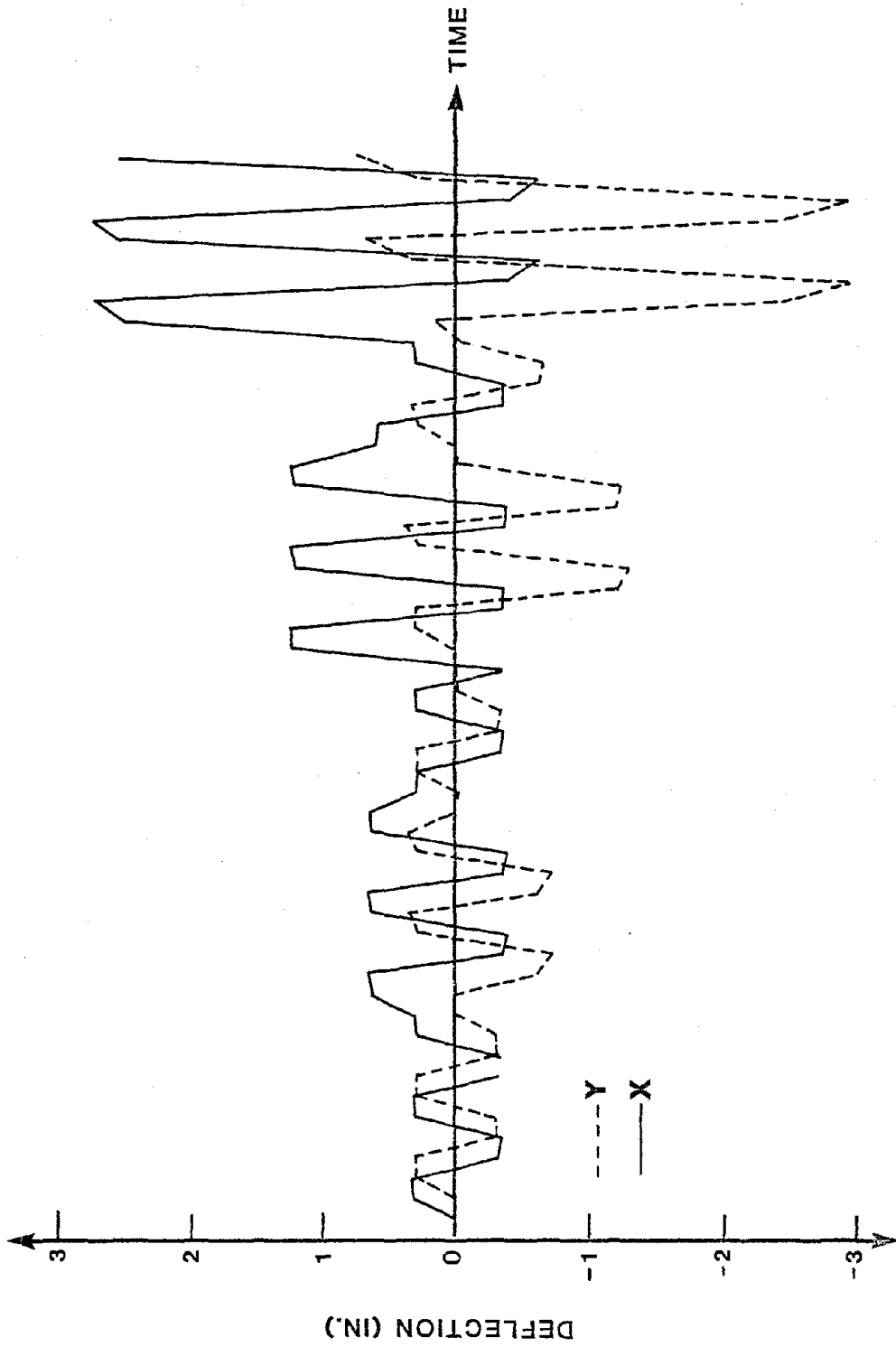


Fig. 4.3. Loading History for Otani's Specimen SP-8.

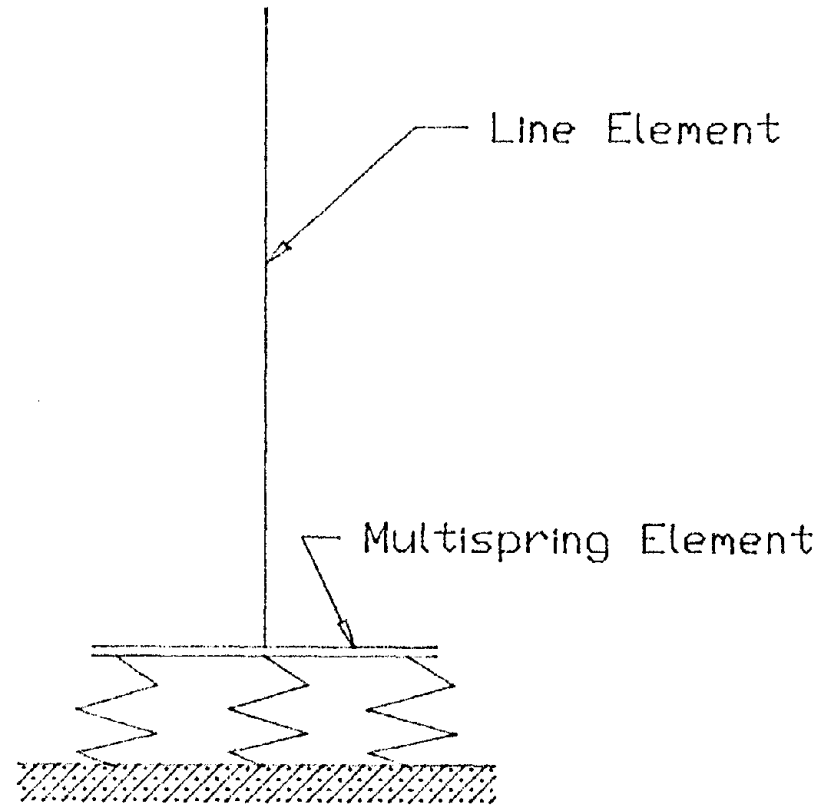


Fig. 4.4. Elevation of the Idealized Cantilever Column Model.

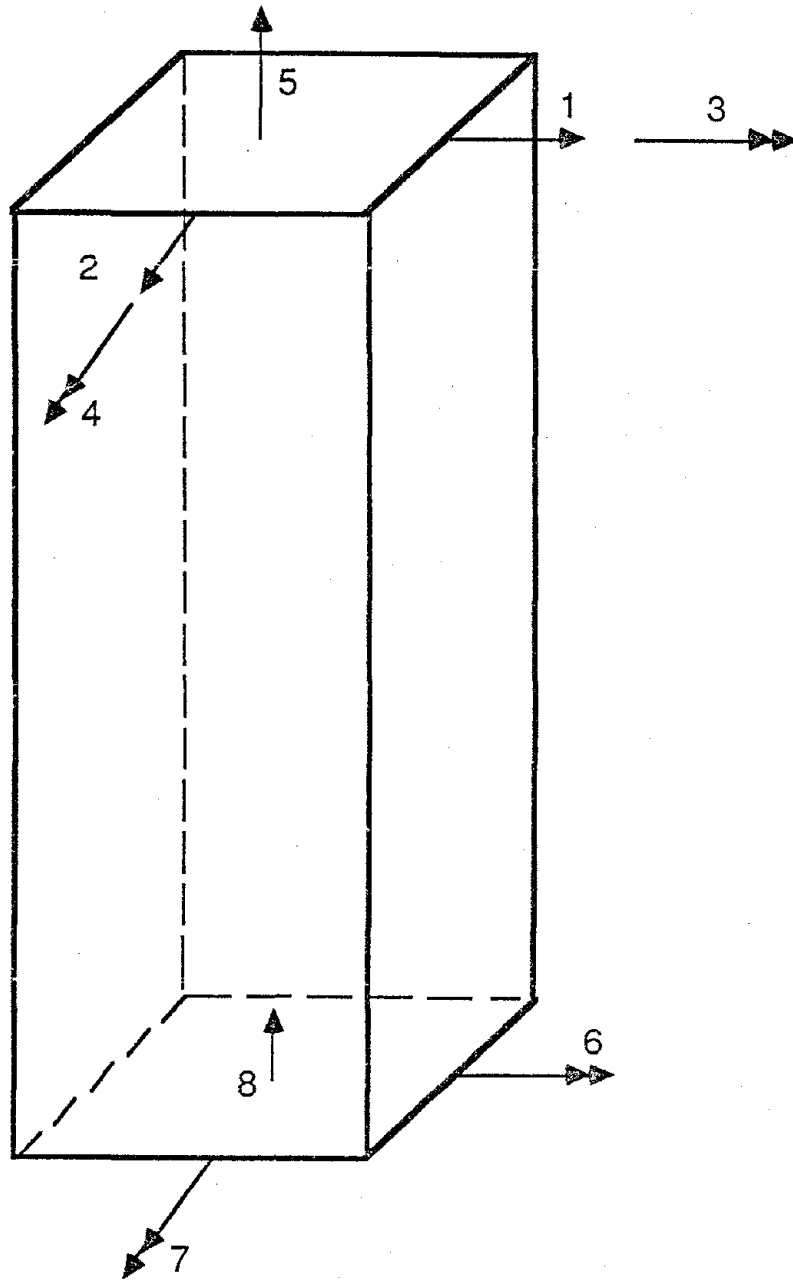


Fig. 4.5. Degrees of Freedom in the Cantilever Model.

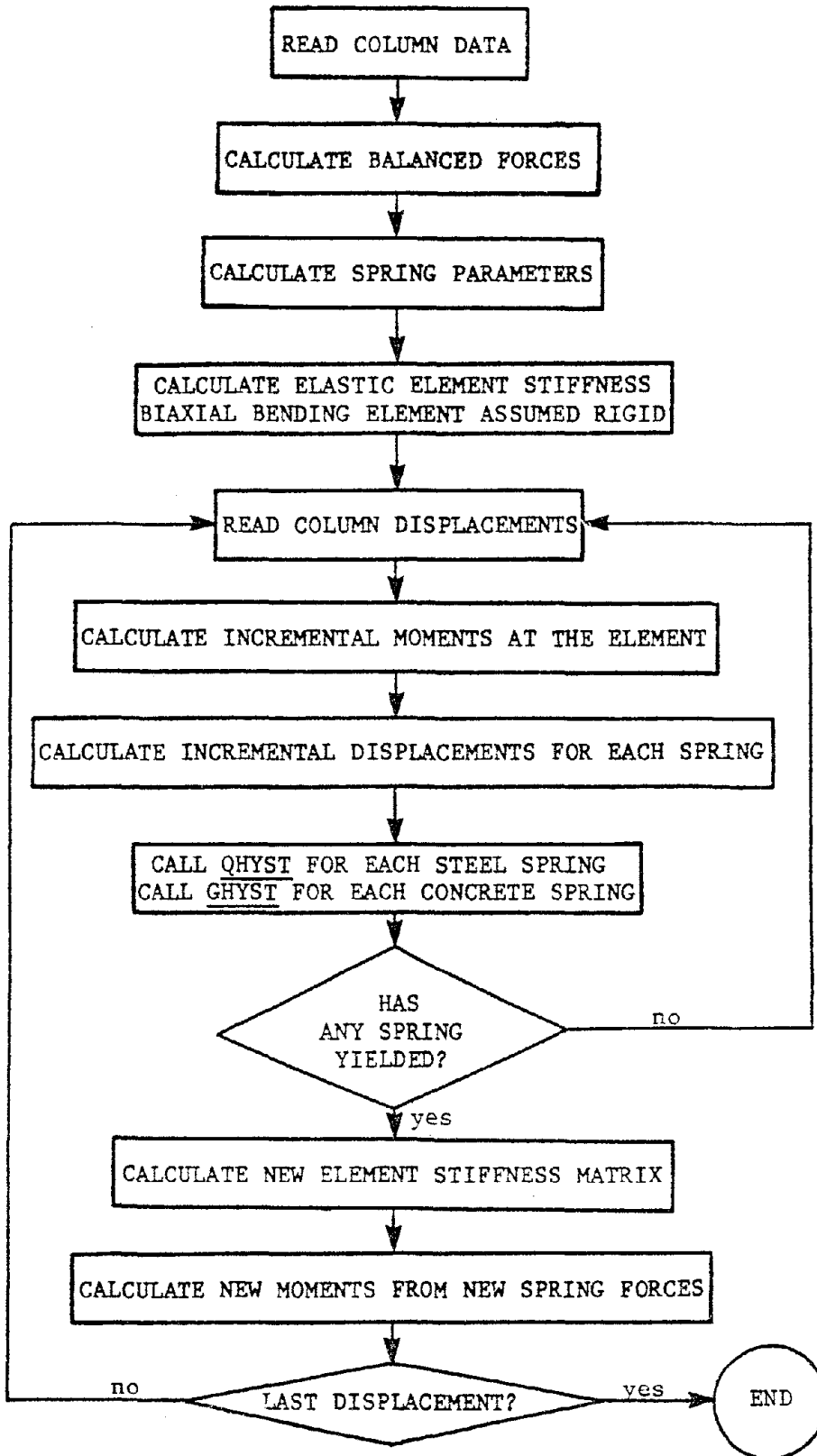


Fig. 4.6. Flowchart for Program APPDIS.

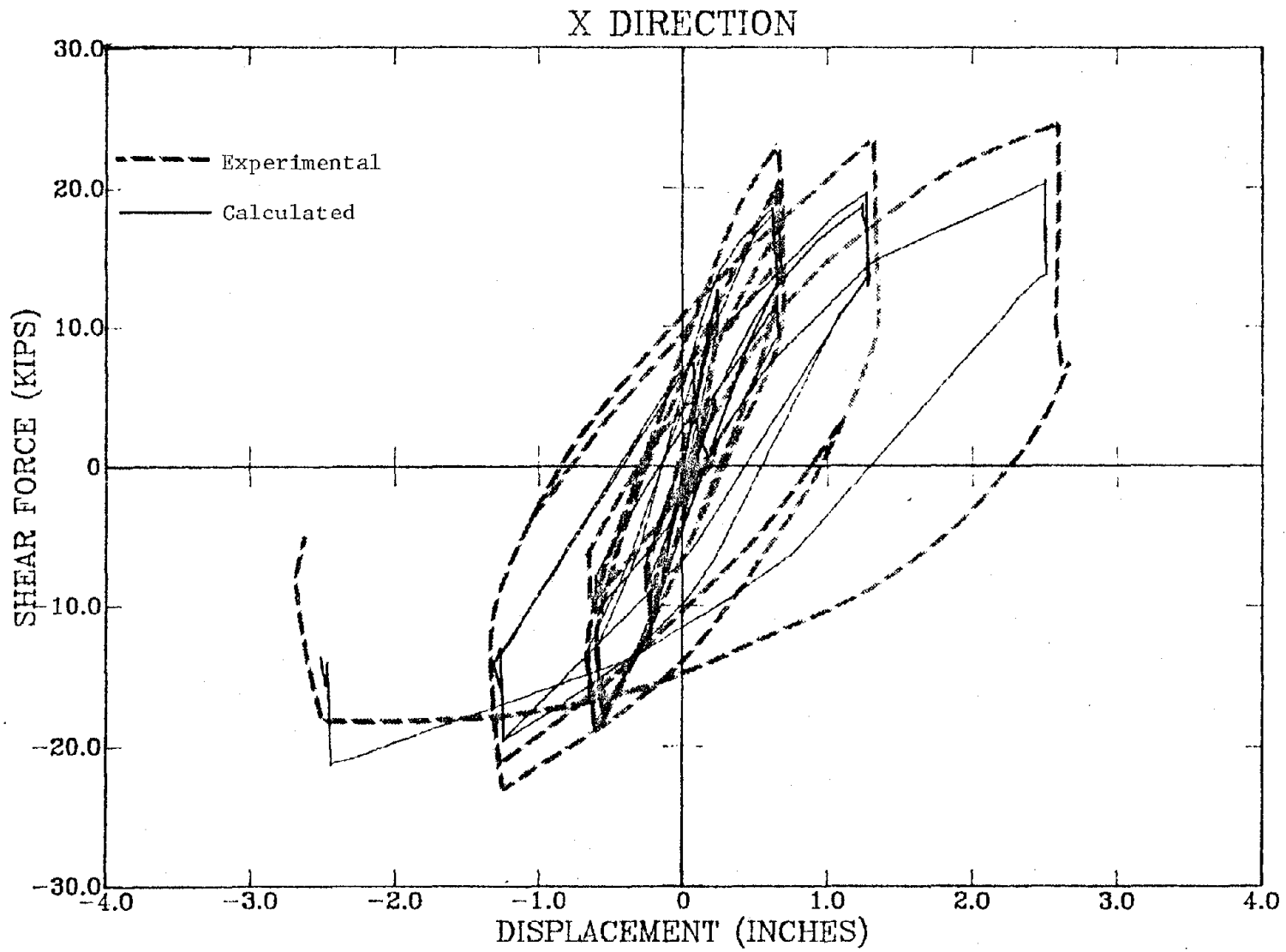


Fig. 4.7. Force-Deflection Curve for SP-7. BTO = 0.5.

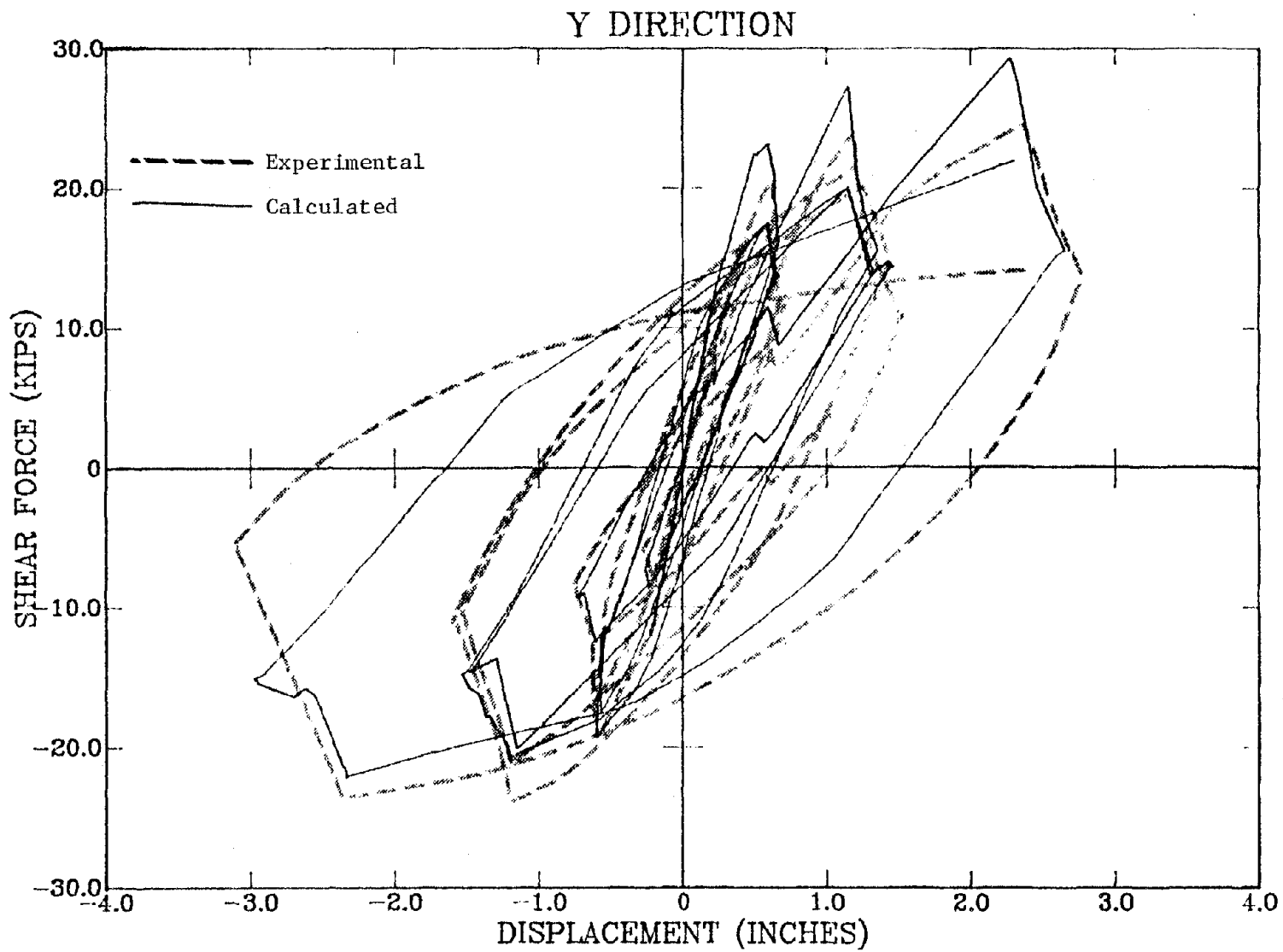


Fig. 4.8. Force-Deflection Curve for SP-7. BTO = 0.5.

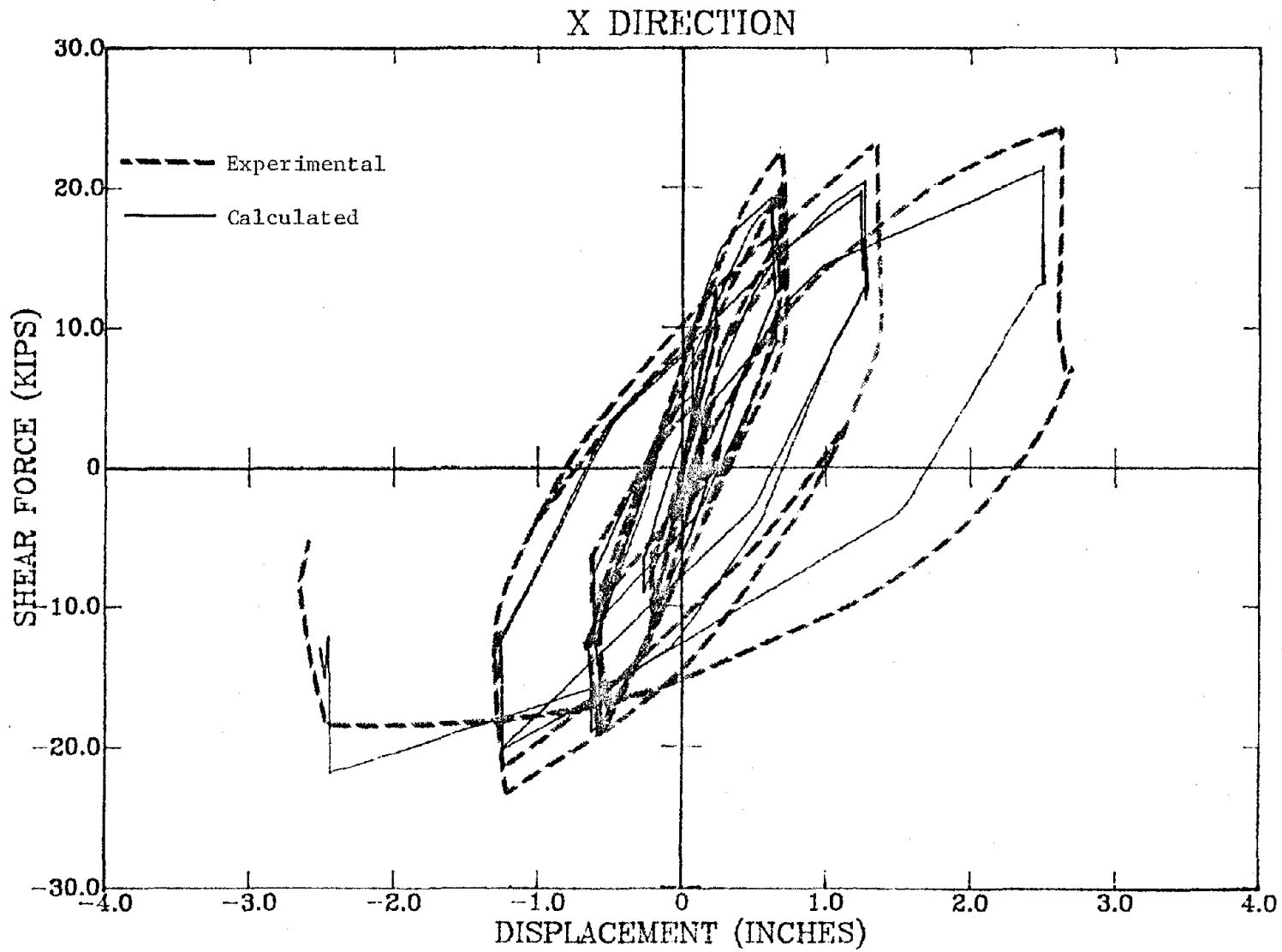


Fig. 4.9. Force-Deflection Curve for SP-7. BTO = 0.2.

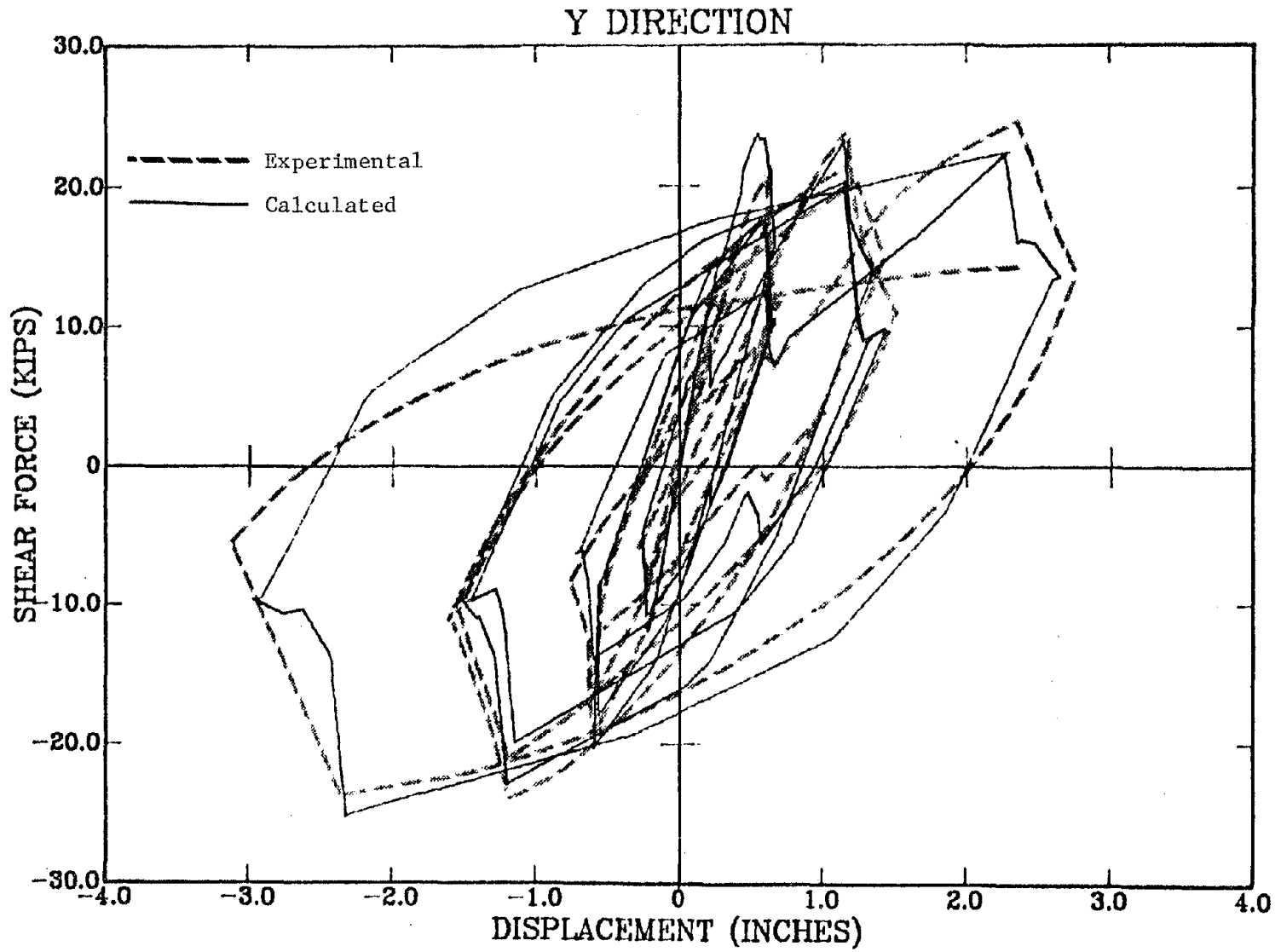


Fig. 4.10. Force-Deflection Curve for SP-7. BTO = 0.2.

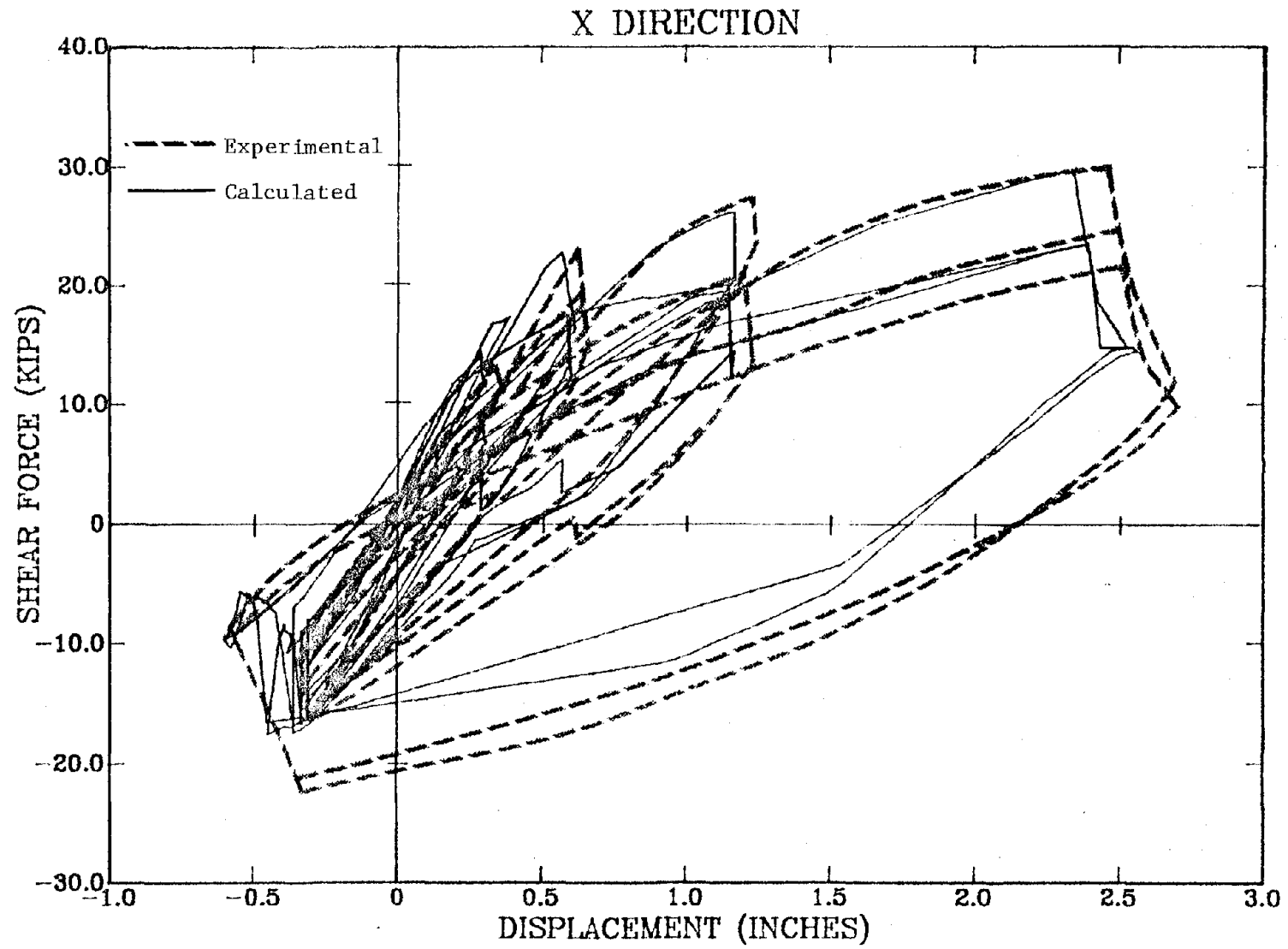


Fig. 4.11. Force-Deflection Curve for SP-8. BTO = 0.2.

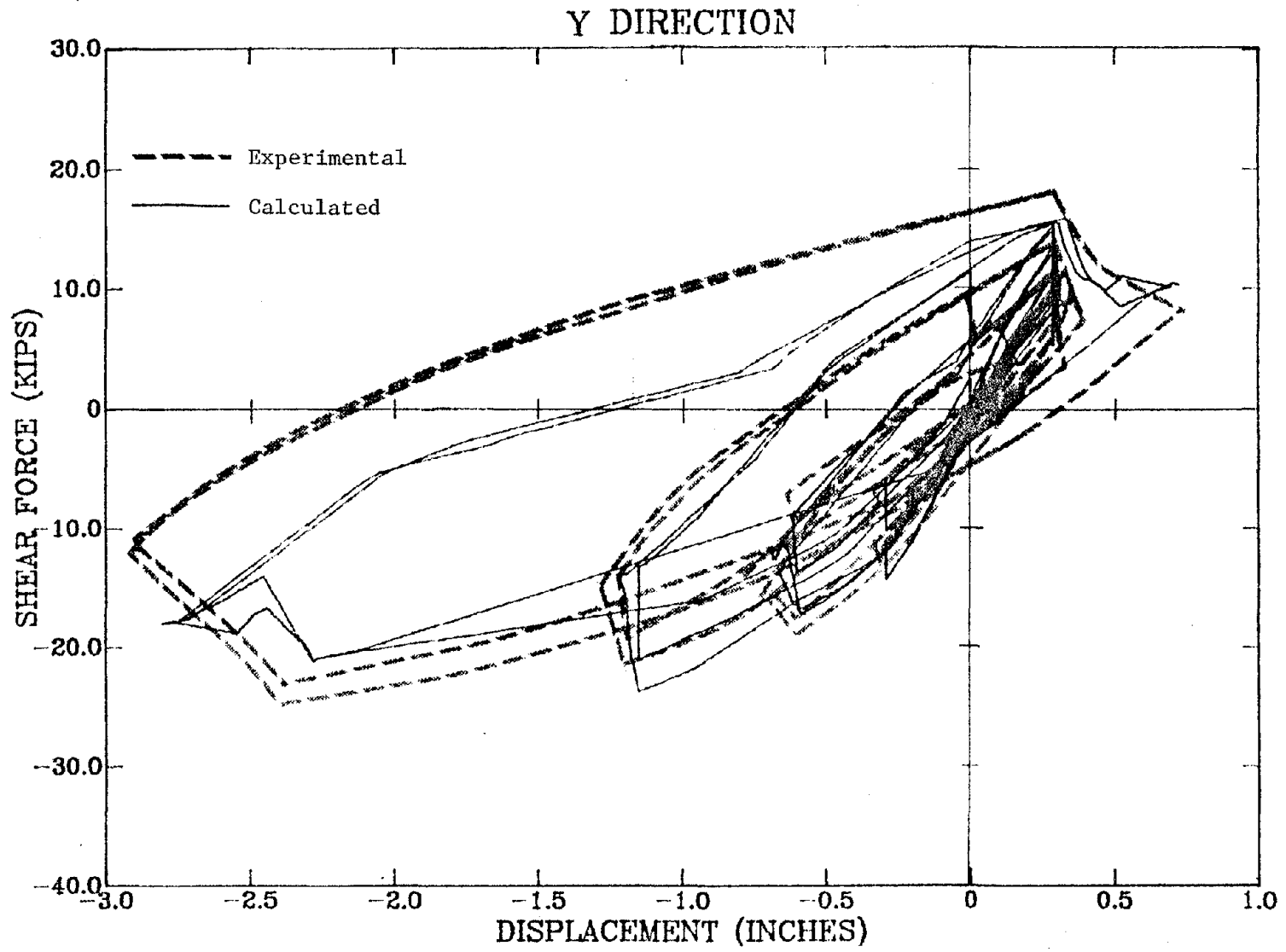


Fig. 4.12. Force-Deflection Curve for SP-8. BTO = 0.2.

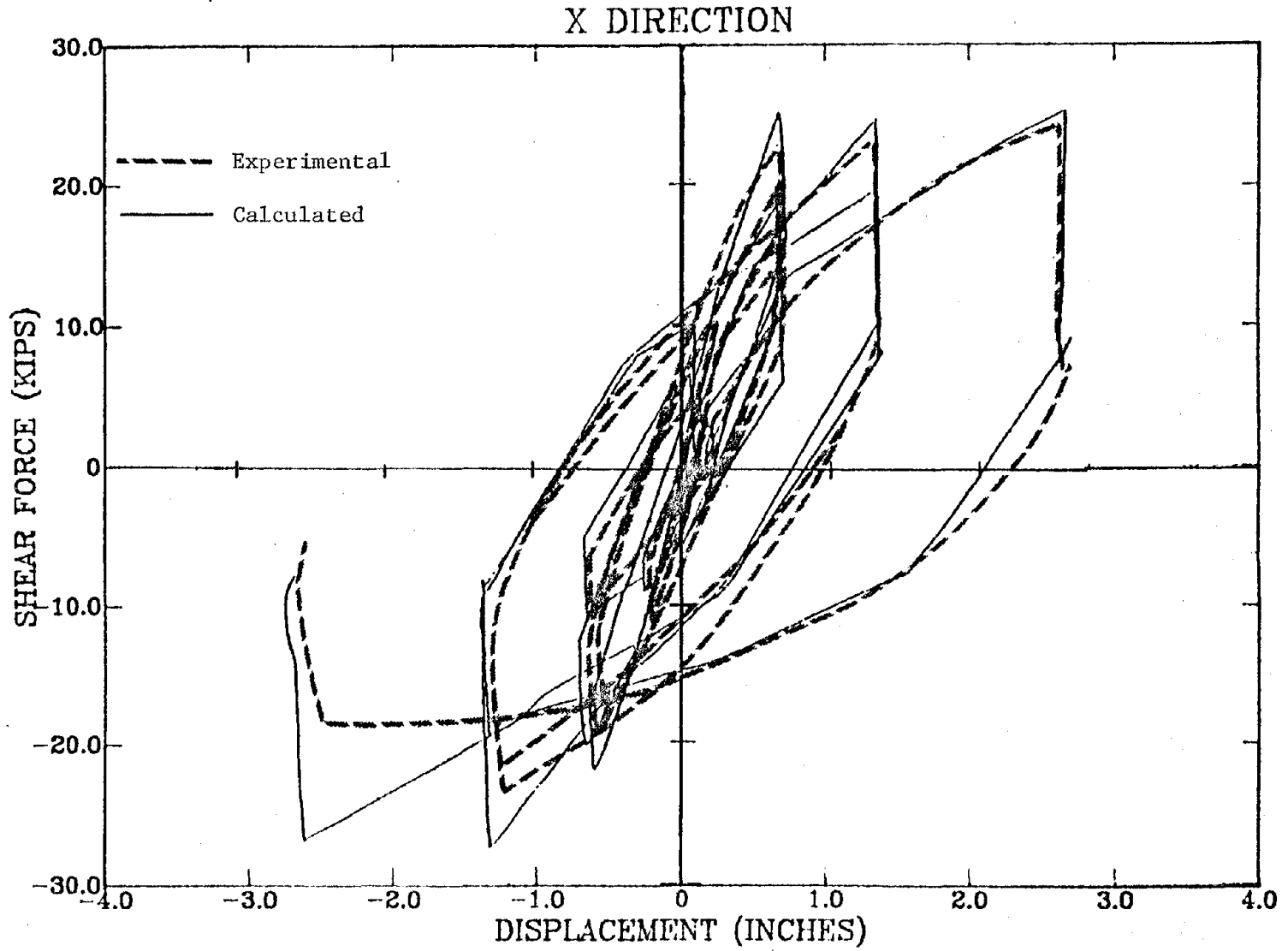


Fig. 4.13. Force-Deflection Curve for SP-7.

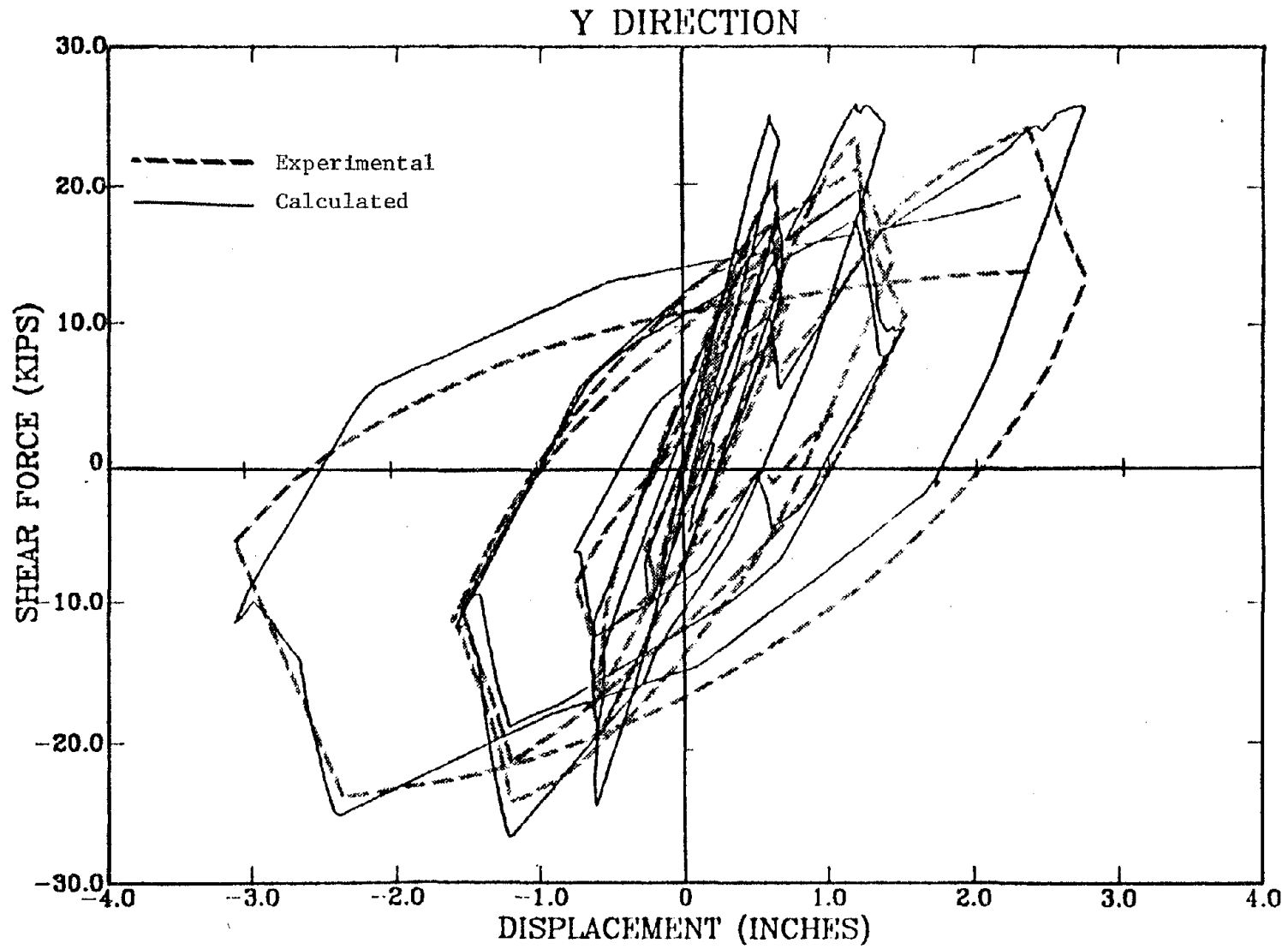


Fig. 4.14. Force-Deflection Curve for SP-7.

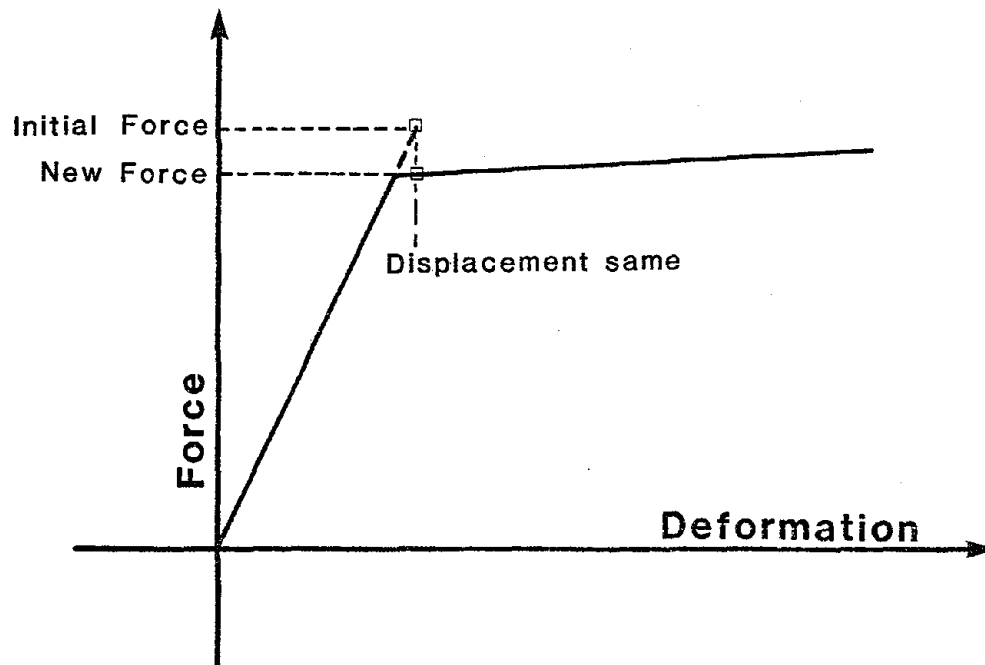


Fig. 4.15. Illustration of Spring Force "Overshoot".

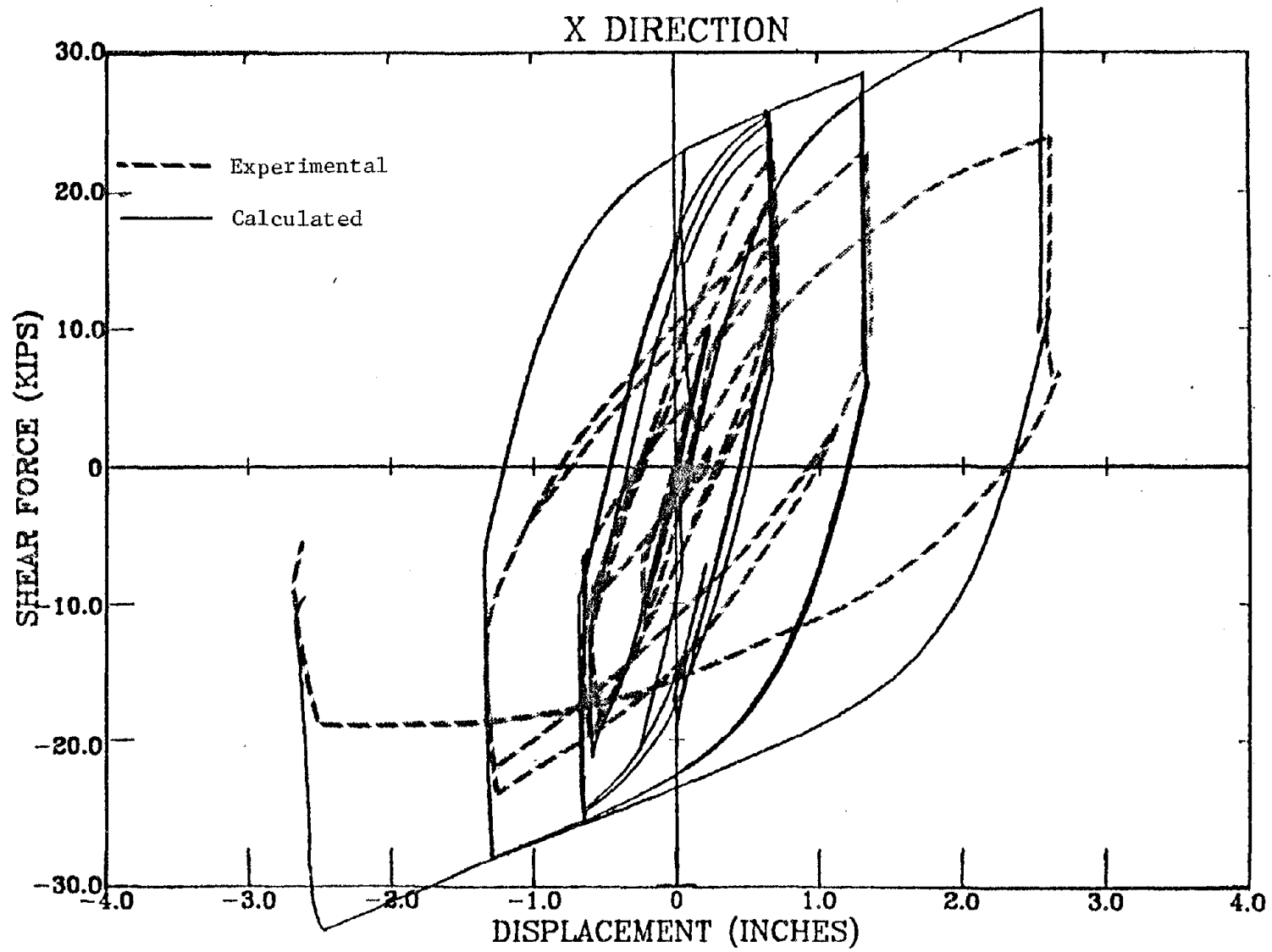


Fig. 4.16. Force-Deflection Curve for SP-7 Using the Bilinear Yield Surface Model.

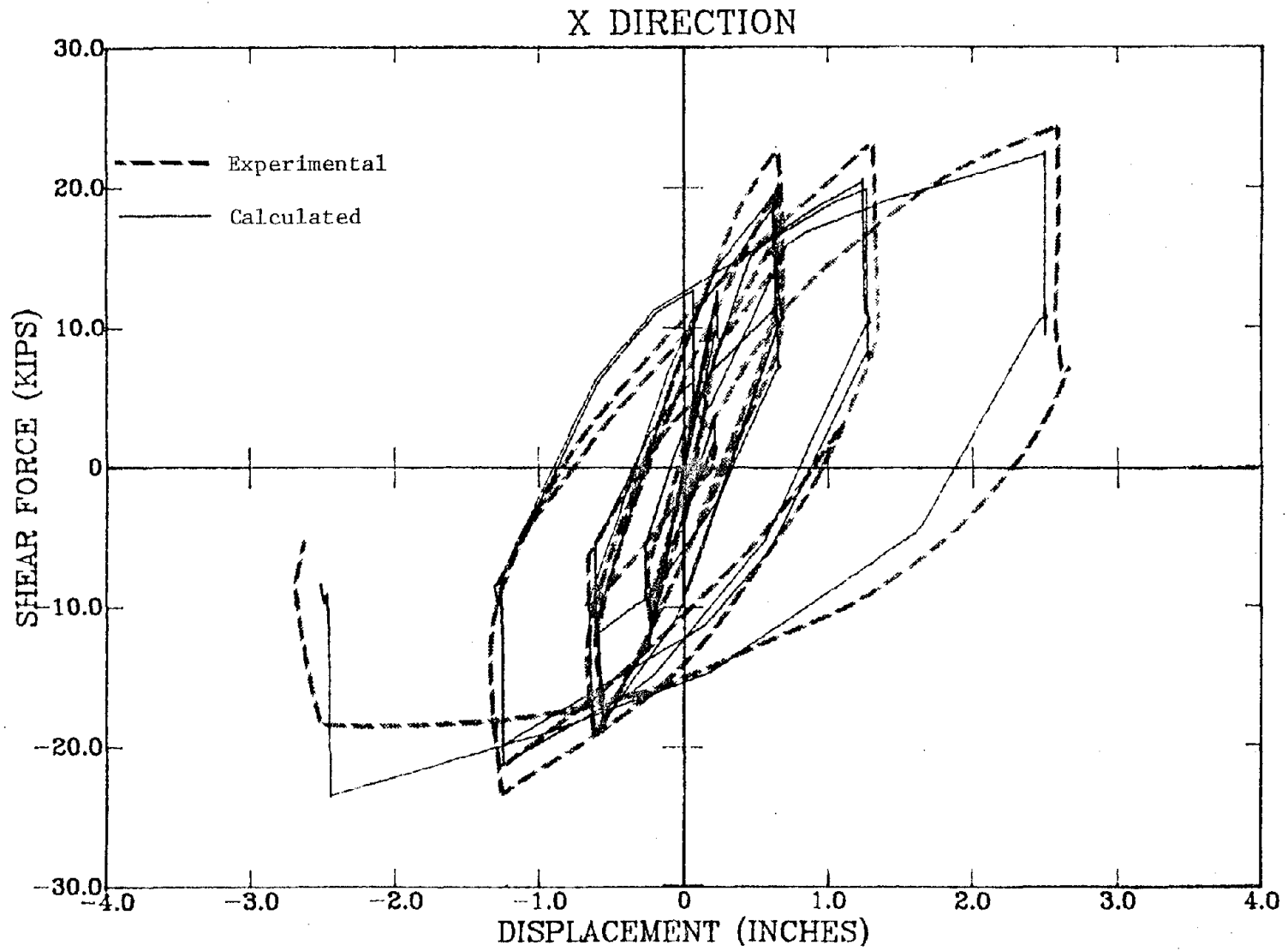


Fig. 4.17. Force-Deflection Curve for SP-7 using 5-Spring Element. BTO = 0.2.

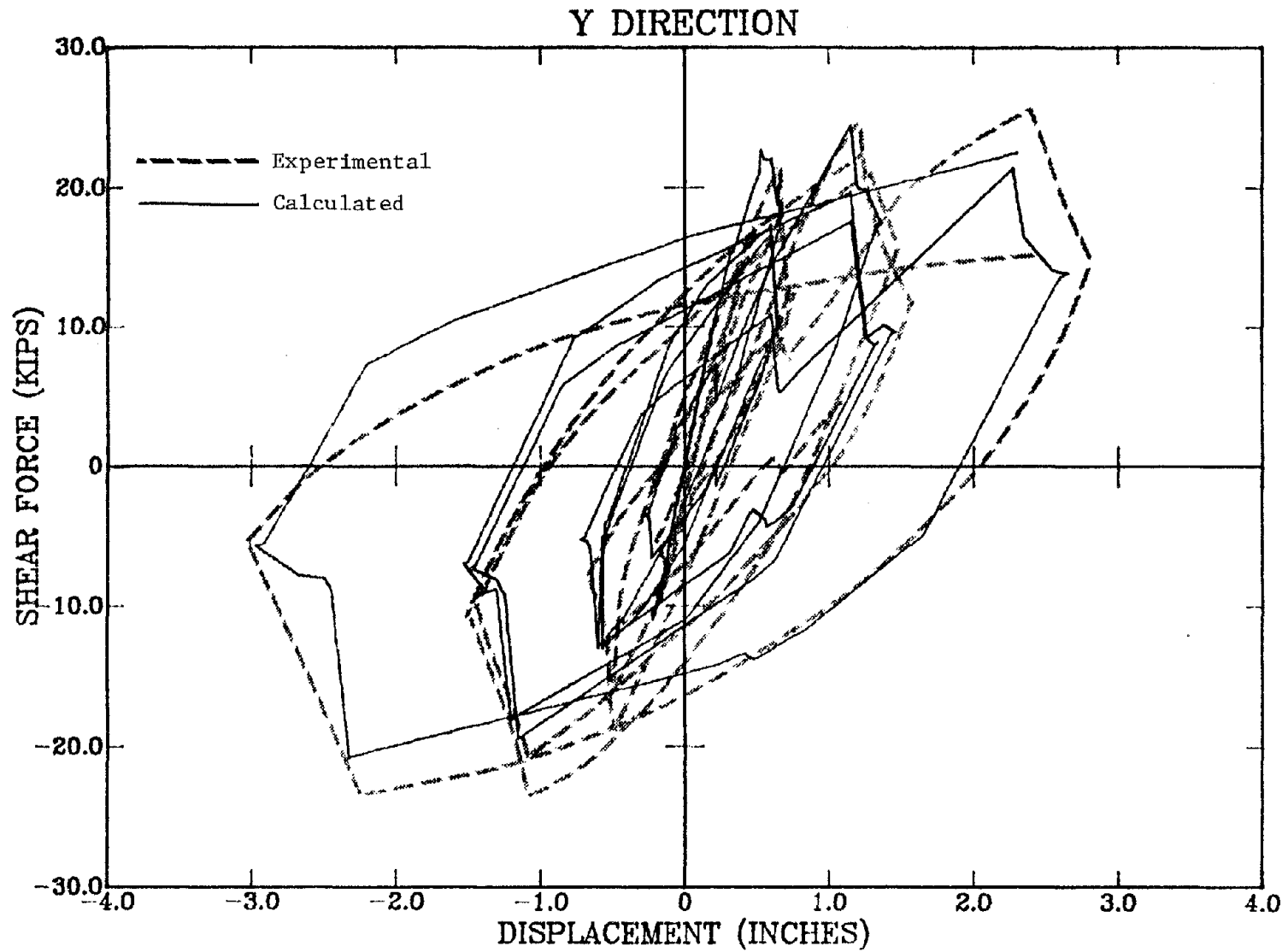


Fig. 4.18. Force-Deflection Curve for SP-7 Using 5-Spring Element. $B_{T0} = B_{T1} = 0.2$.

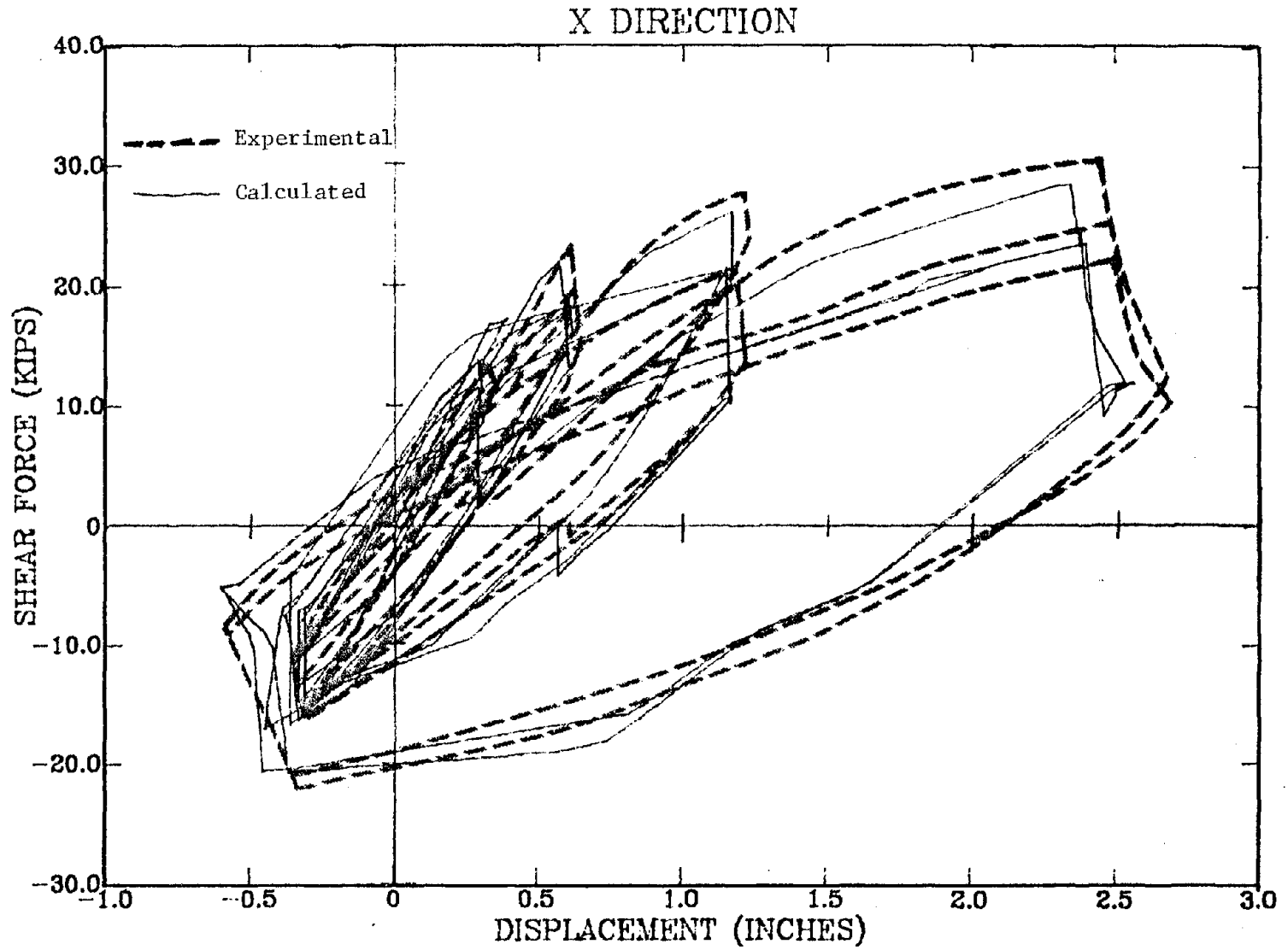


Fig. 4.19. Force-Deflection Curve for SP-8 Using 5-Spring Element. BTO = BT1 = 0.2.

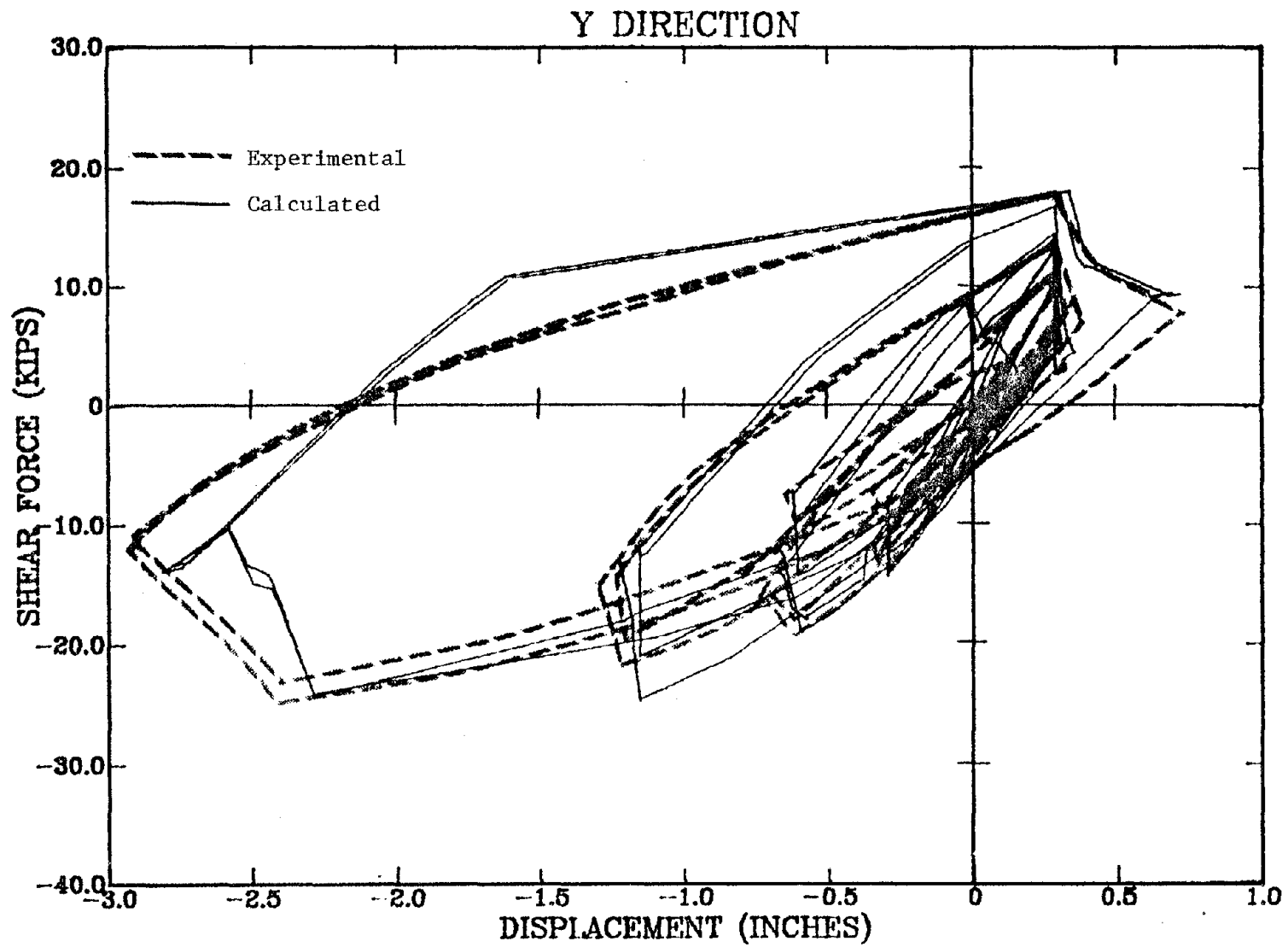


Fig. 4.20. Force-Deflection Curve for SP-8 Using 5-Spring Element. $BTO = BT1 = 0.2$.

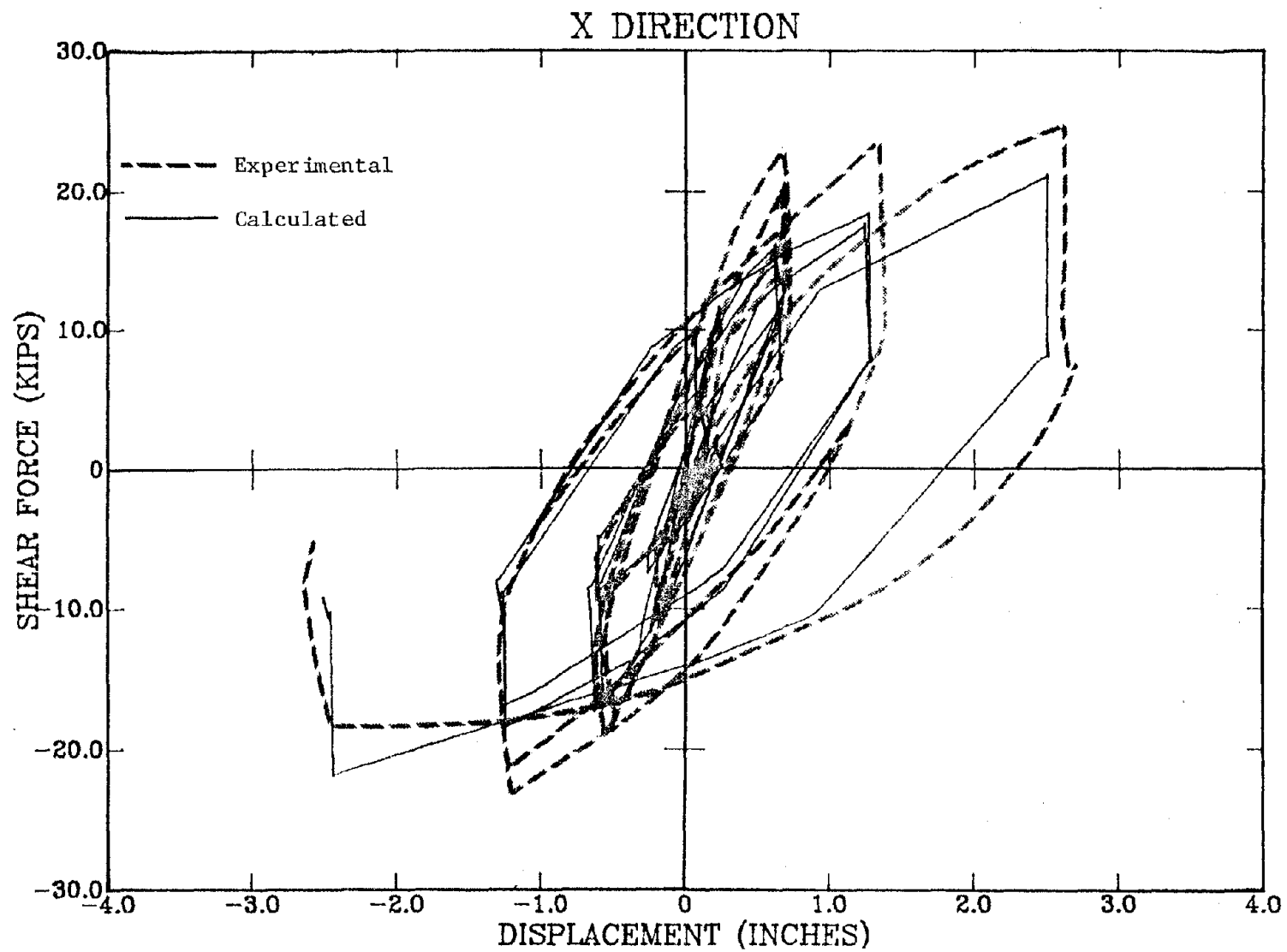


Fig. 4.21. Force-Deflection Curve for SP-7 Using 5-Spring Element. $BT0 = BT1 = 0.4$.

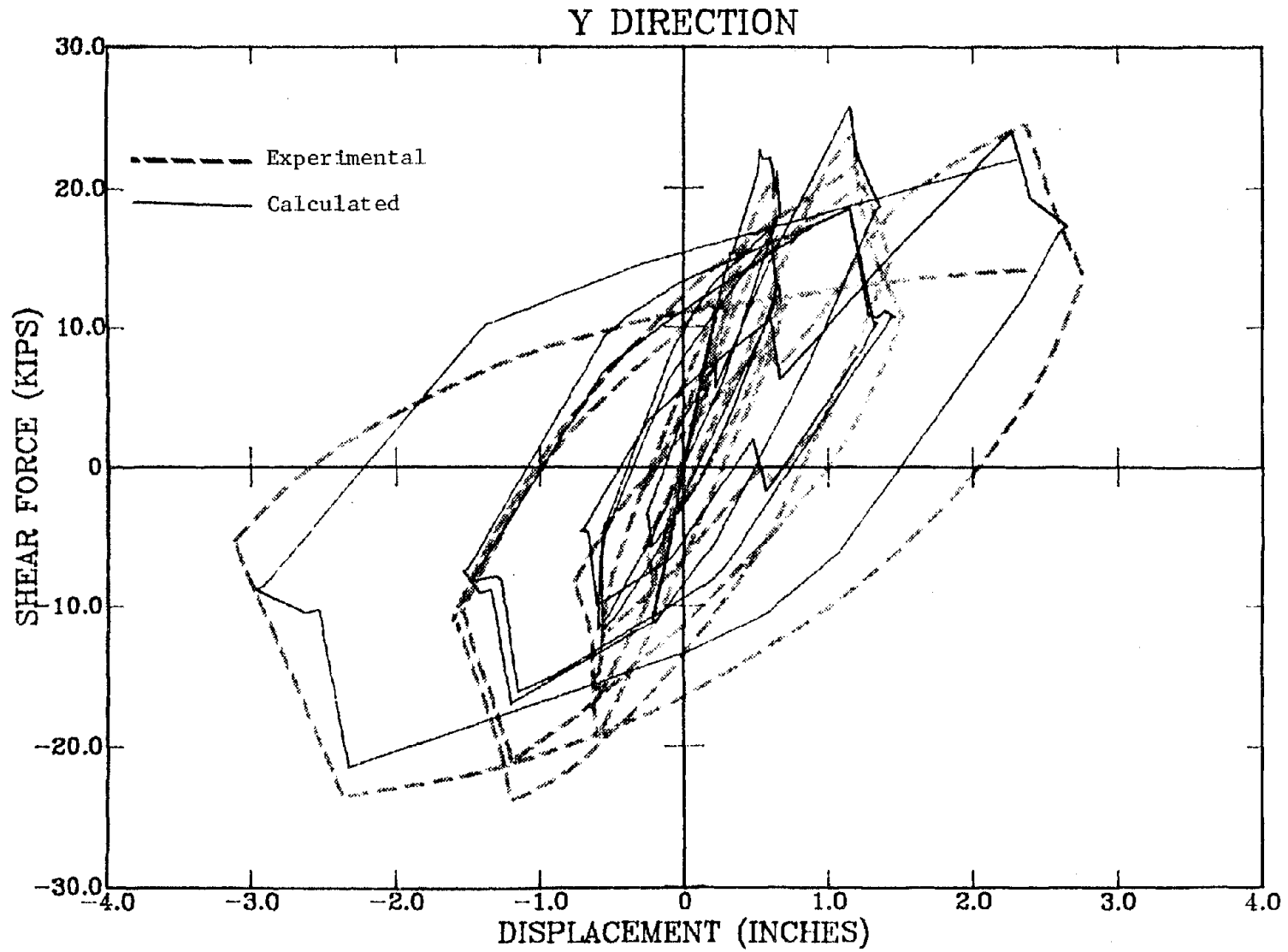


Fig. 4.22. Force-Deflection Curve for SP-7 Using 5-Spring Element. $BT_0 = BT_1 = 0.4$.

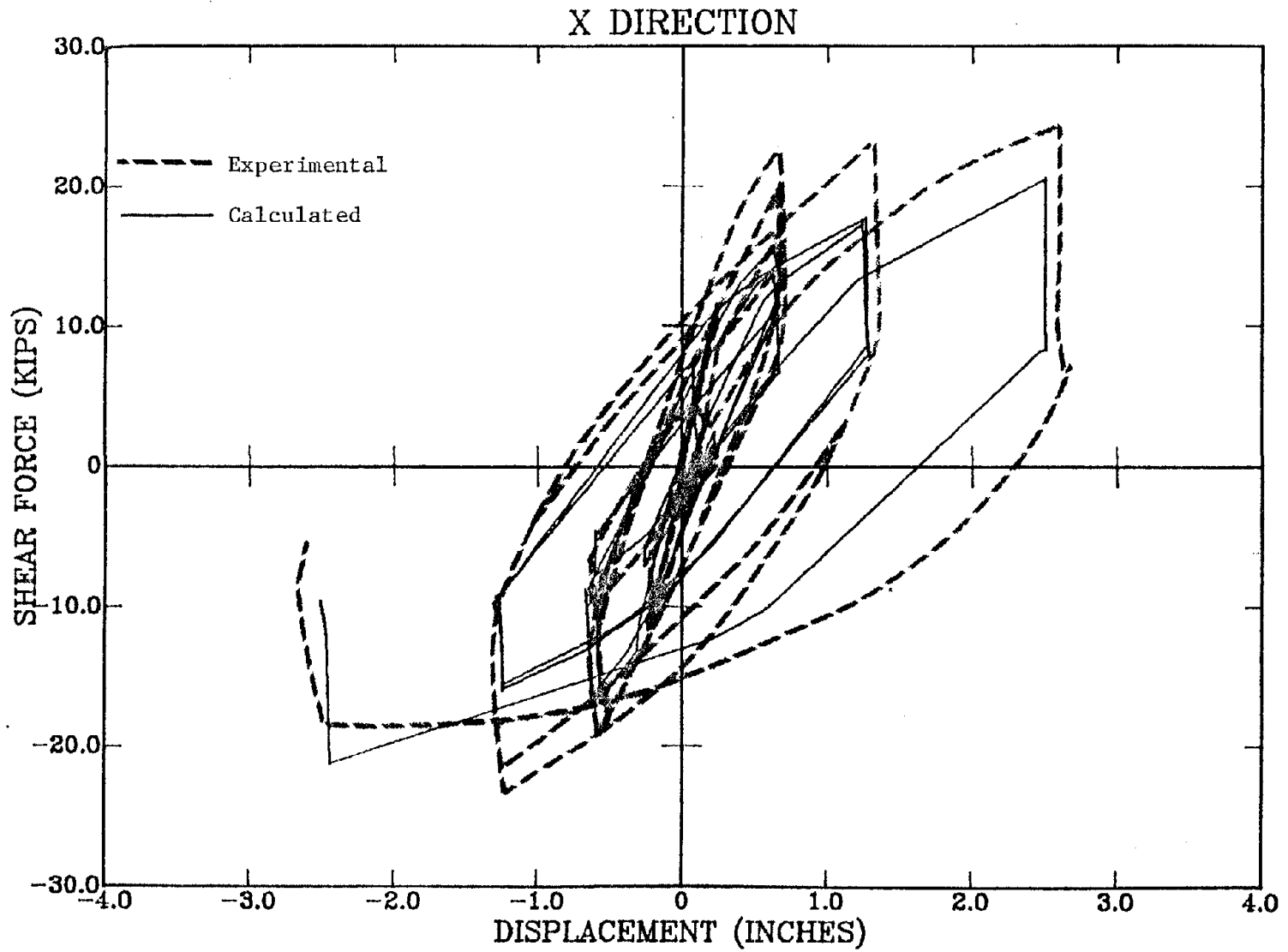


Fig. 4.23. Force-Deflection Curve for SP-7 Using 5-Spring Element. $BT_0 = 0.4$, $BT_1 = 0.7$.

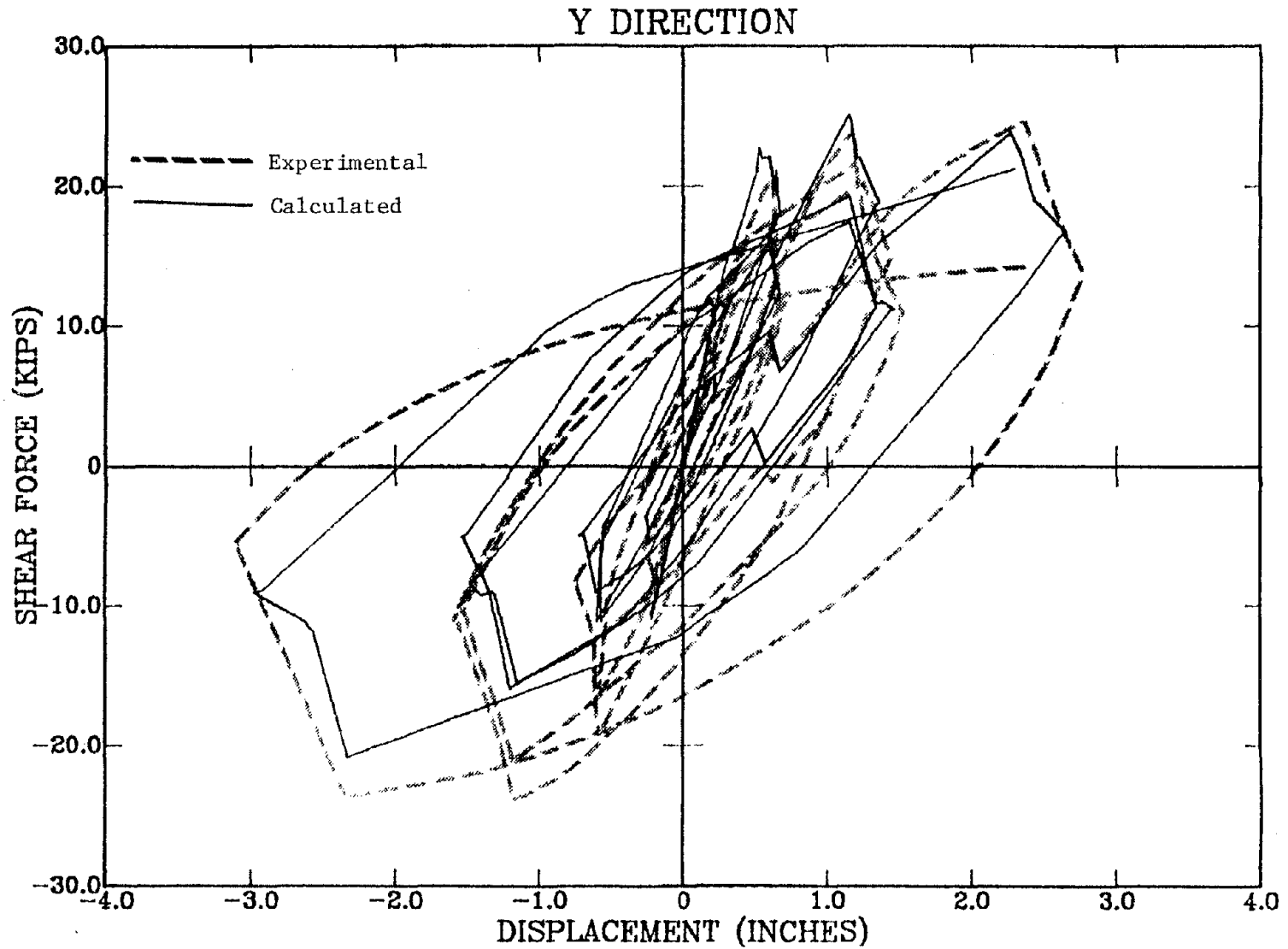


Fig. 4.24. Force-Deflection Curve for SP-7 Using 5-Spring Element. $BTO = 0.4$, $BT1 = 0.7$.

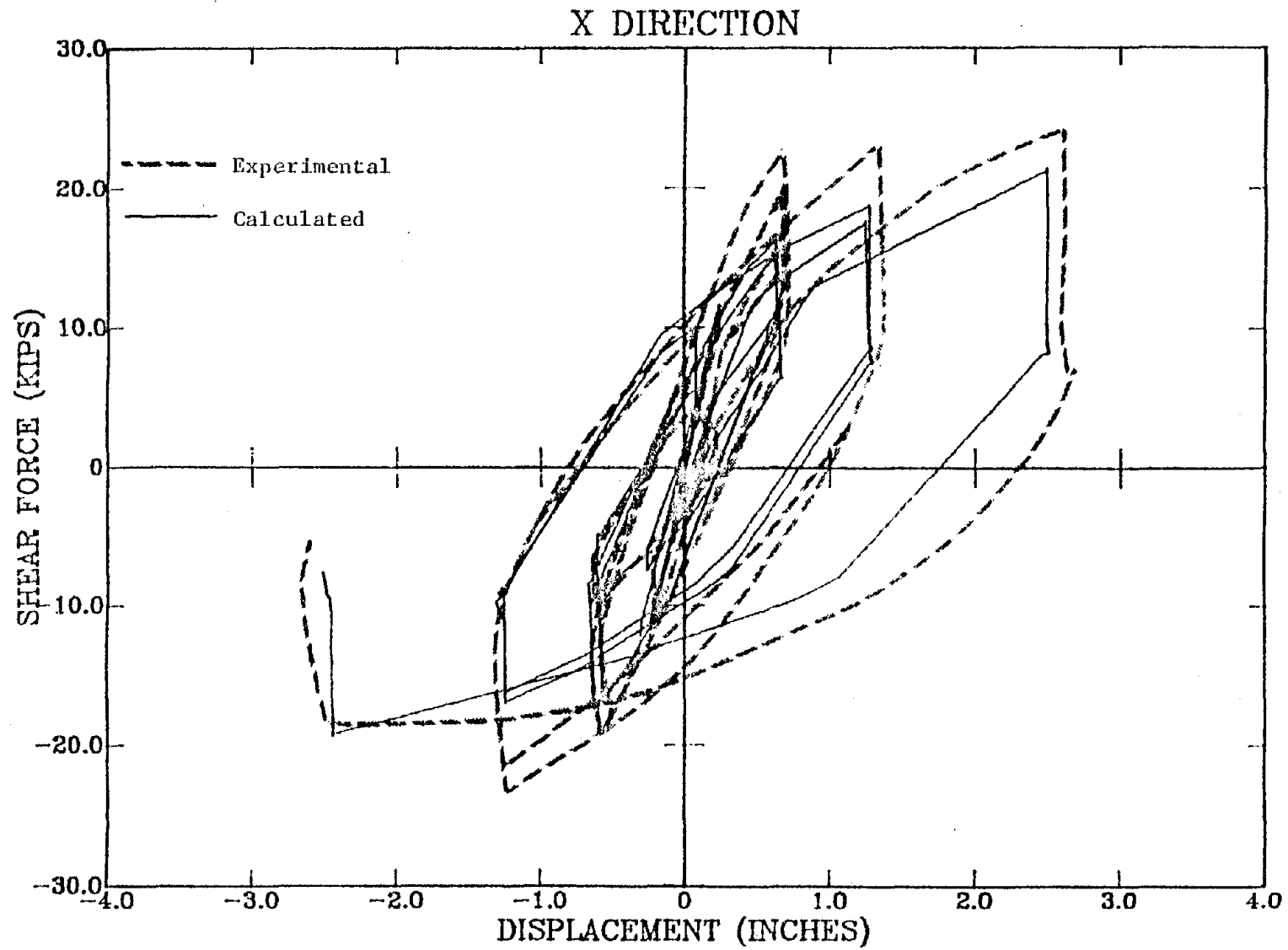


Fig. 4.25. Force-Deflection Curve for SP-7 Using 5-Spring Element. $BTO = 0.4$, $BTI = 0.3$.

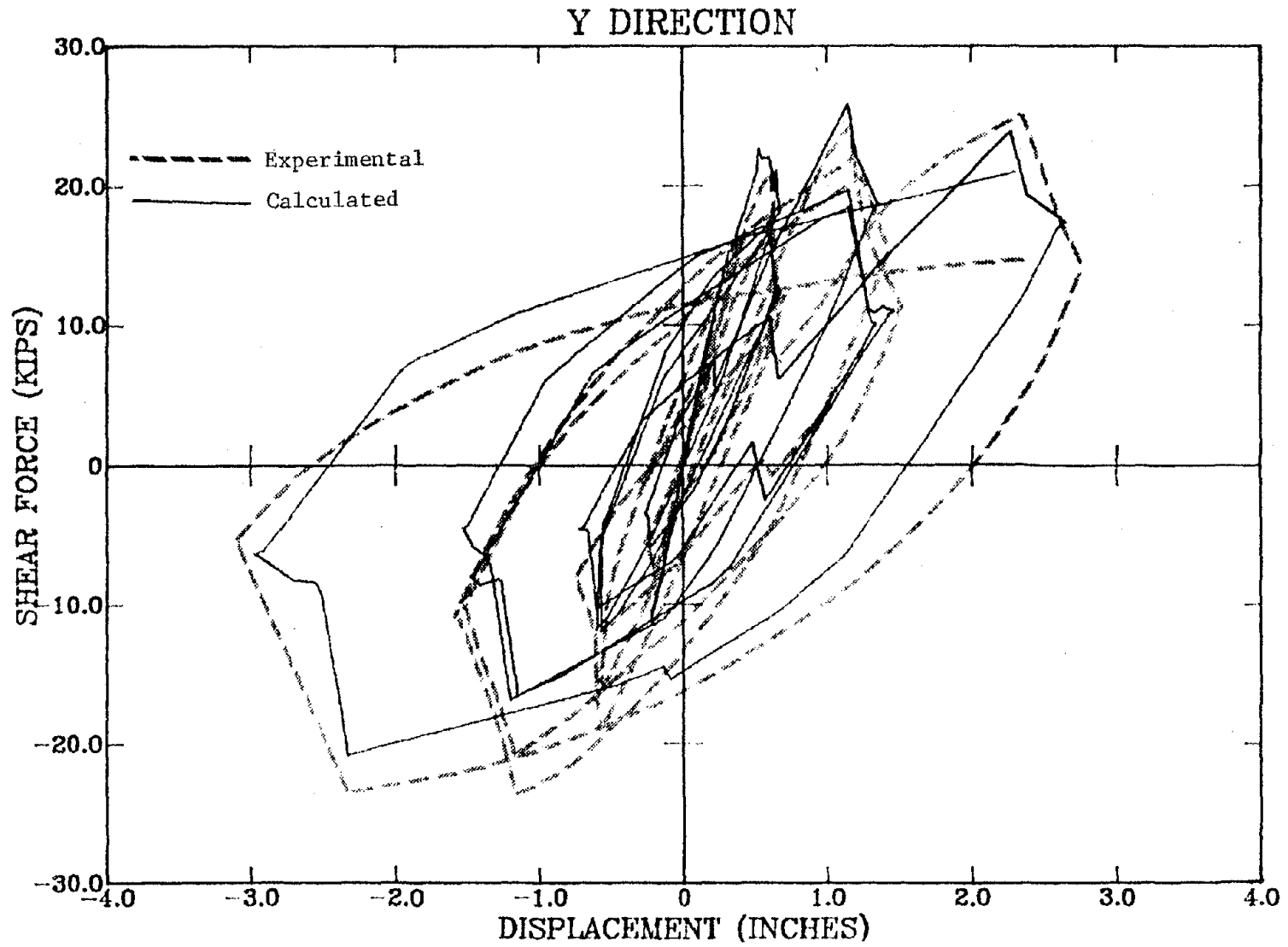


Fig. 4.26. Force-Deflection Curve for SP-7 Using 5-Spring Element. BTO = 0.4, BT1 = 0.3.

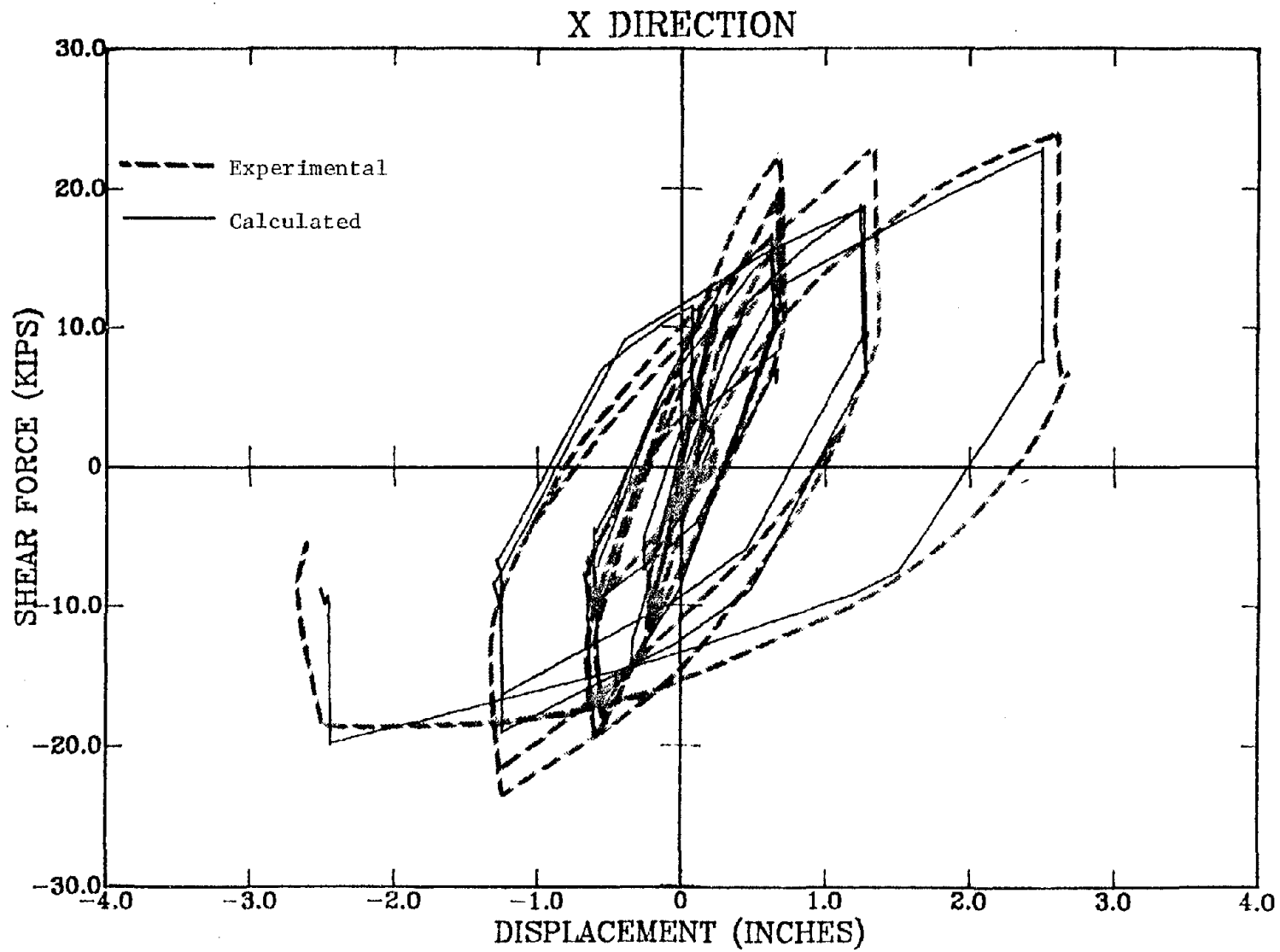


Fig. 4.27. Force-Deflection Curve for SP-7 Using 5-Spring Element. $K_y = 5\% K_{se}$.

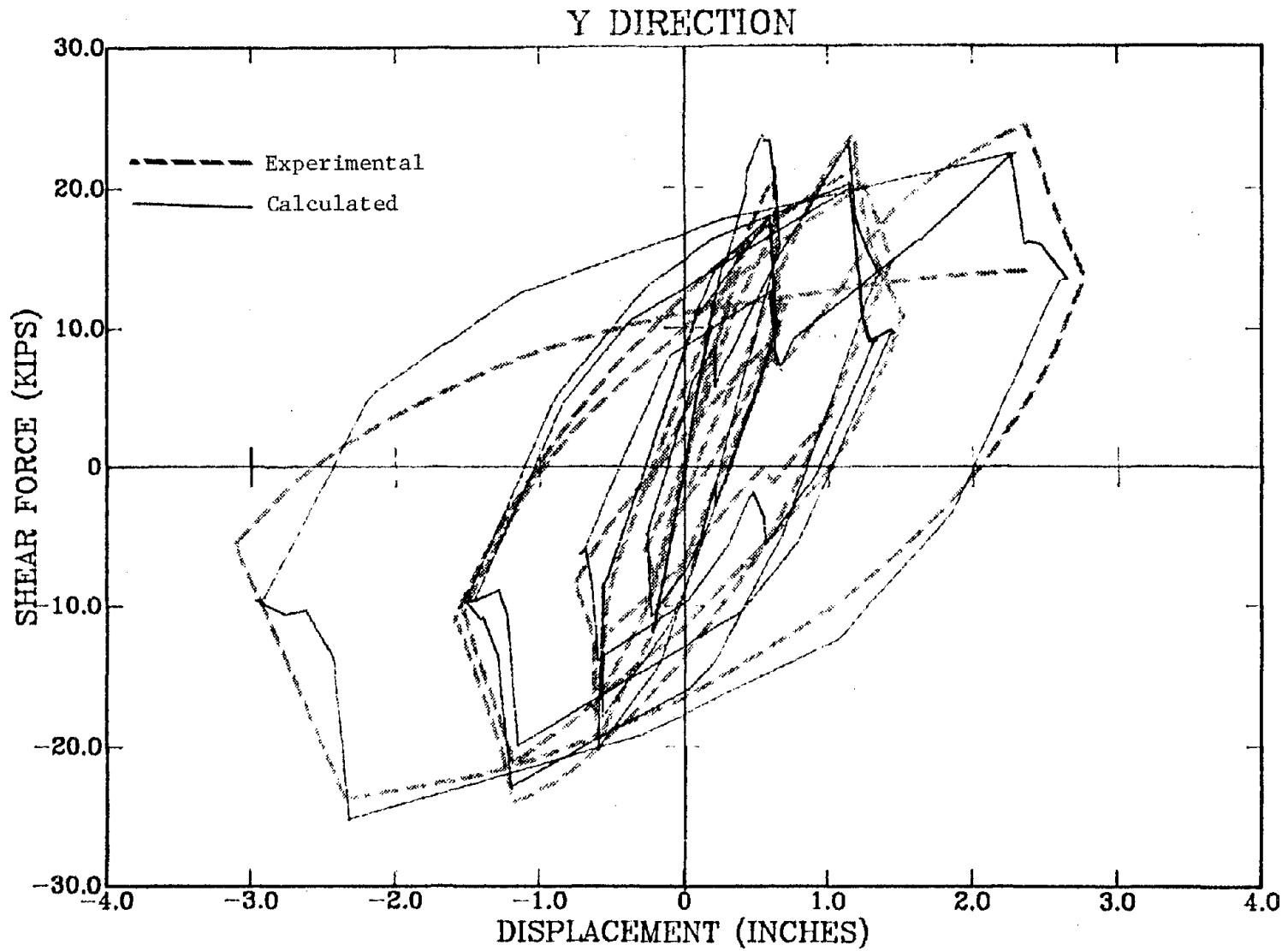


Fig. 4.28. Force-Deflection Curve for SP-7 Using 5-Spring Element. $K_y = 5\% K_{se}$.

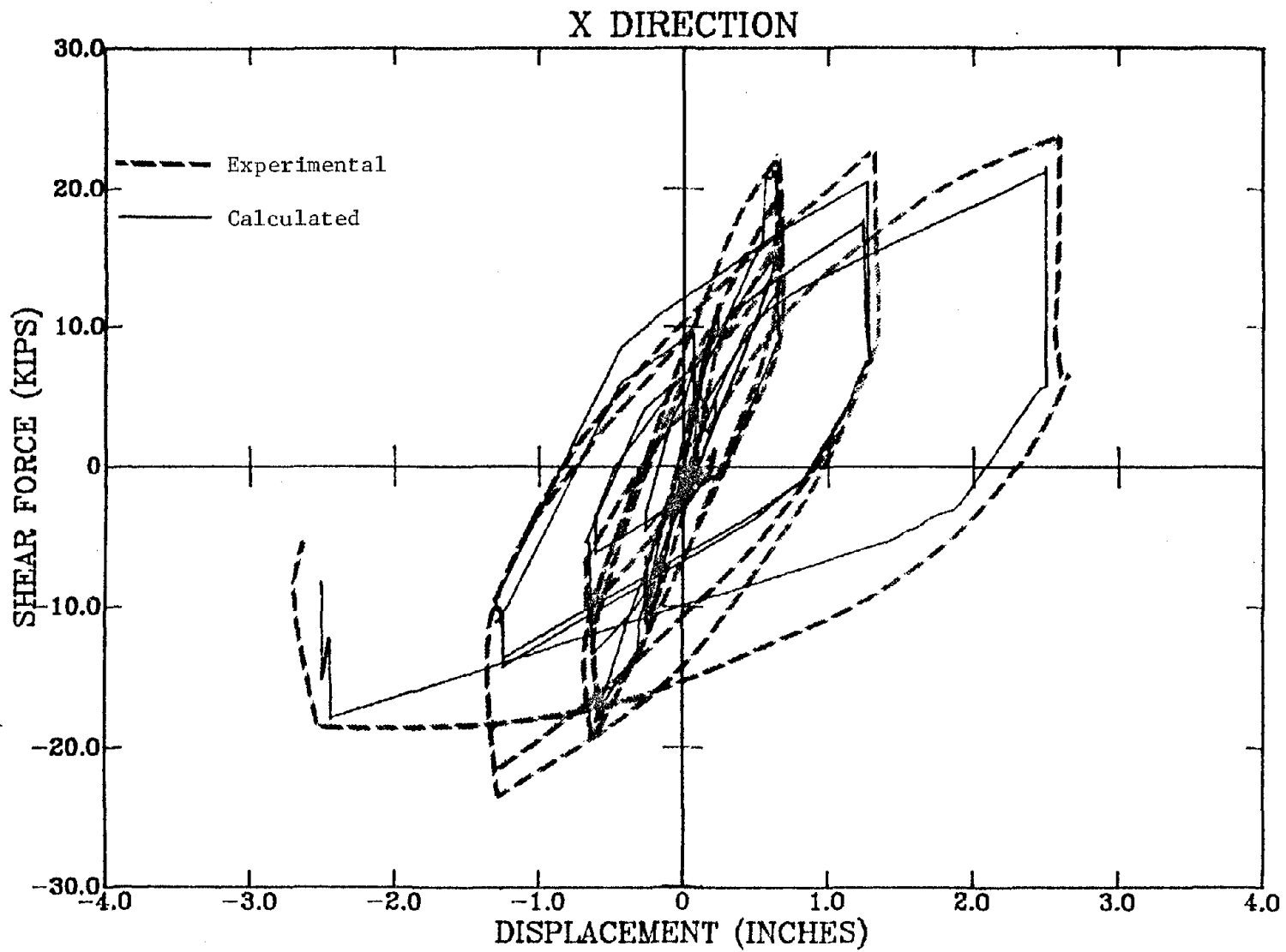


Fig. 4.29. Force-Deflection Curve for SP-7 Using 5-Spring Element. $K_y = 0.2\% K_{se}$.

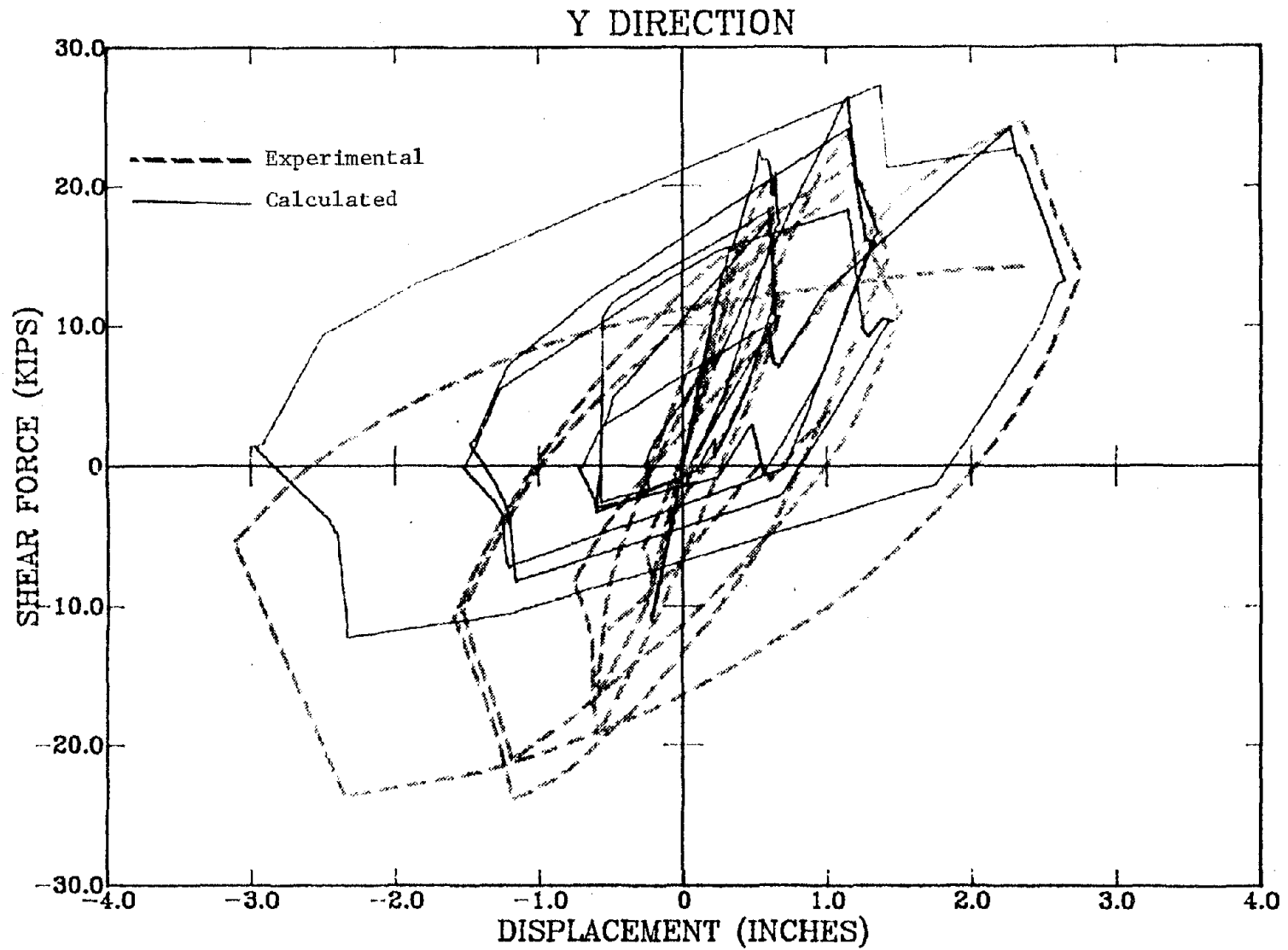


Fig. 4.30. Force-Deflection Curve for SP-7 Using 5-Spring Element. $K_y = 0.2\% K_{se}$.

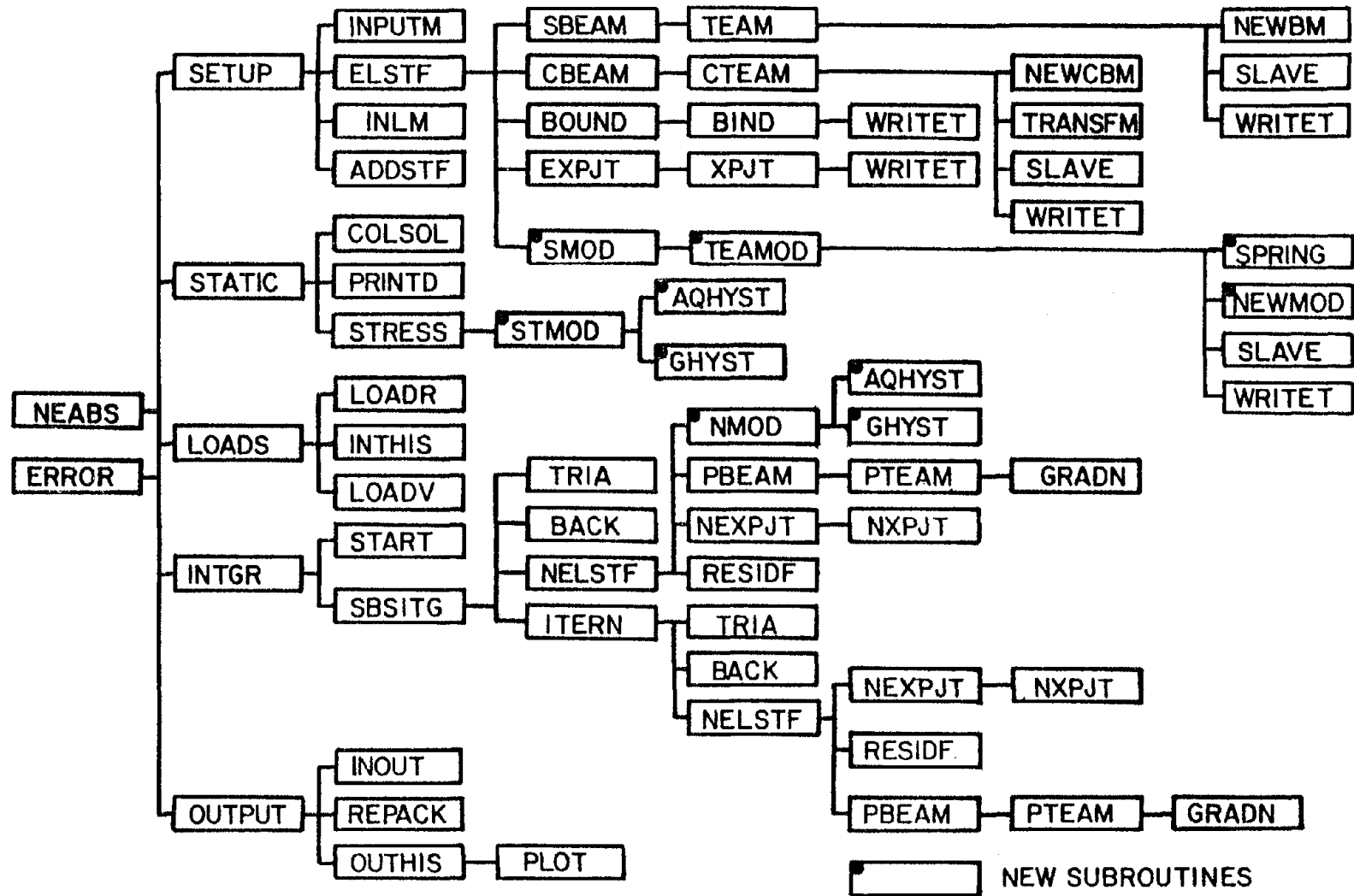


Fig. 5.1. Subroutine Organization of NEABS and NEABS-86.

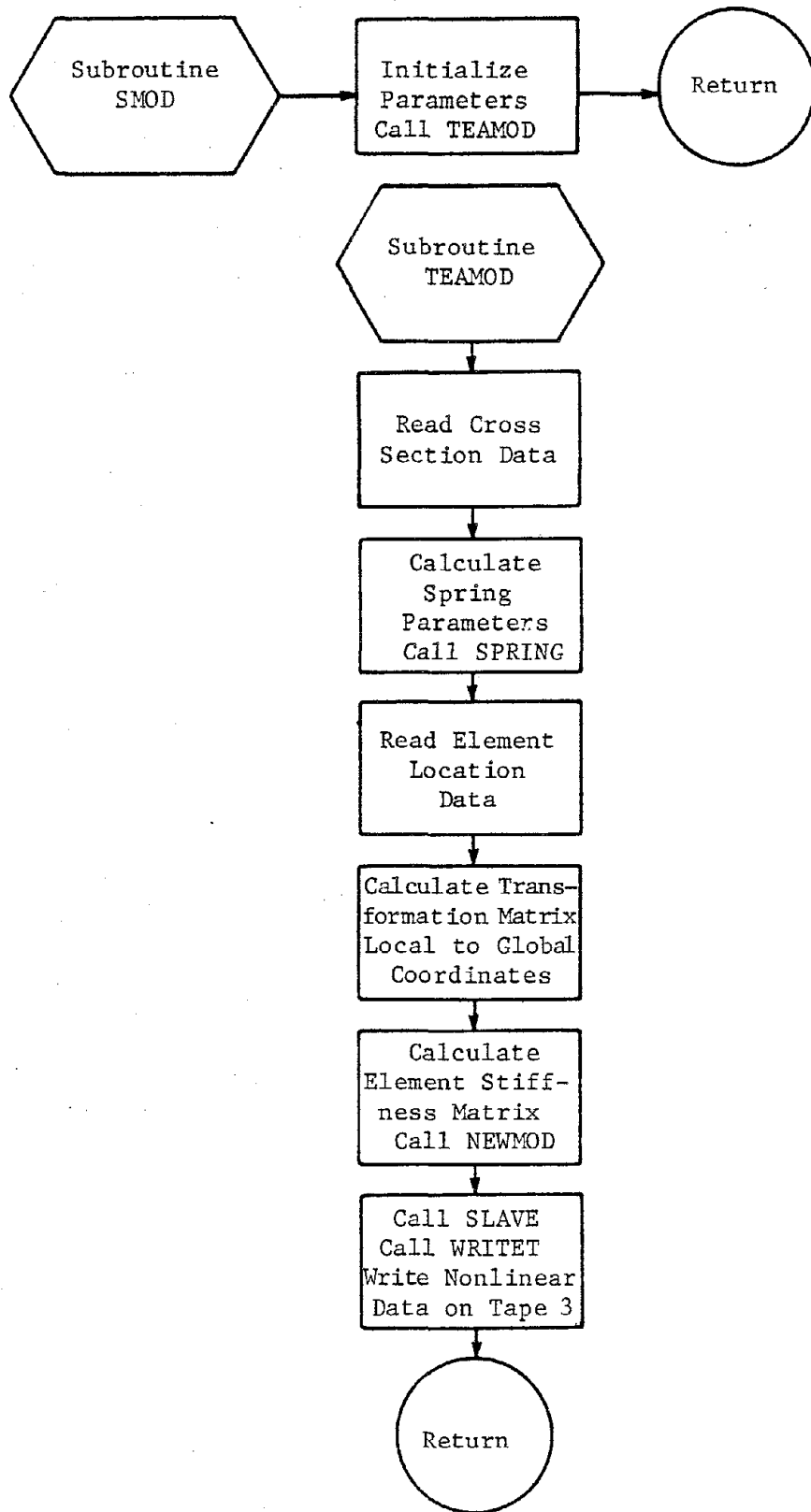


Fig. 5.2. Flowchart for Subroutines SMOD and TEAMOD.

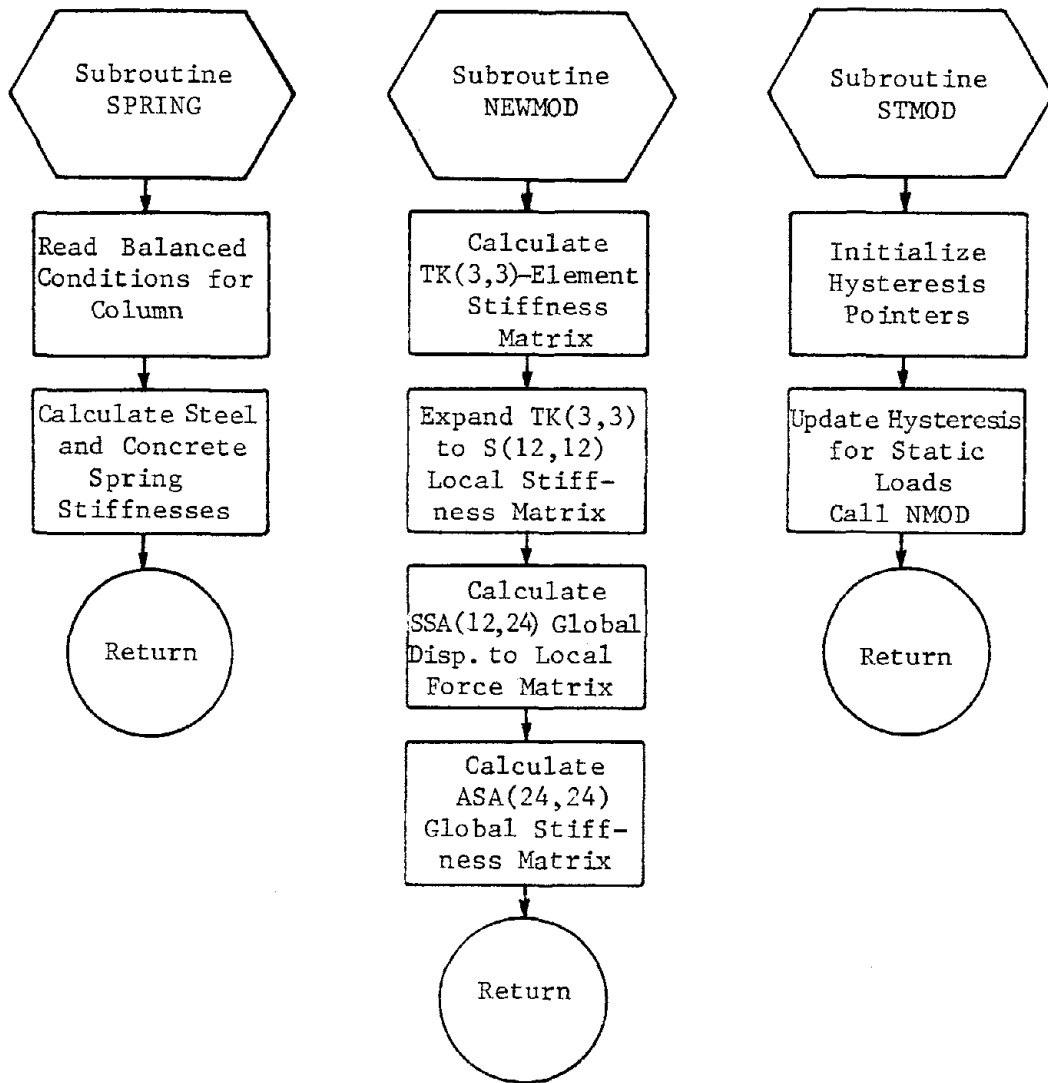


Fig. 5.3. Flowcharts for Subroutines SPRING, NEWMOD, and STMOD.

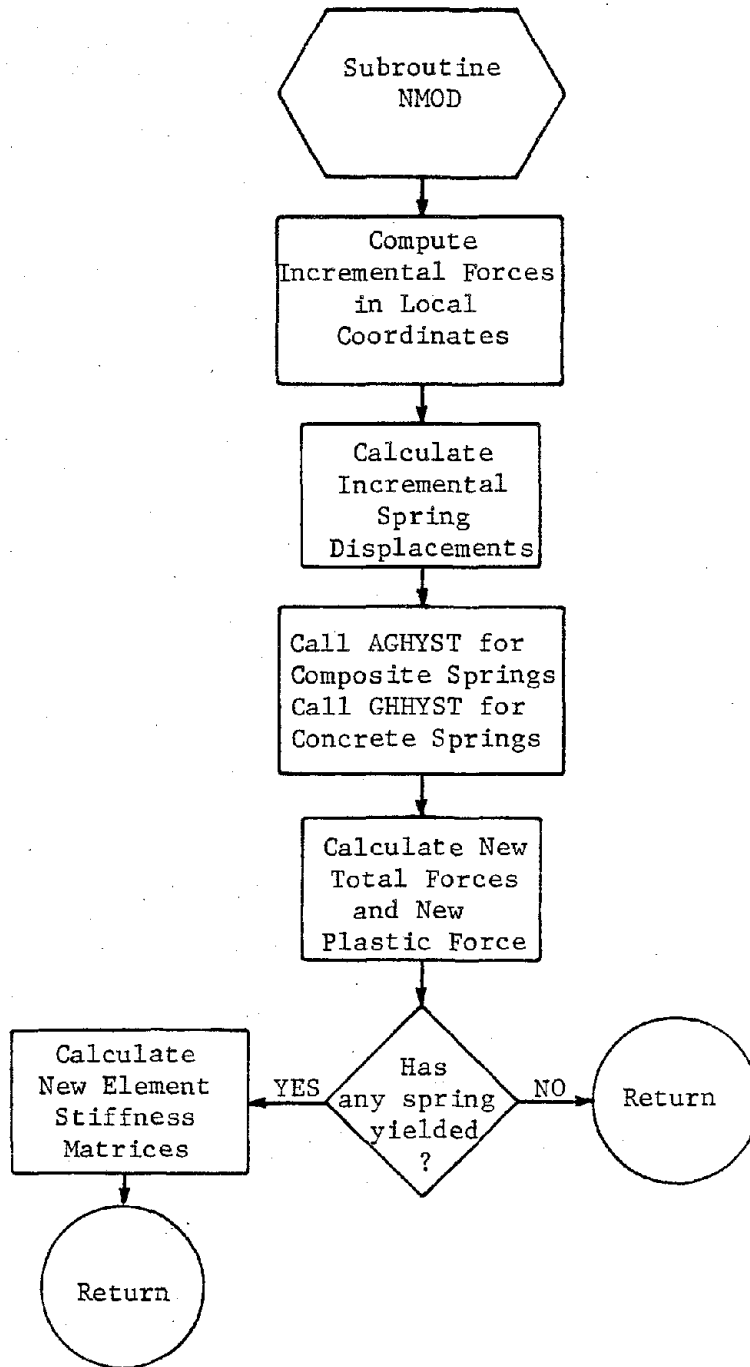


Fig. 5.4. Flowchart for Subroutine NMOD.

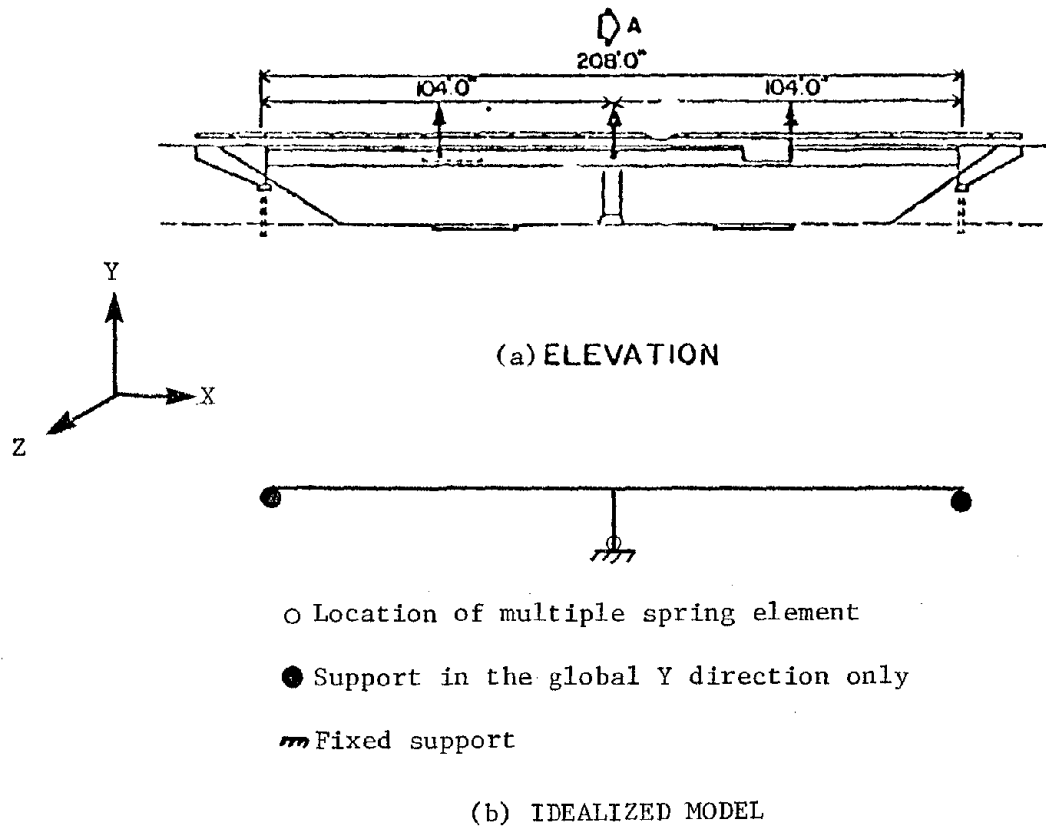


Fig. 6.1. Elevation and Model of the Meloland Overpass.

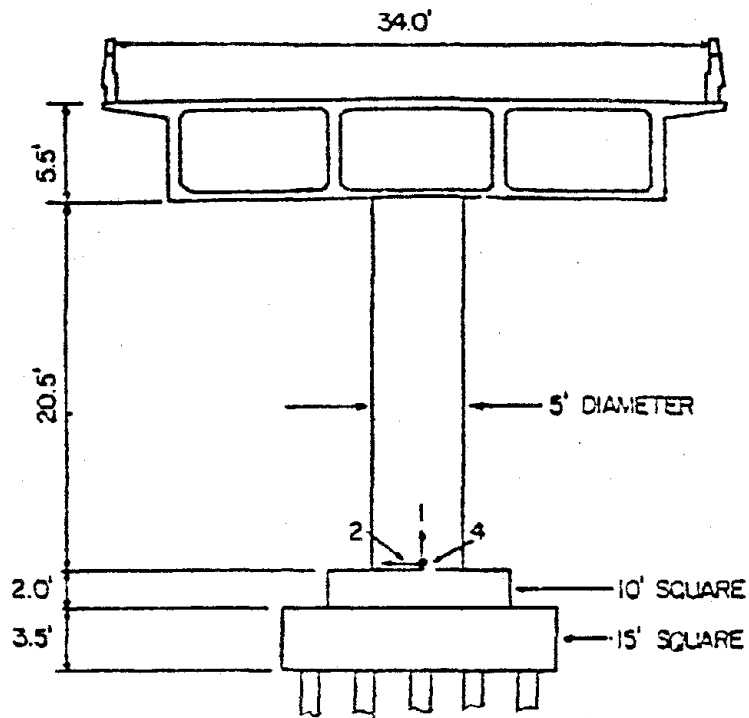


Fig. 6.2. Elevation of Meloland Overpass.

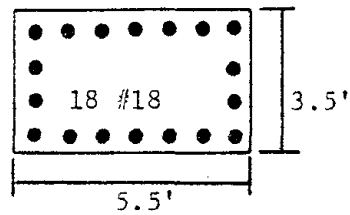


Fig. 6.3. Pier Cross Section for the Rectangular Column Model.

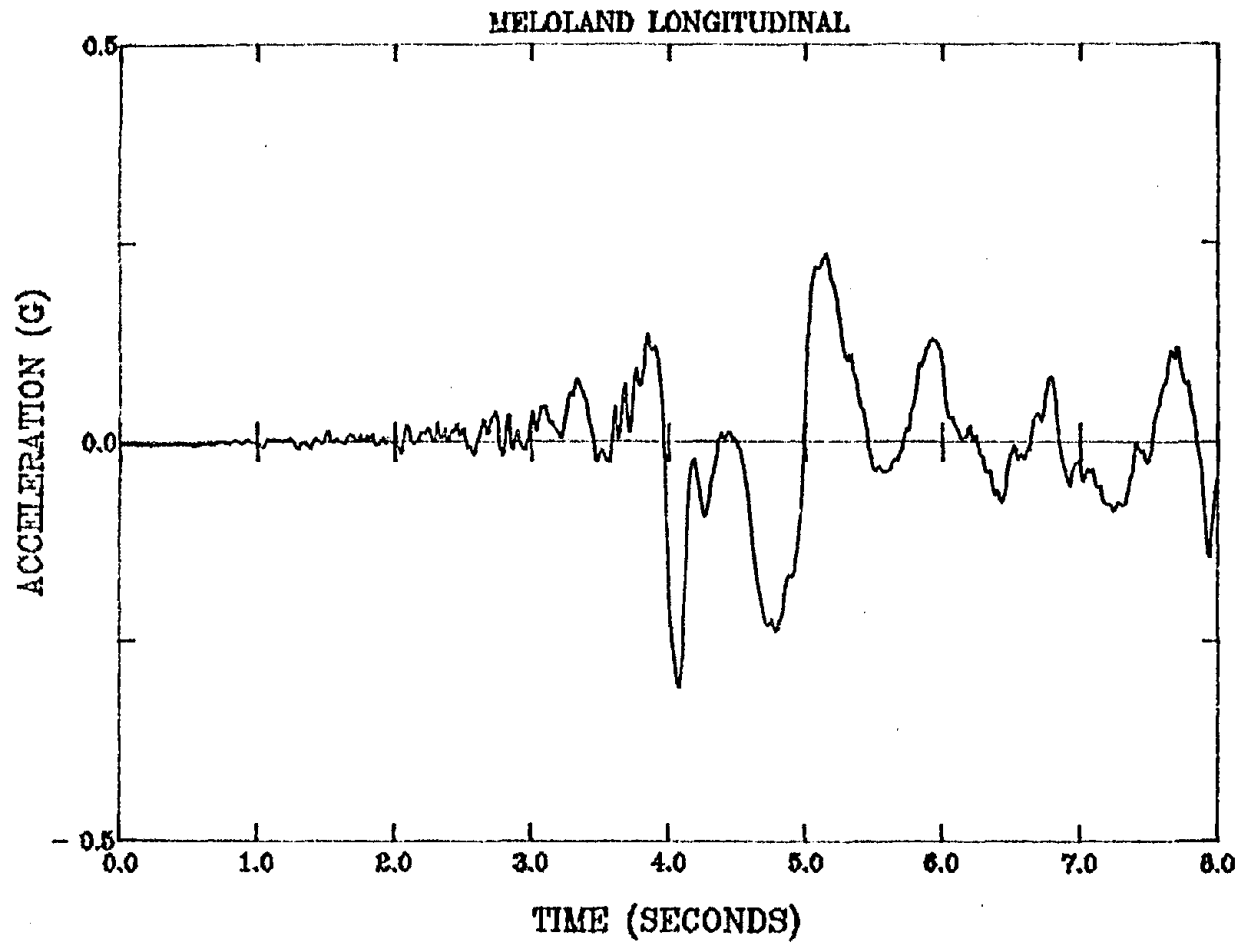


Fig. 6.4. The 1979 Imperial Valley Earthquake.

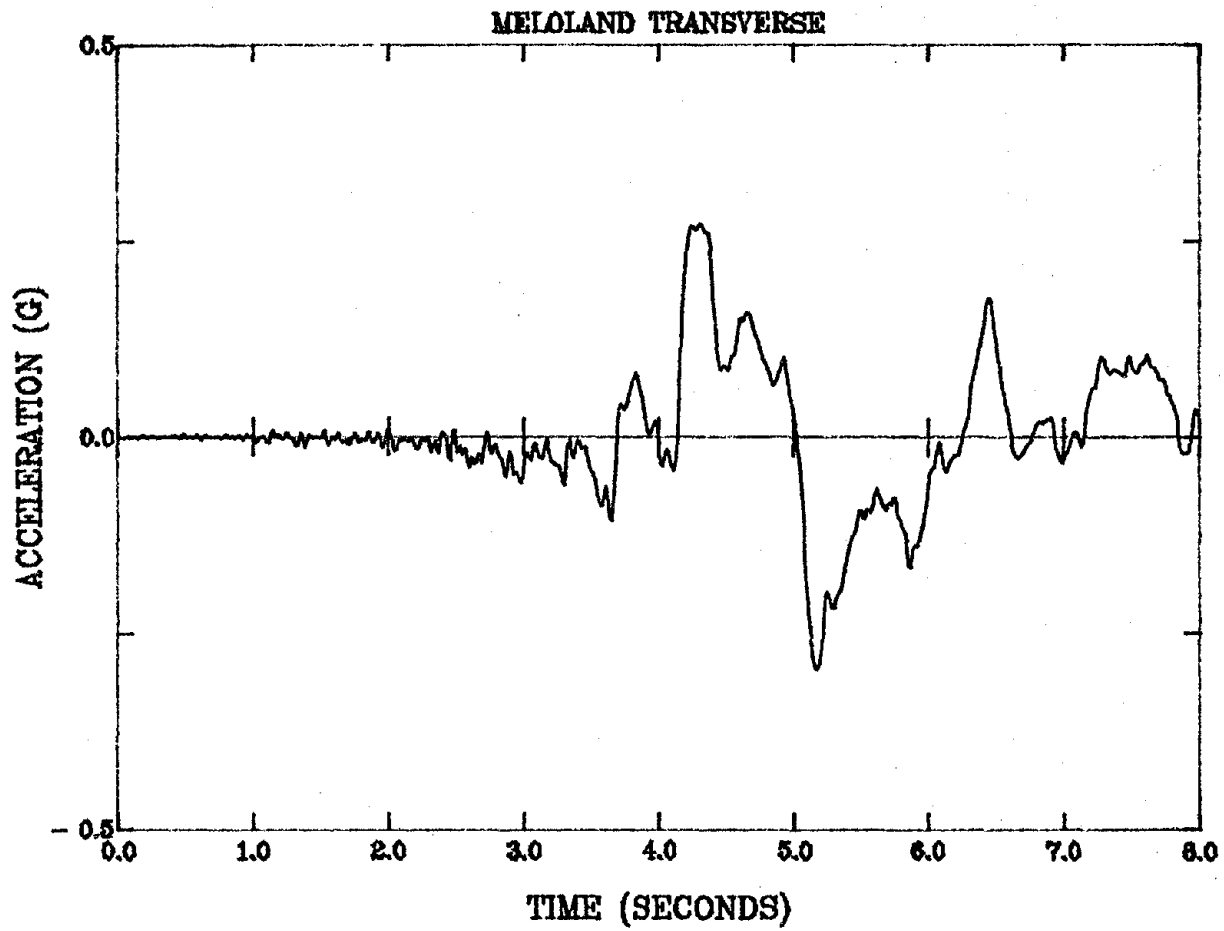


Fig. 6.5. The 1979 Imperial Valley Earthquake.

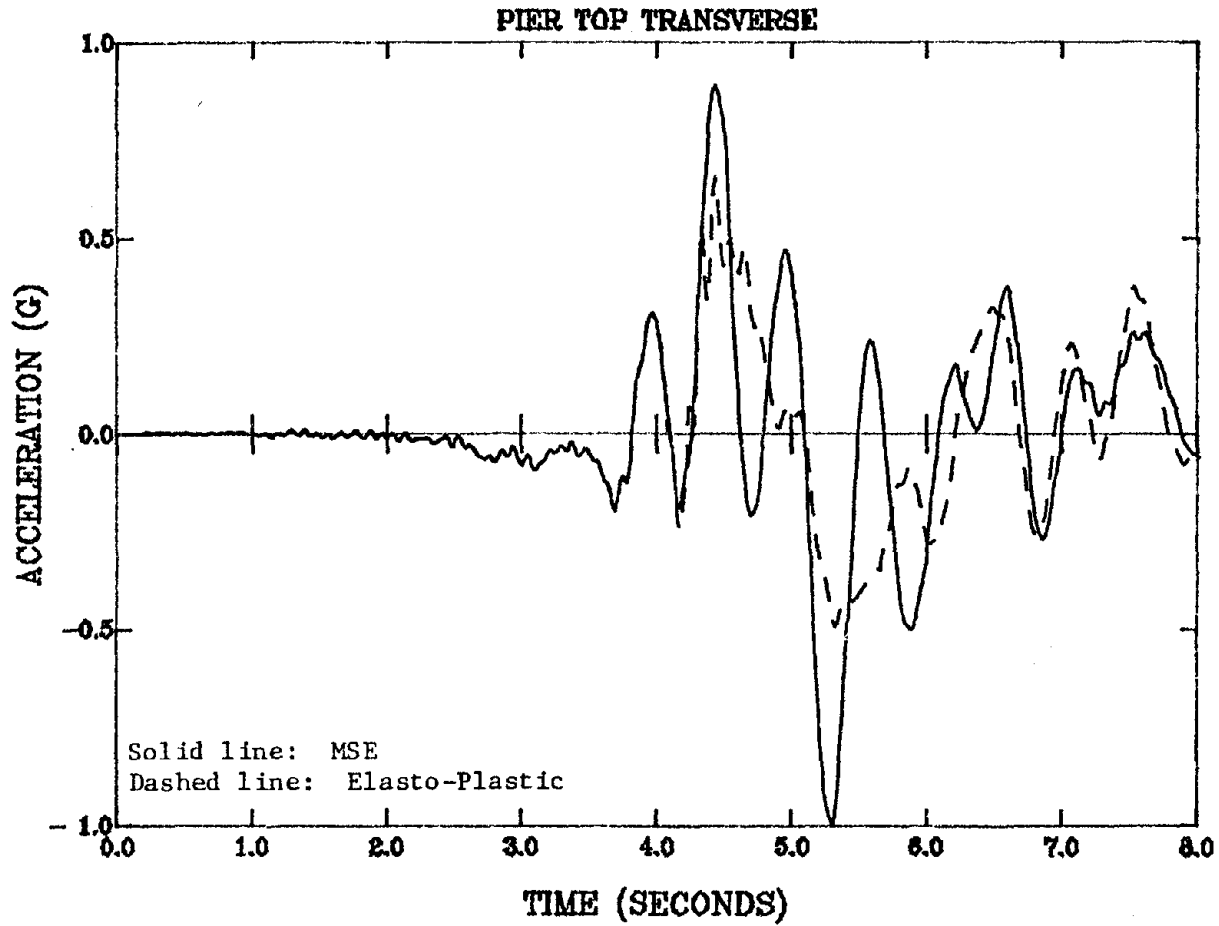


Fig. 6.6. Meloland Overpass Model Response. Imperial Valley Earthquake *1.0. (round column)

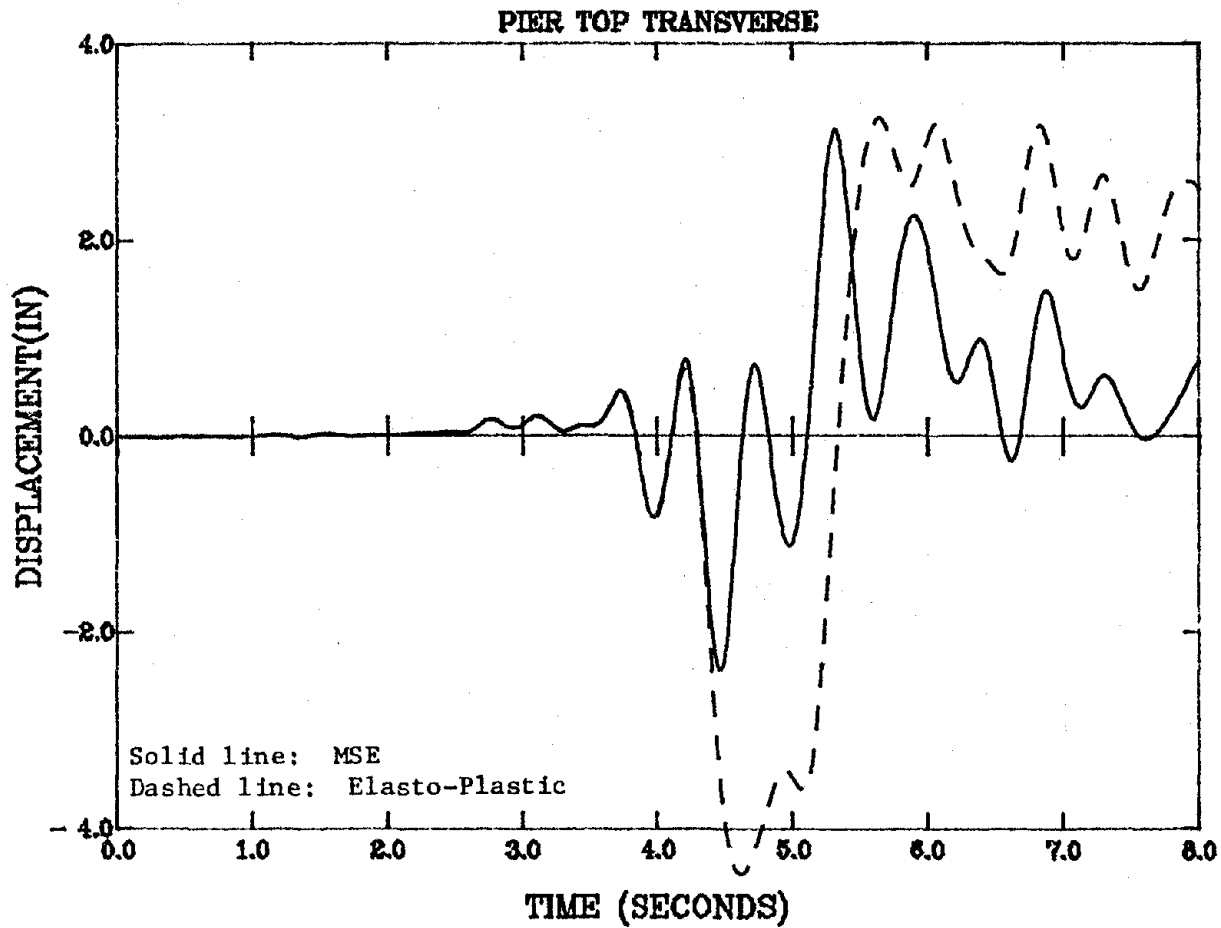


Fig. 6.7. Meloland Overpass Model Response. Imperial Valley Earthquake *1.0. (round column)

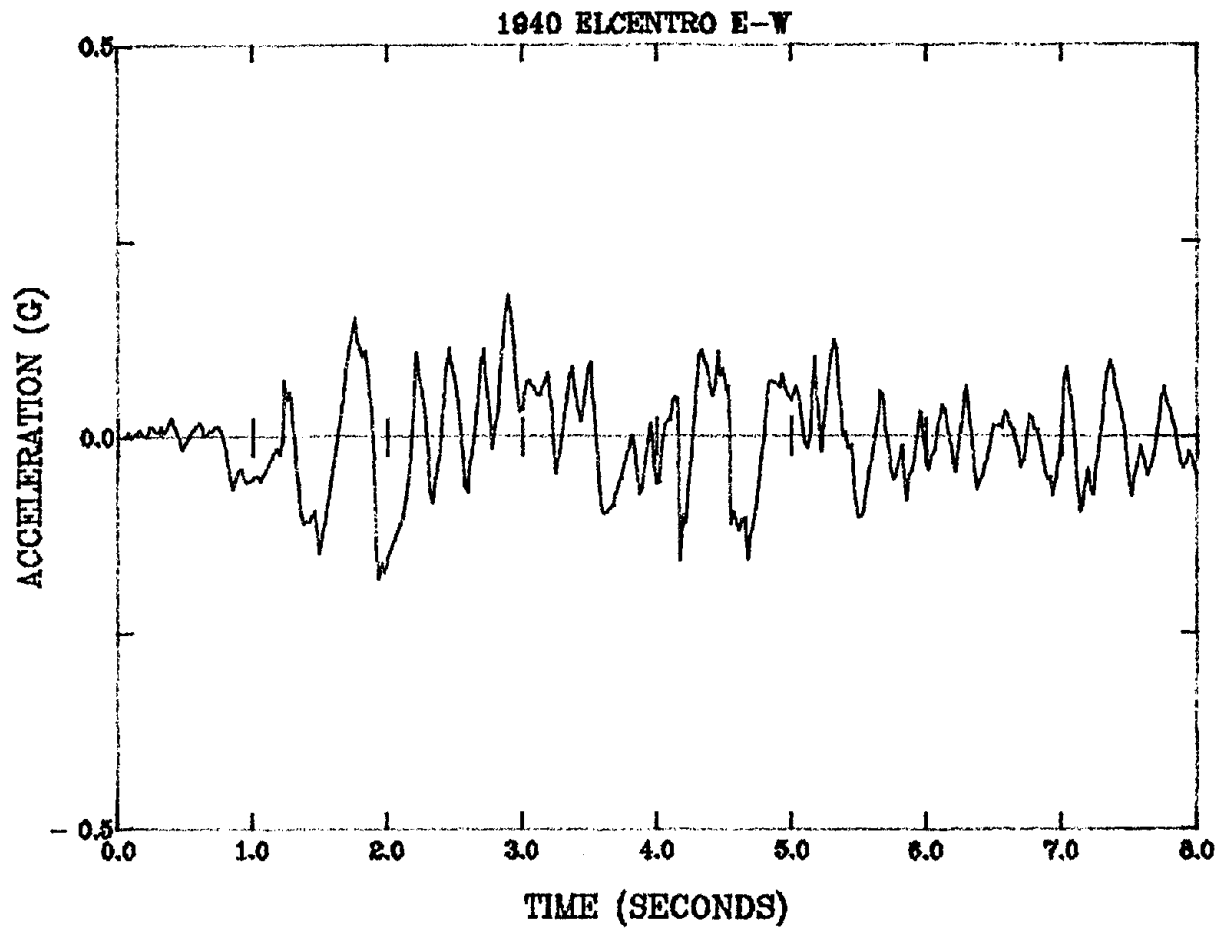


Fig. 6.8. 1940 El Centro Earthquake E-W.

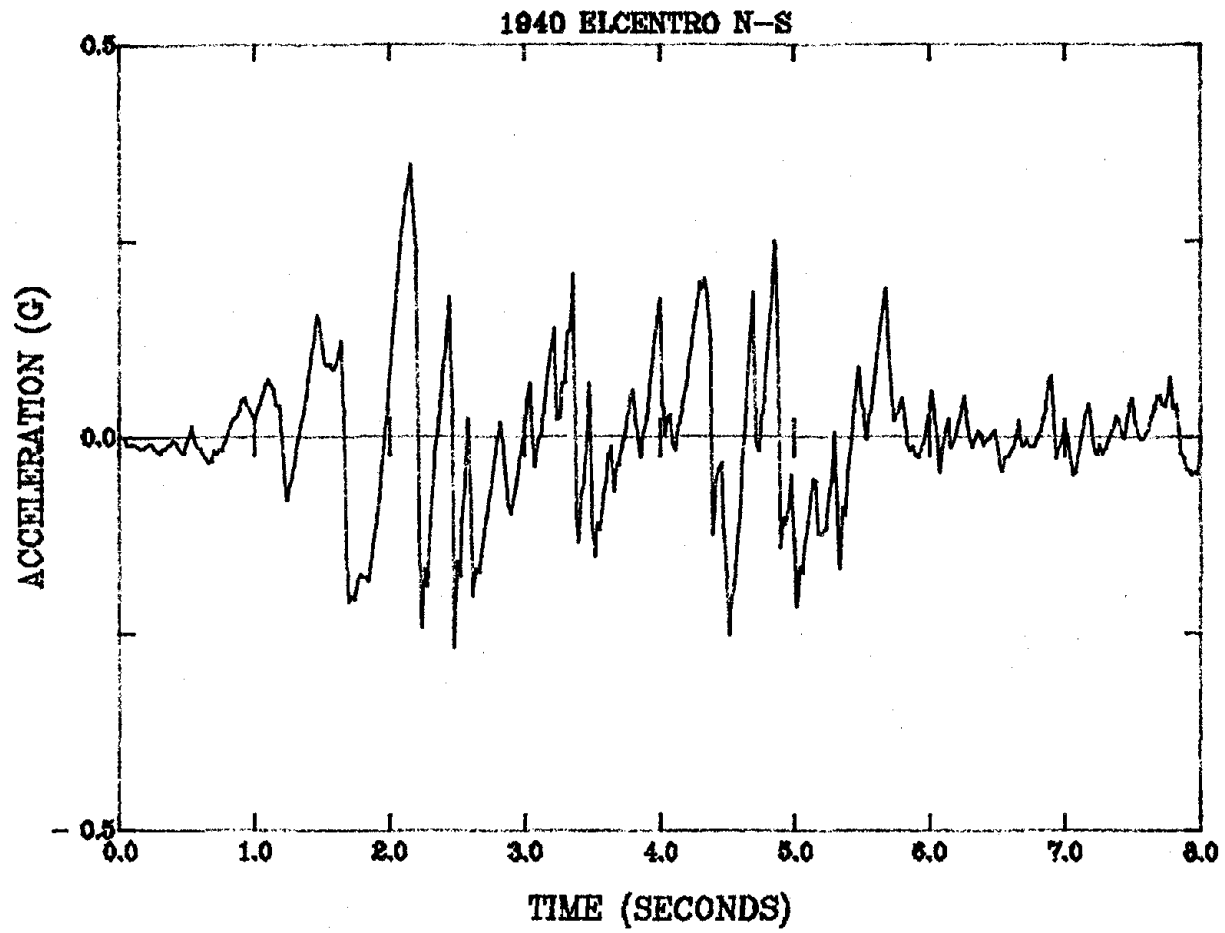


Fig. 6.9. 1940 El Centro Earthquake N-S.

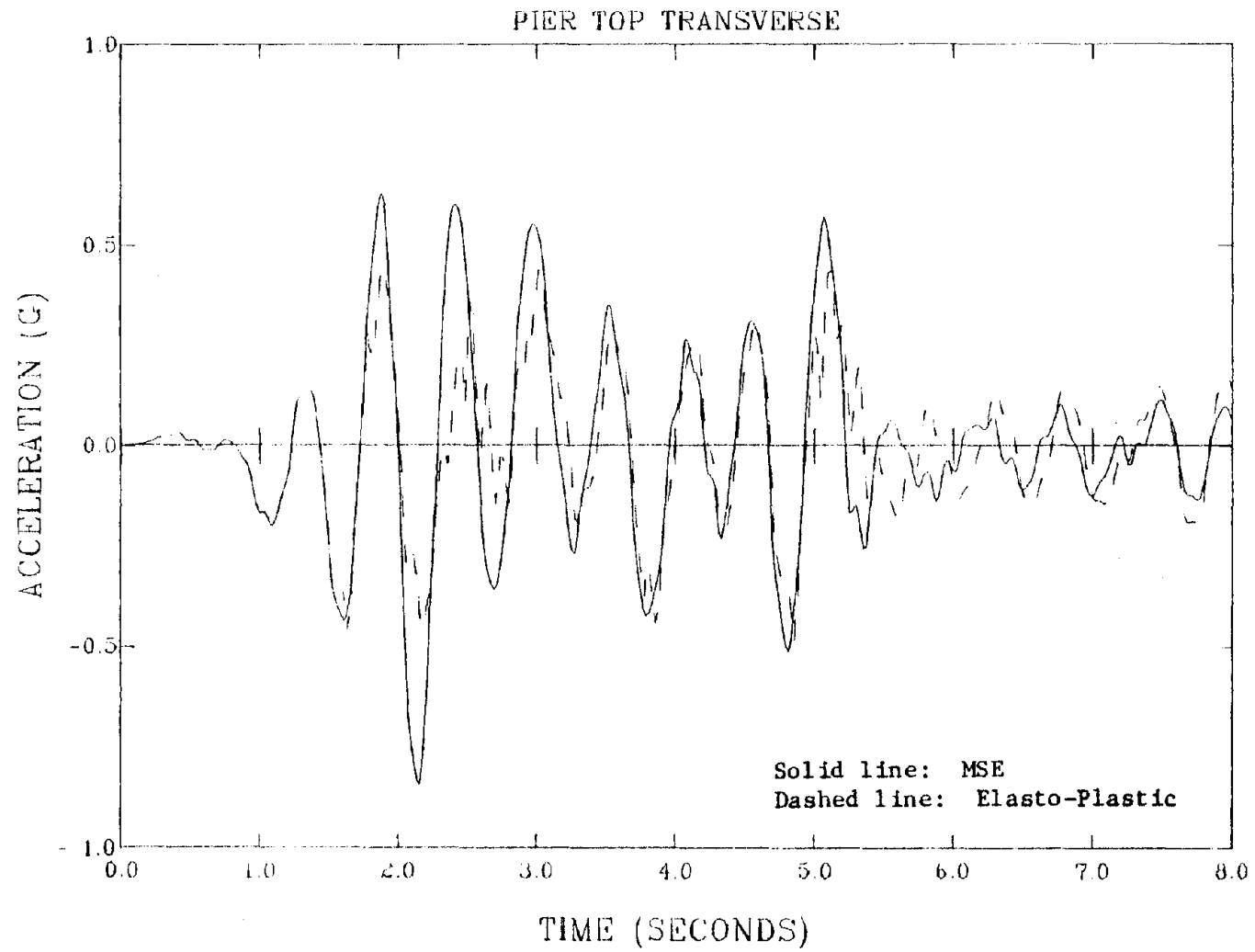


Fig. 6.10. Meloland Overpass Model Response Using El Centro Earthquake *2.0. (round column)

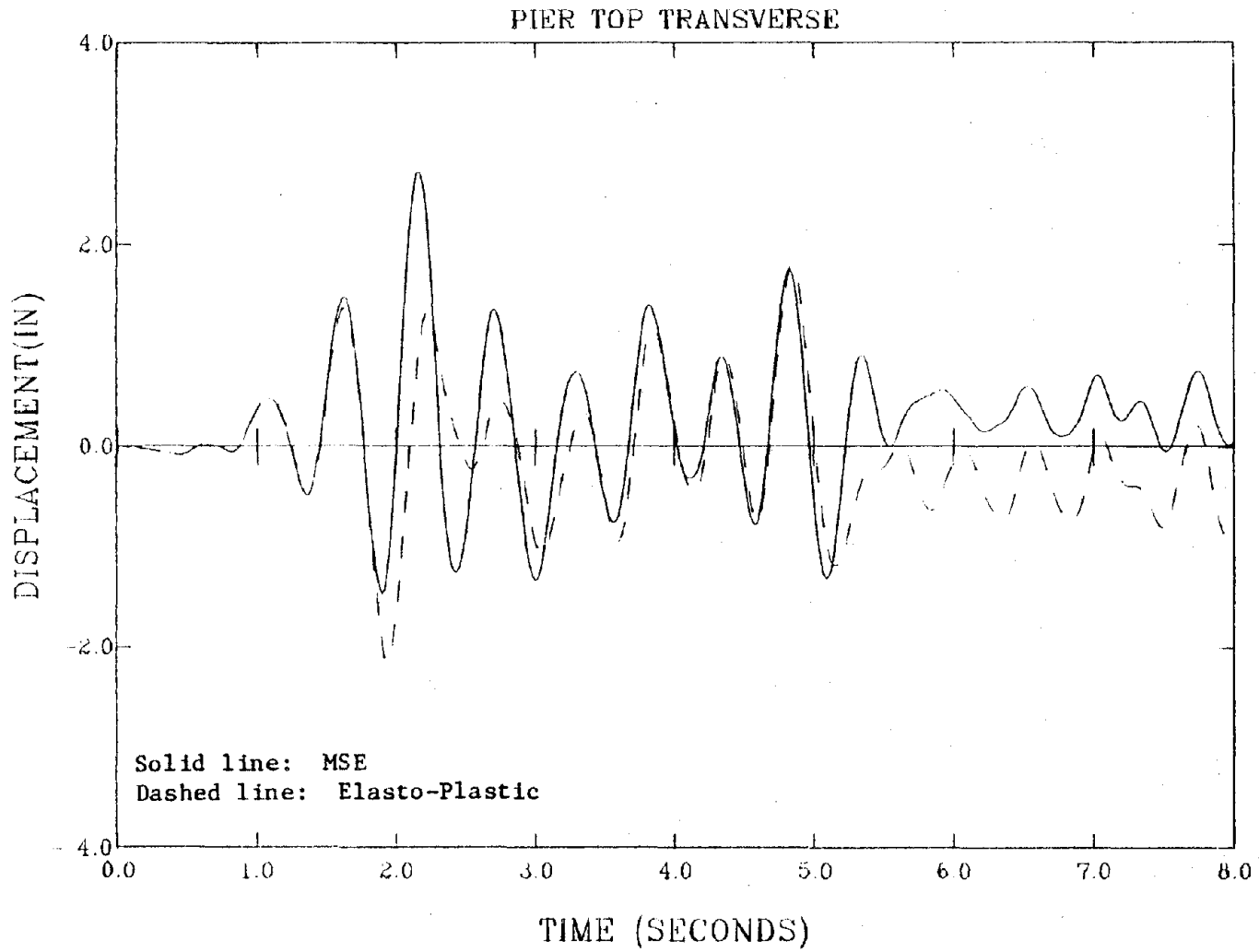


Fig. 6.11. Meloland Overpass Model Response Using El Centro Earthquake *2.0. (round column)

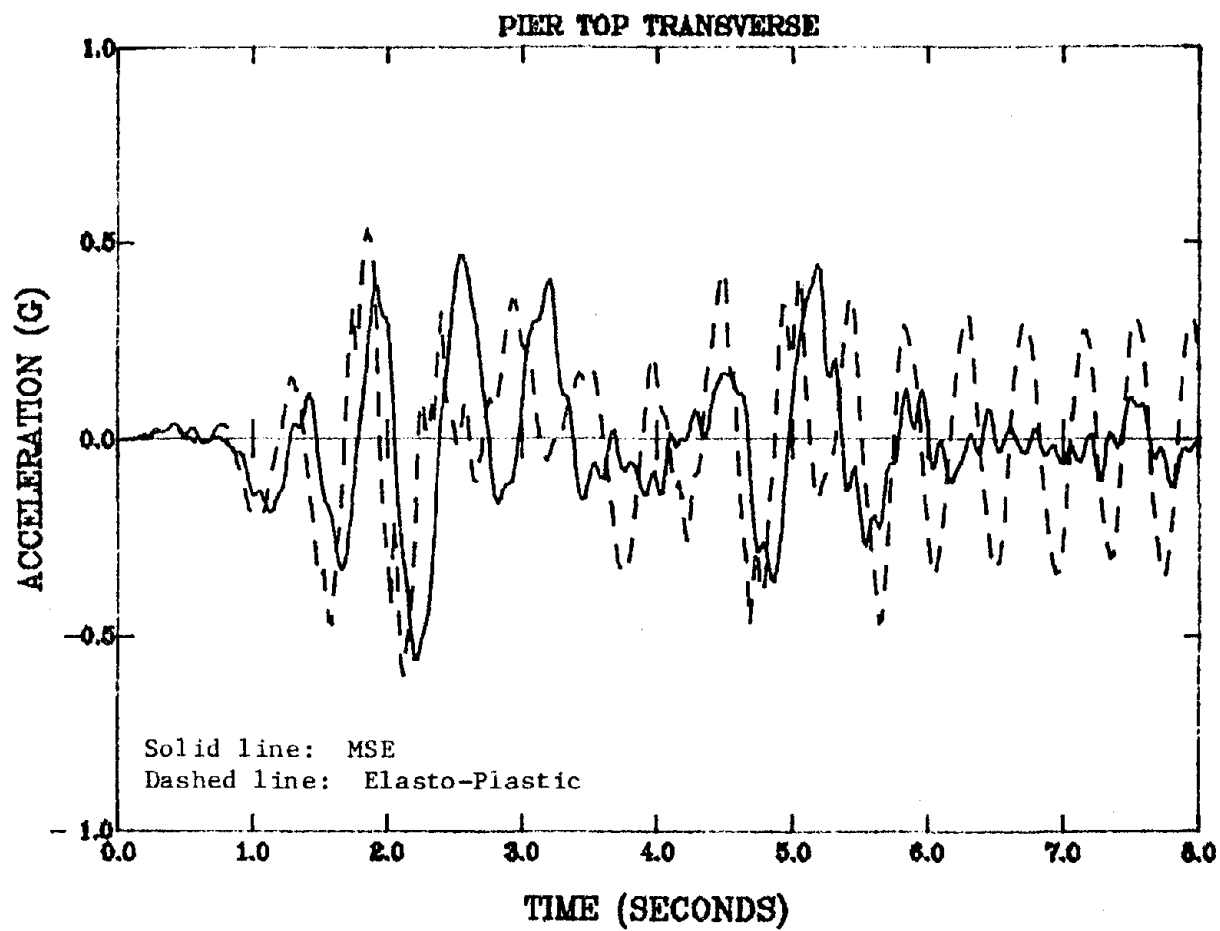


Fig. 6.12. Meloland Overpass Model Response Using El Centro Earthquake *2.0. (rectangular column)

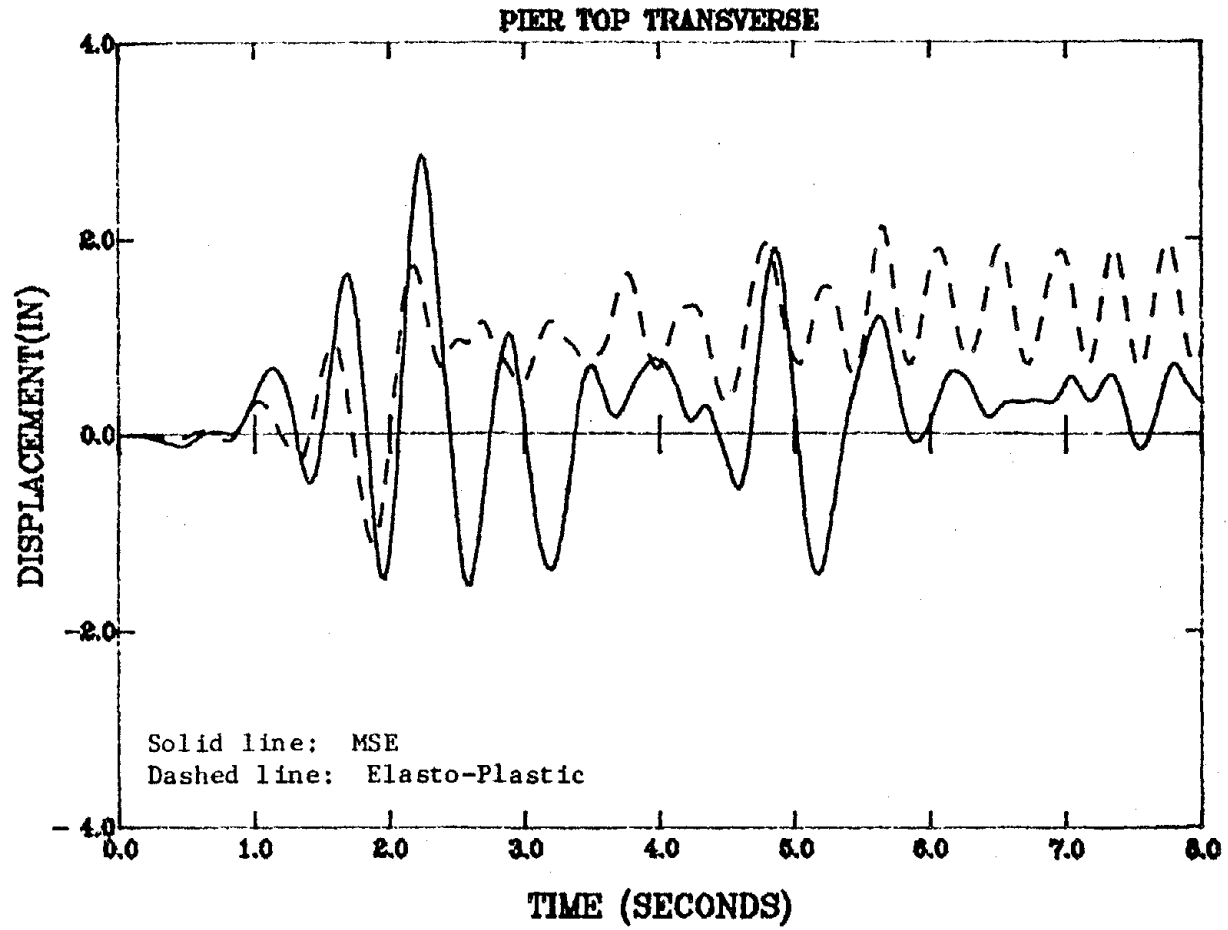


Fig. 6.13. Meloland Overpass Model Response Using El Centro Earthquake *2.0. (rectangular column)

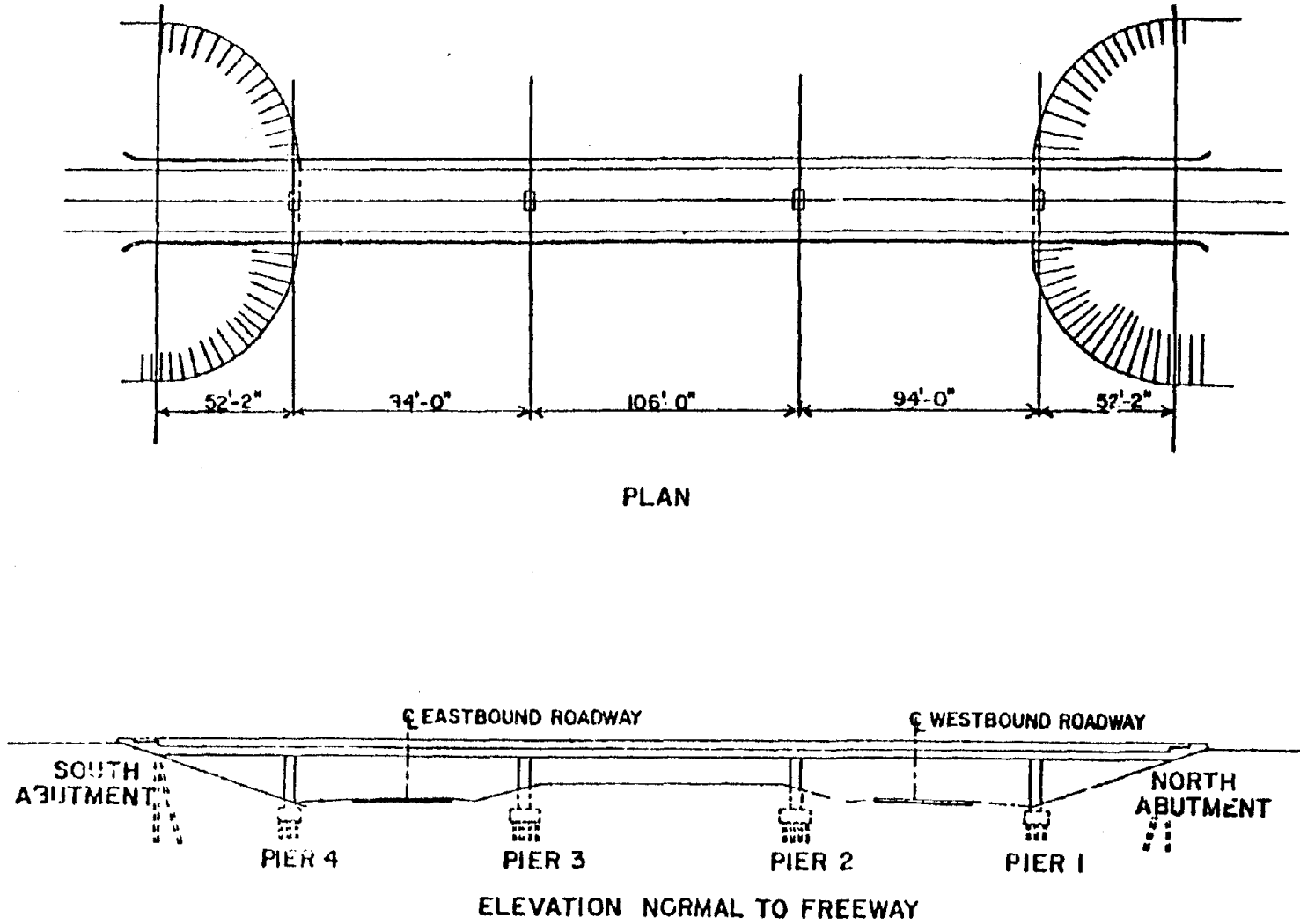


Fig. 6.14. Rose Creek Interchange Plan and Elevation.

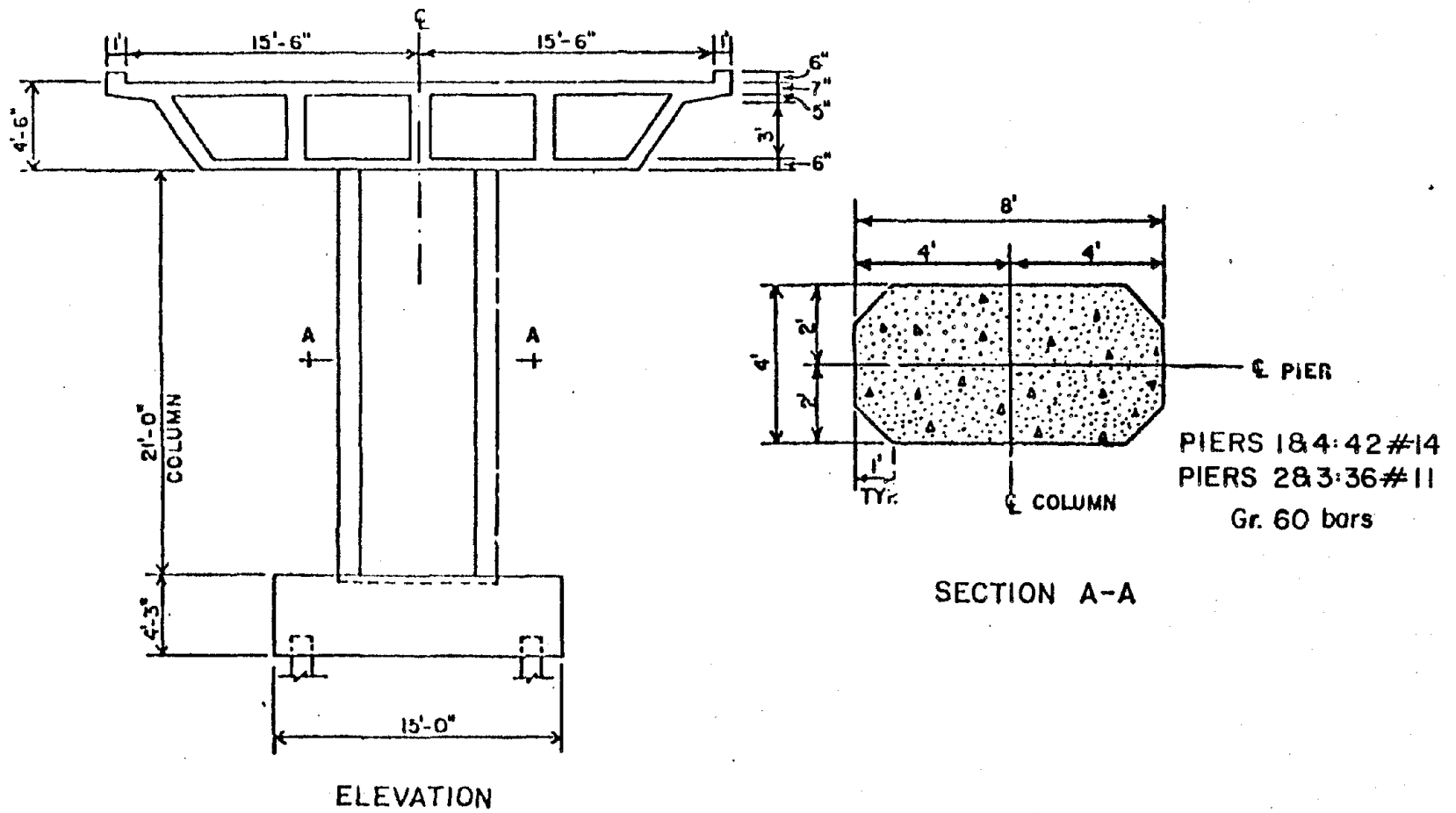


Fig. 6.15. Elevation of Rose Creek Interchange Pier and Column Cross-Section.

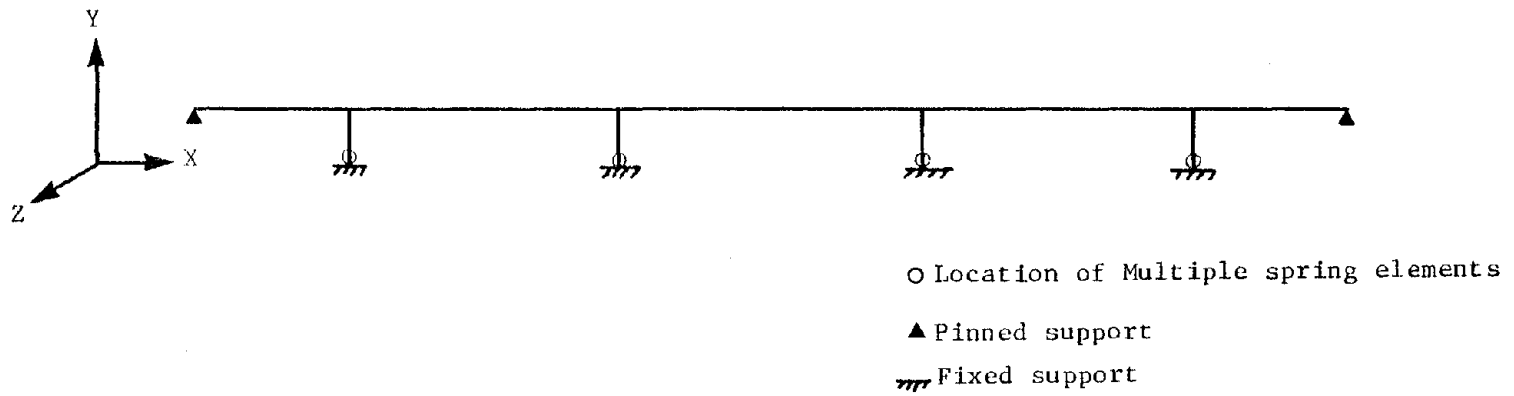


Fig. 6.16. Model of the Rose Creek Interchange.

PIER TOP 1 TRANSVERSE

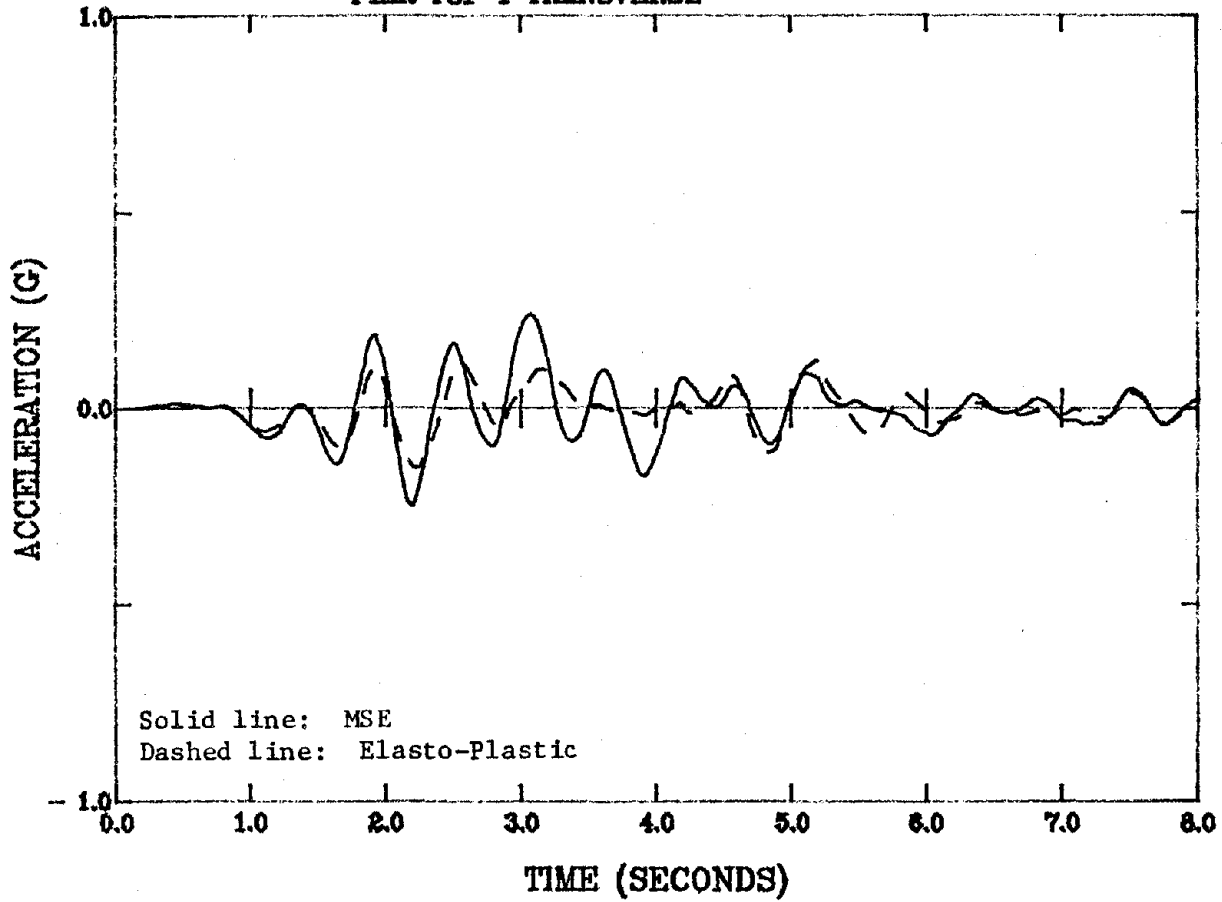


Fig. 6.17. Rose Creek Interchange Model Response (El Centro *1.0).

PIER TOP 2 TRANSVERSE

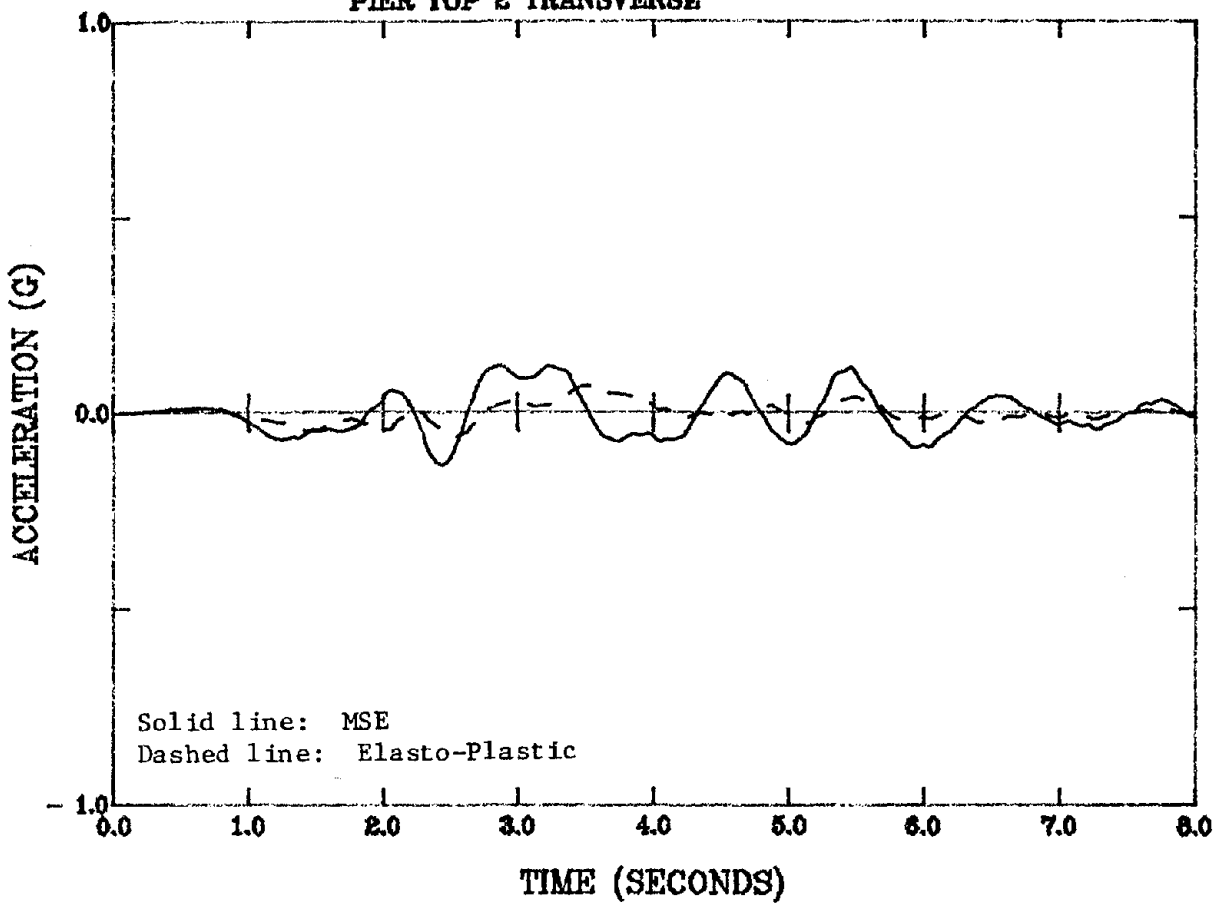


Fig. 6.18. Rose Creek Interchange Model Response (El Centro *1.0).

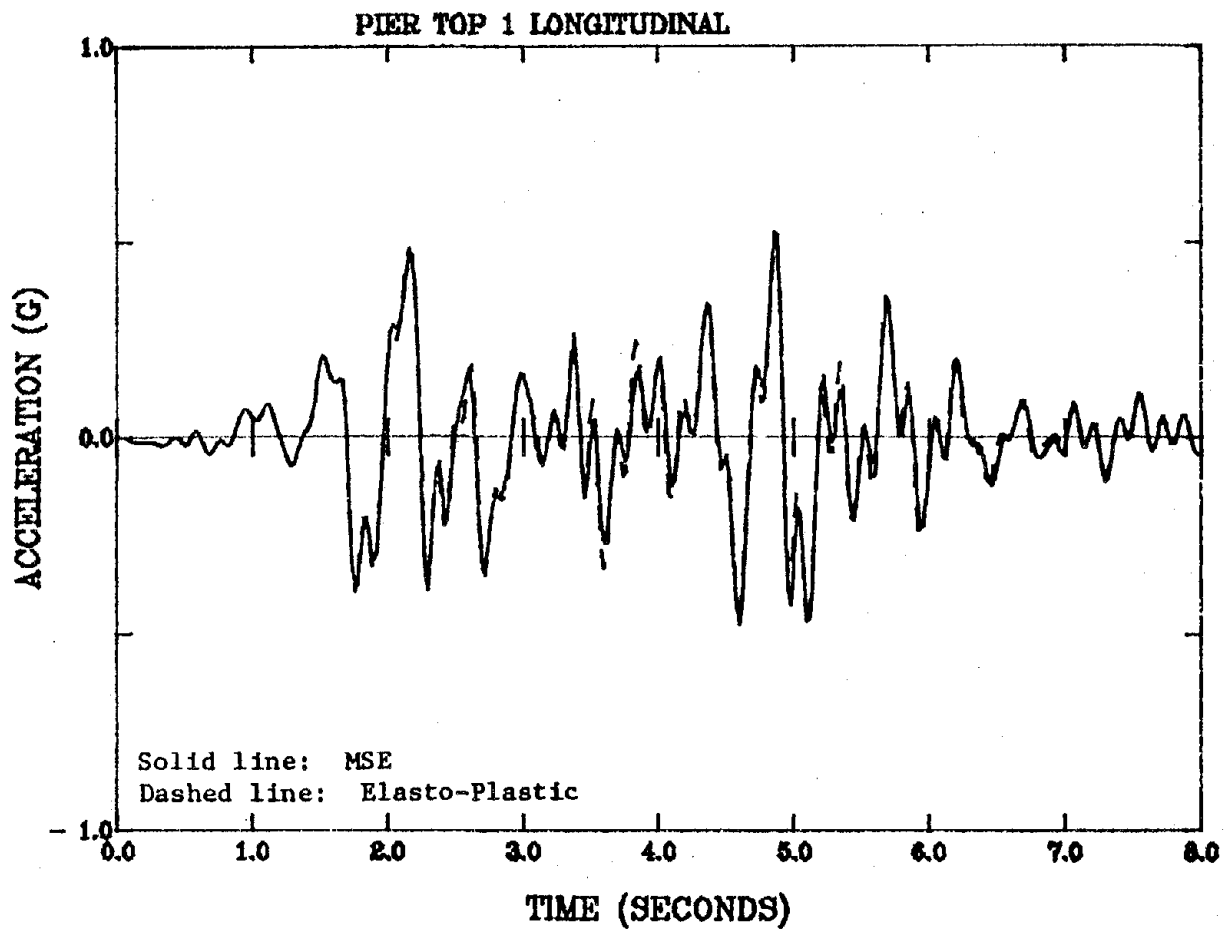


Fig. 6.19. Rose Creek Interchange Model Response (El Centro *1.0).

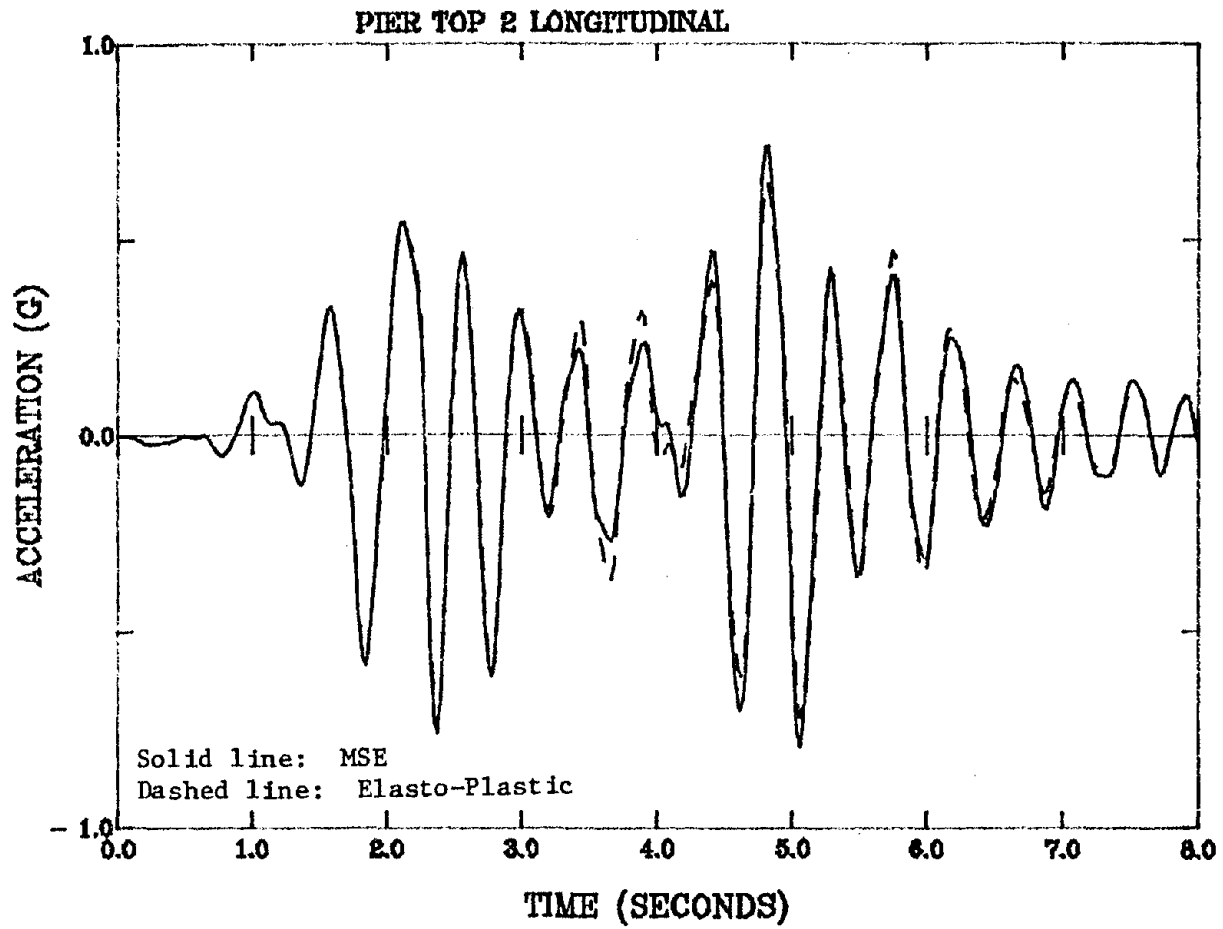


Fig. 6.20. Rose Creek Interchange Model Response (El Centro *1.0).

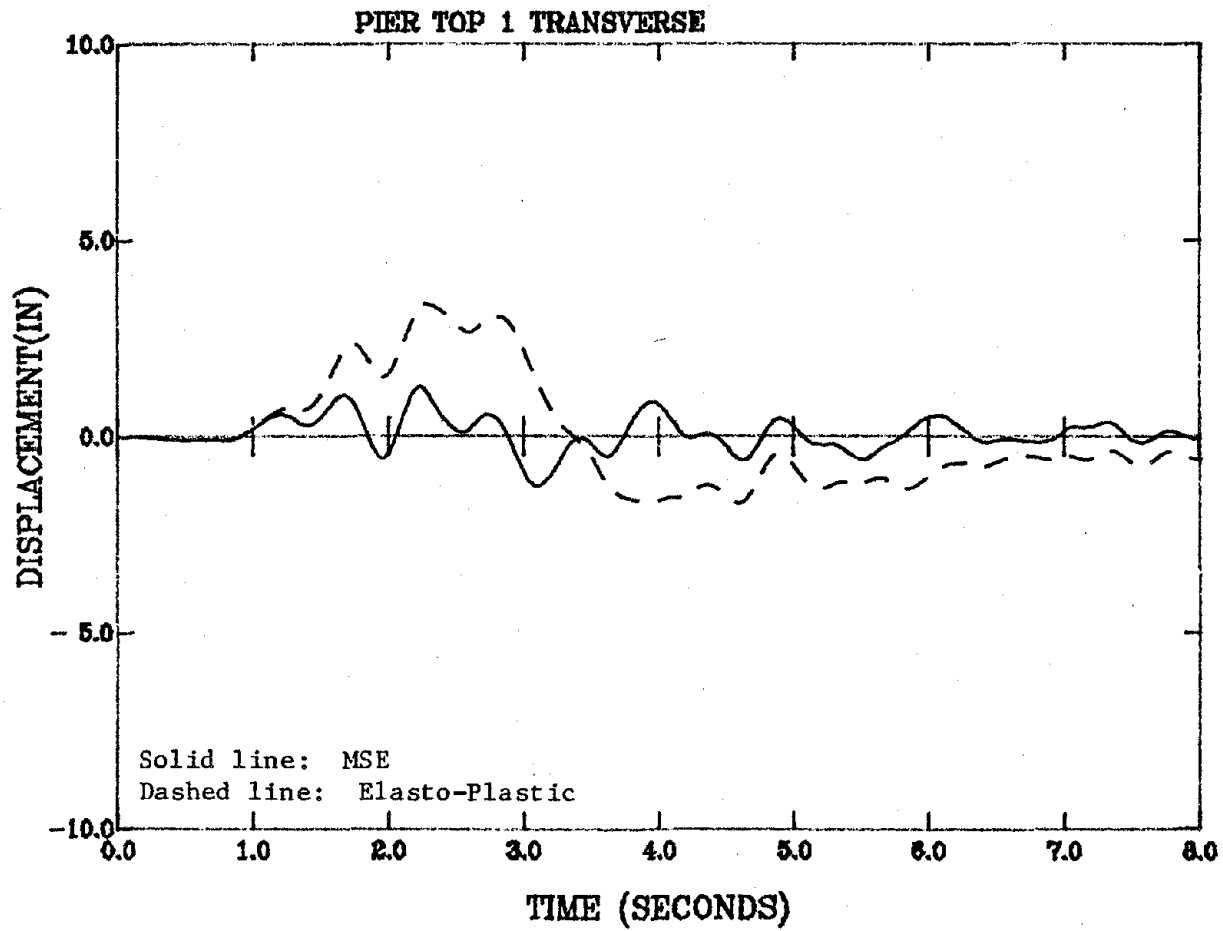


Fig. 6.21. Rose Creek Interchange Model Response (El Centro *1.0).

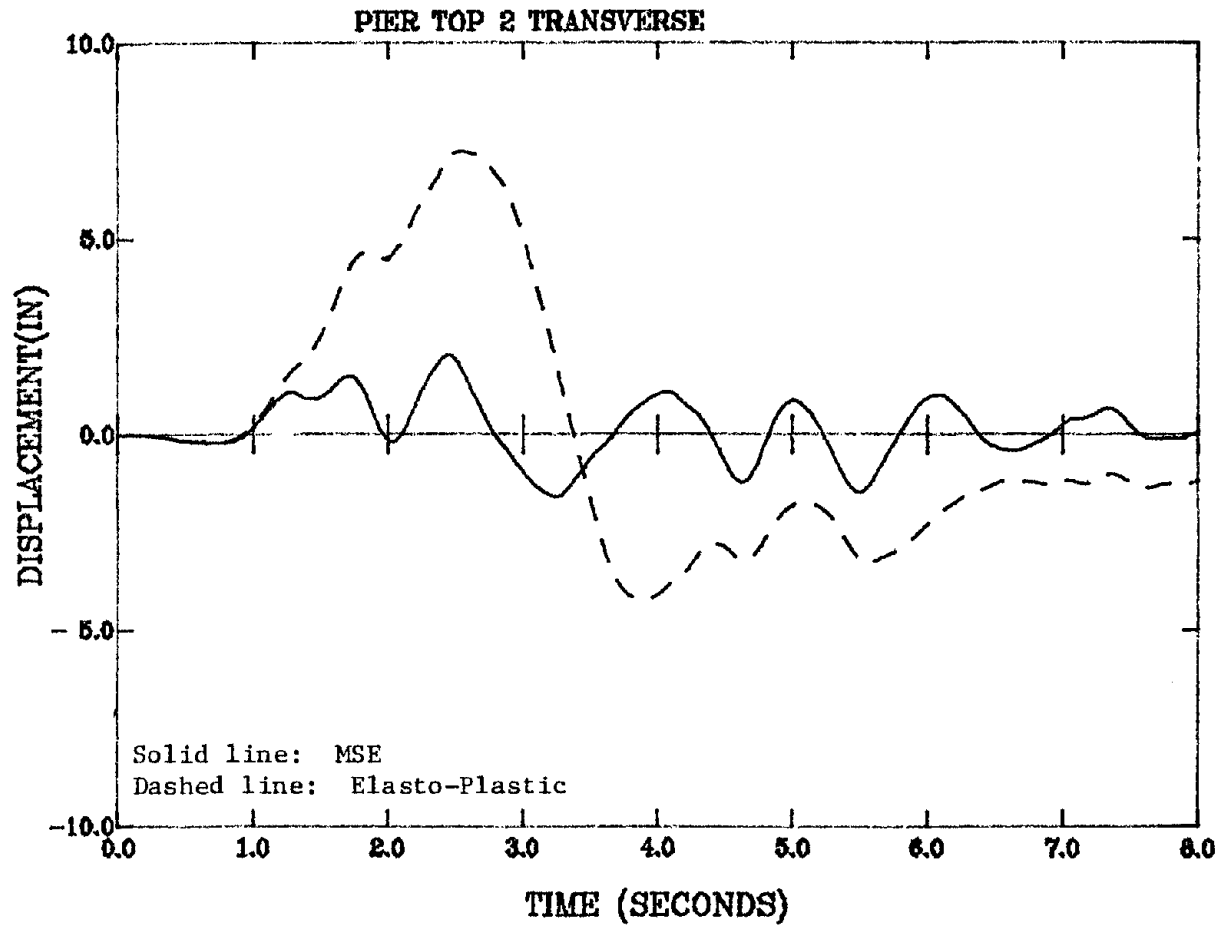


Fig. 6.22. Rose Creek Interchange Model Response (El Centro *1.0).

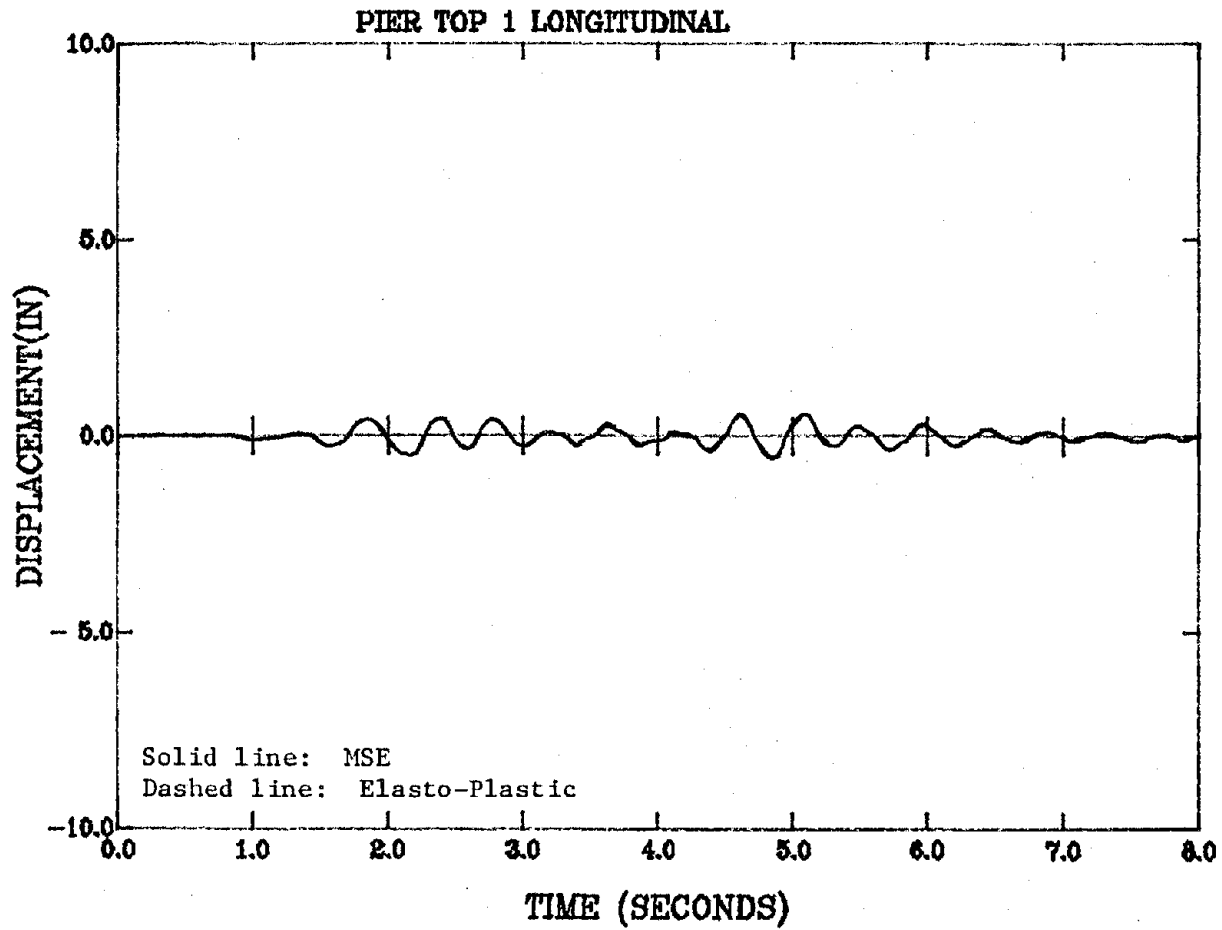


Fig. 6.23. Rose Creek Interchange Model Response (El Centro *1.0).

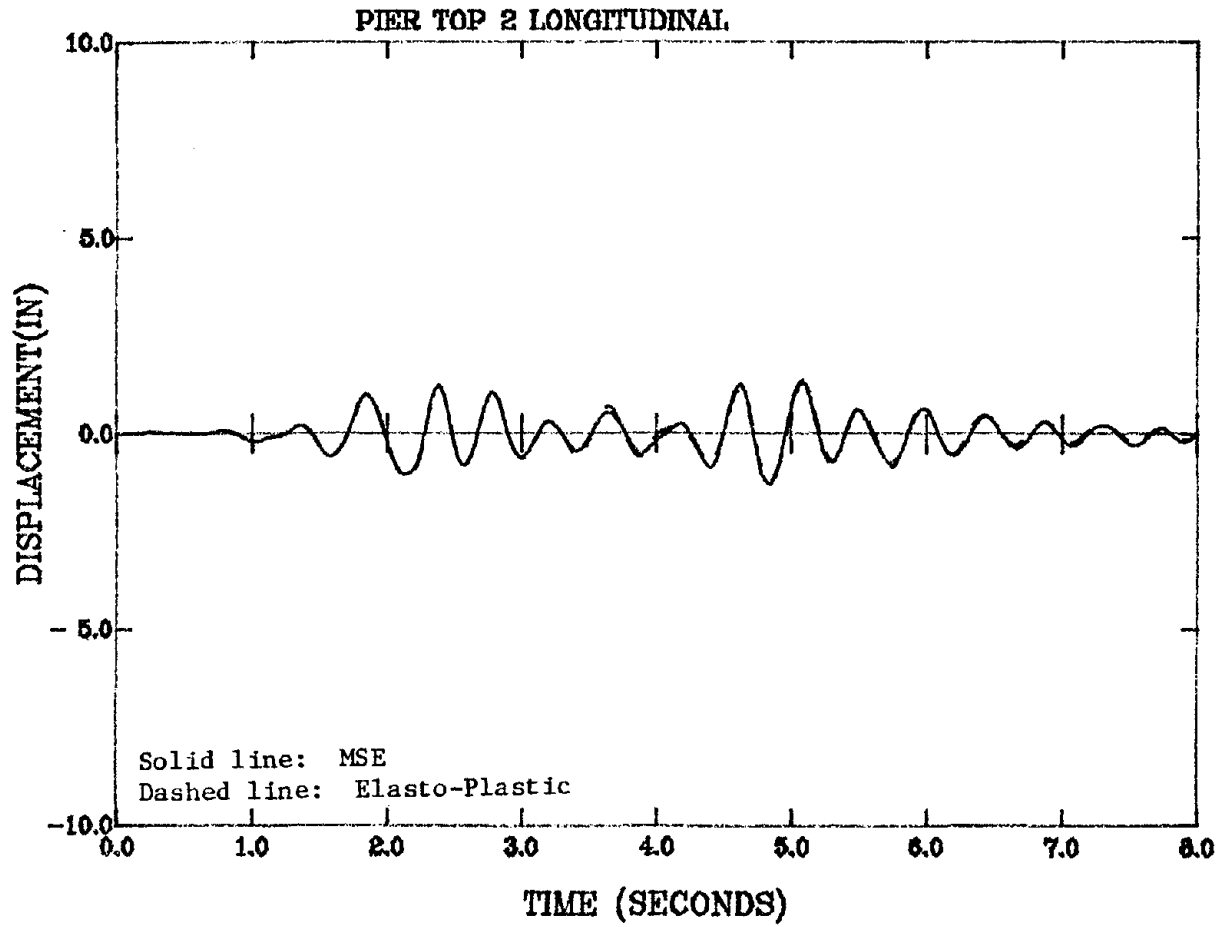


Fig. 6.24. Rose Creek Interchange Model Response (El Centro *1.0).

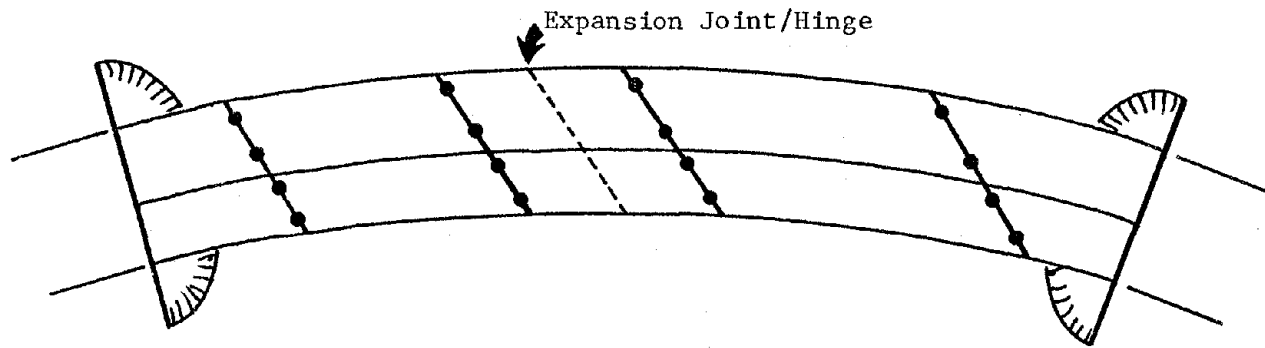


Fig. 6.25. Diagram of the Flamingo Road Overpass.

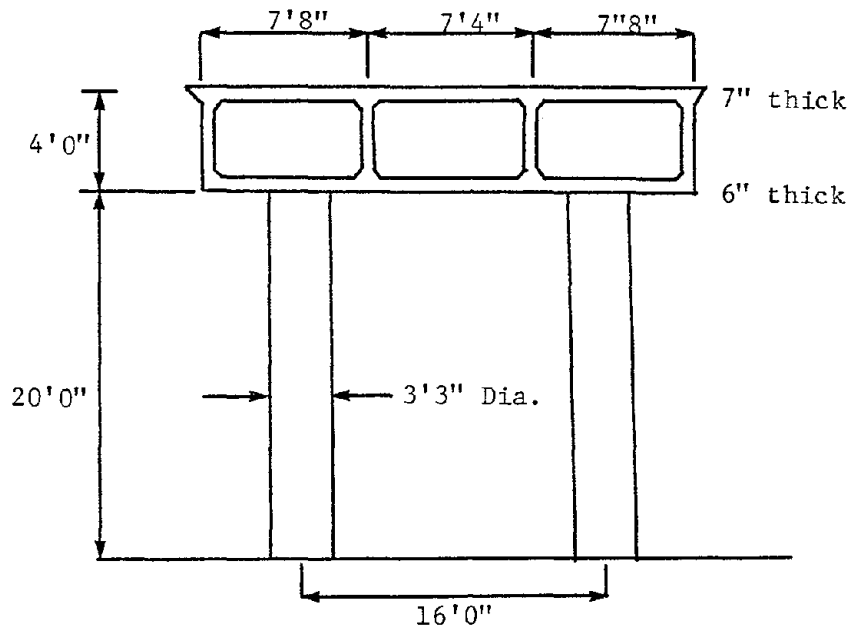


Fig. 6.26. Idealized Pier Elevation for Flamingo Road Overpass.

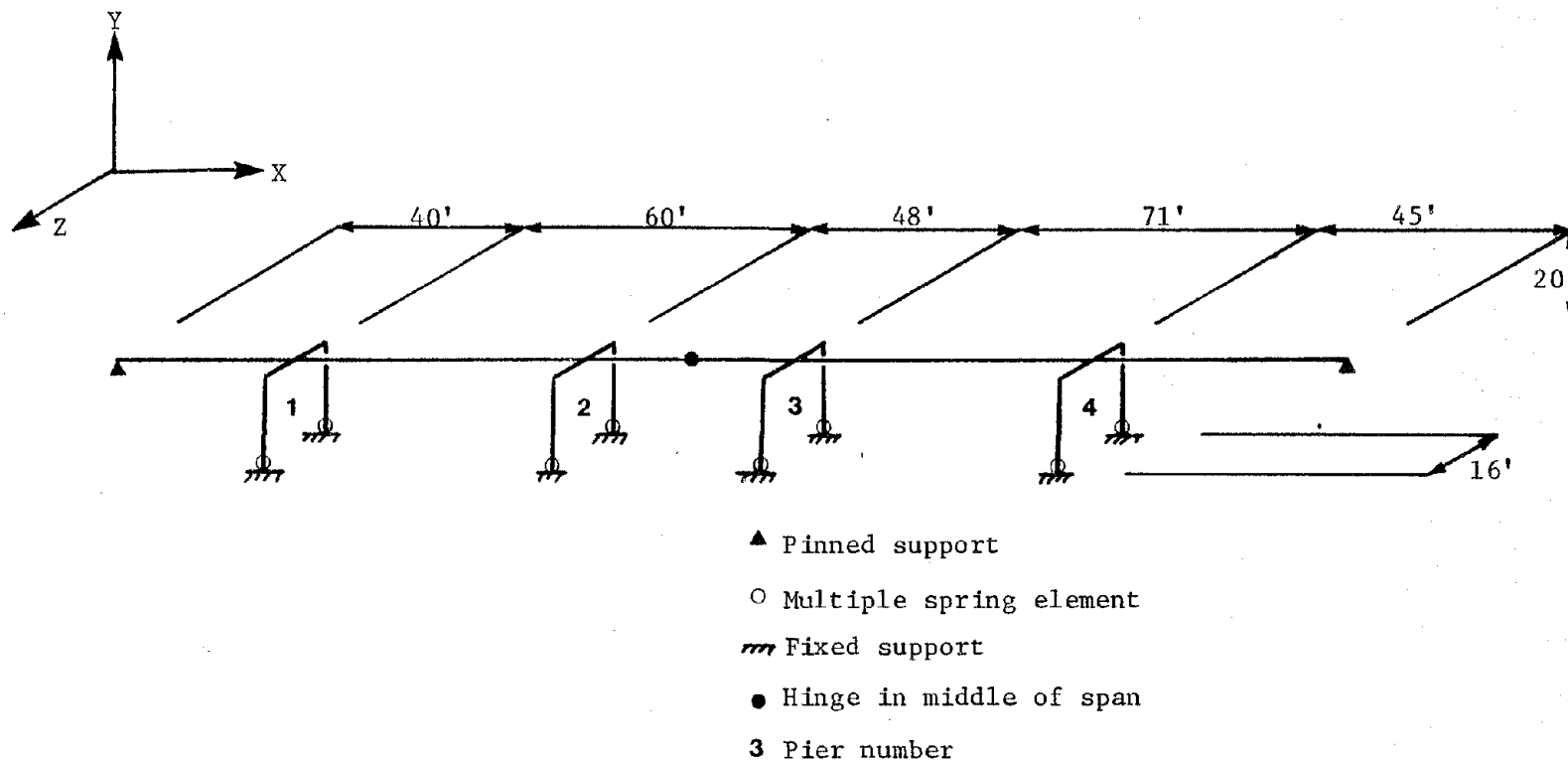


Fig. 6.27. Flamingo Road Overpass Model.

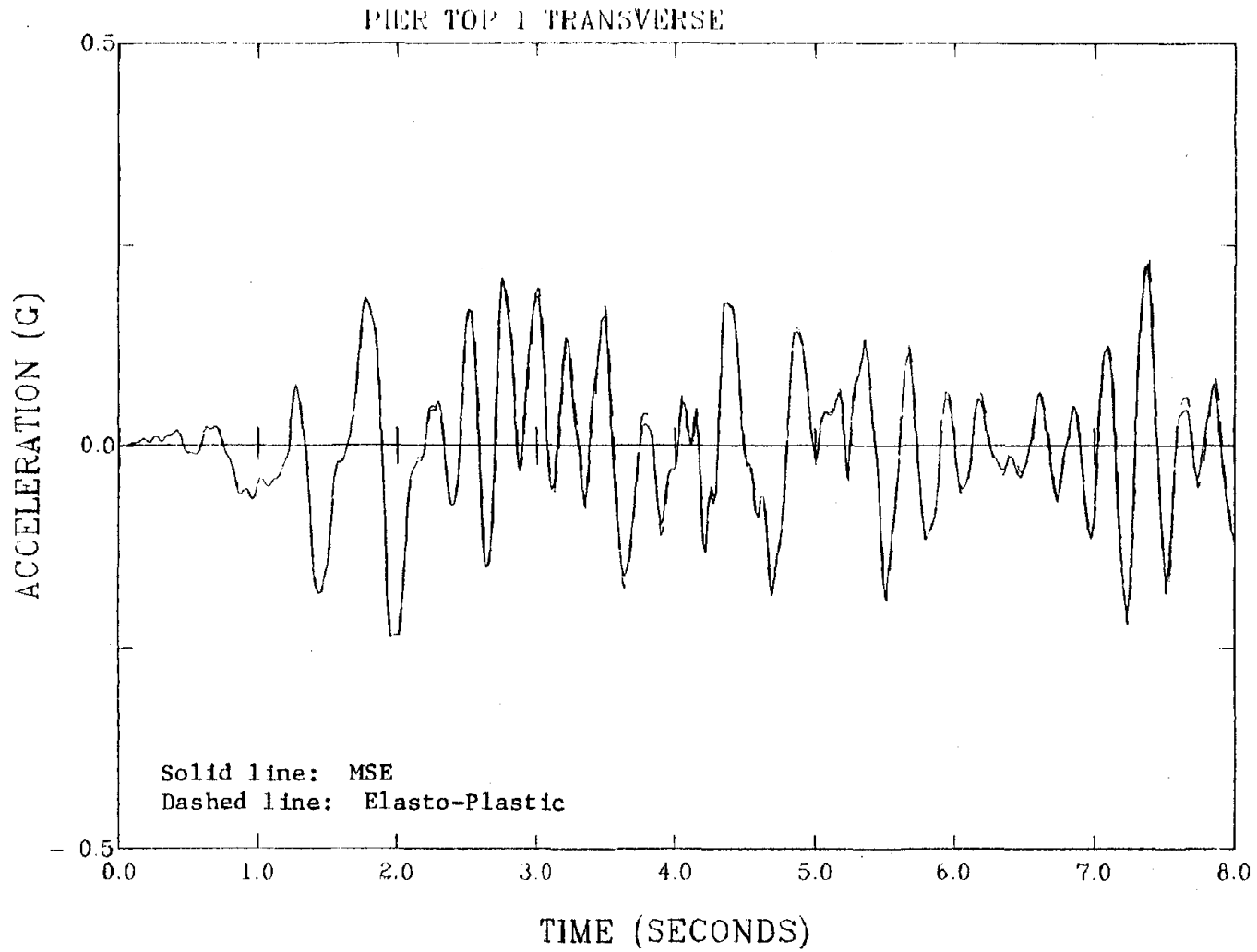


Fig. 6.28. Flamingo Road Overpass Model Response Using El Centro *1.0.

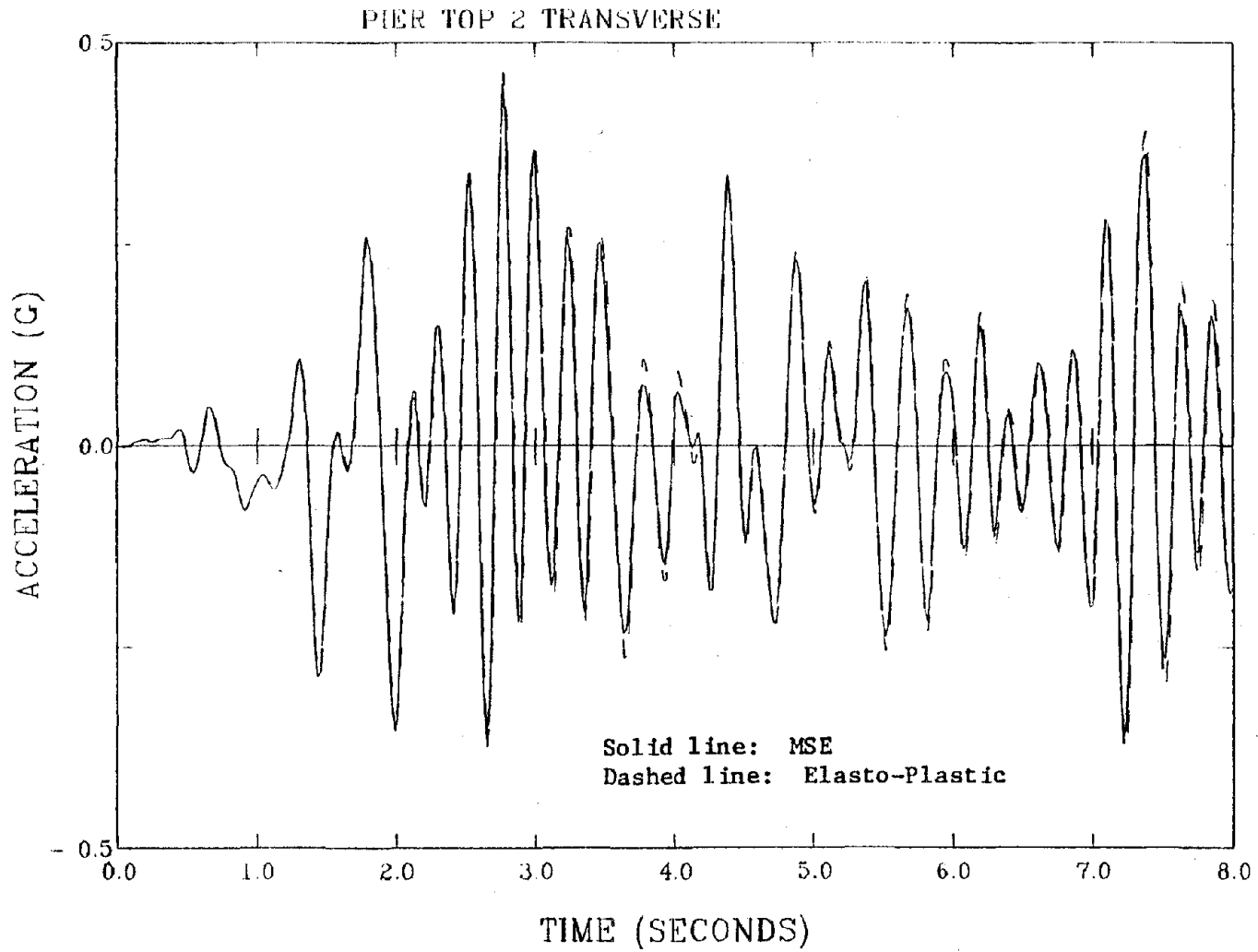


Fig. 6.29. Flamingo Road Overpass Model Response Using El Centro *1.0.

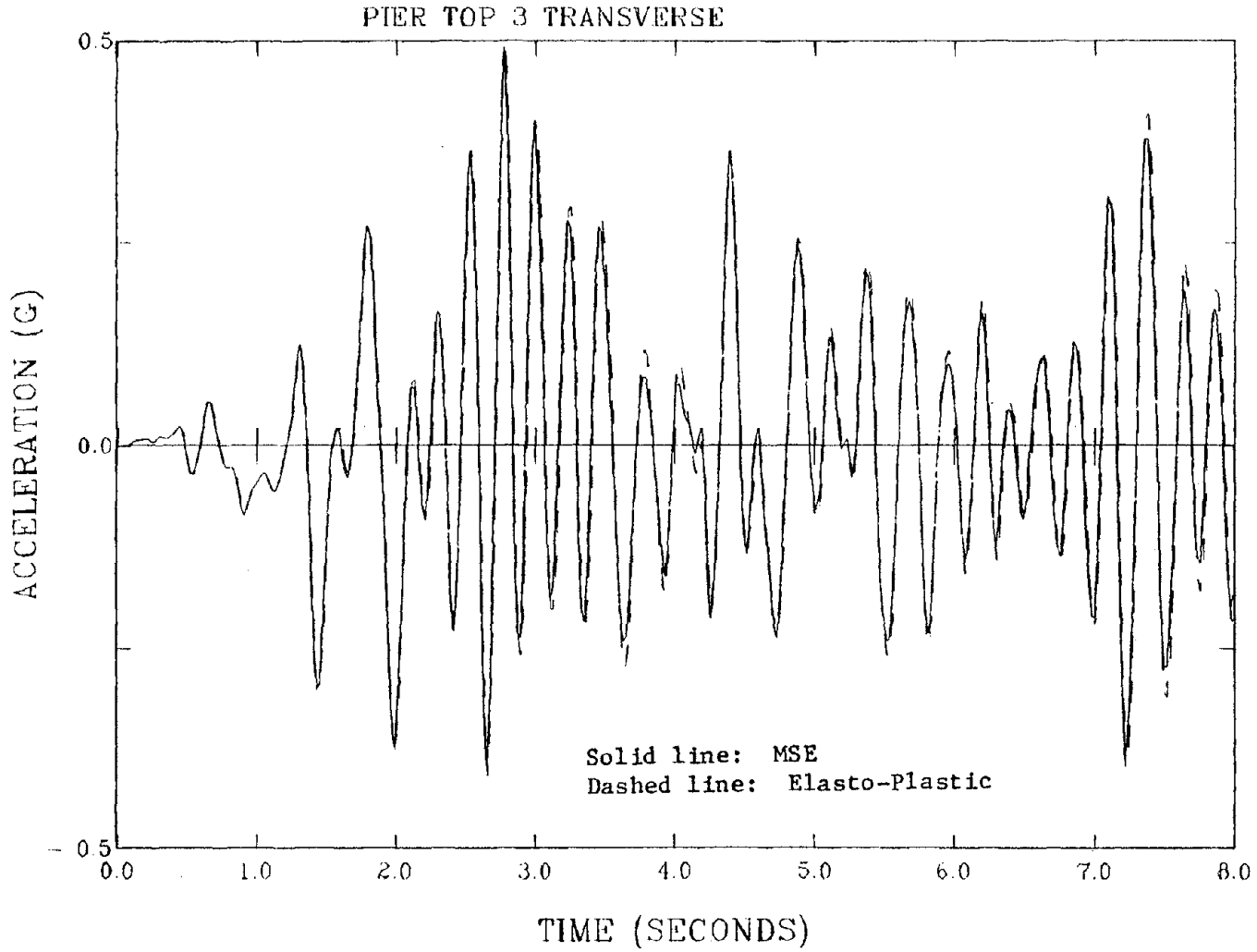


Fig. 6.30. Flamingo Road Overpass Model Response Using El Centro *1.0.

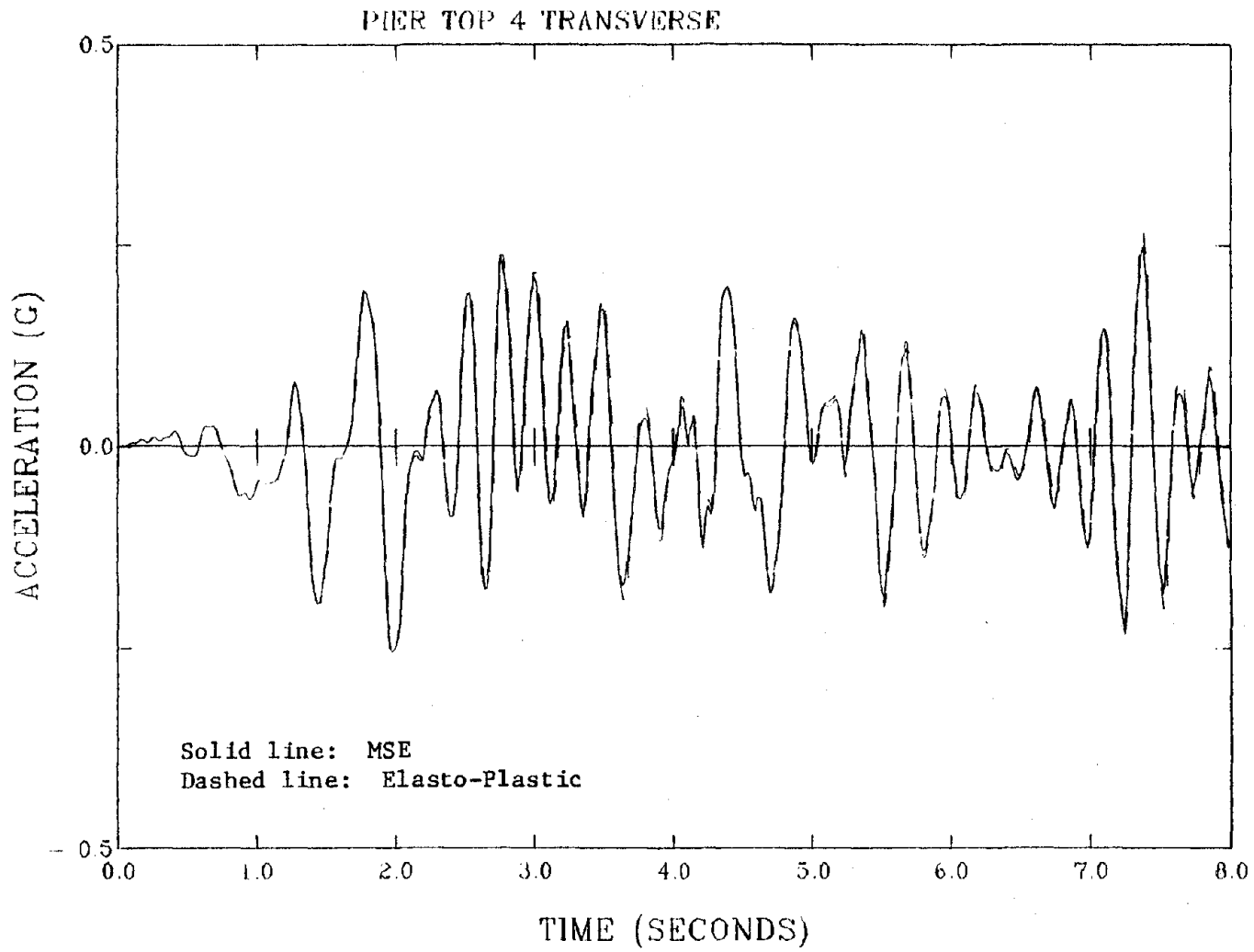


Fig. 6.31. Flamingo Road Overpass Model Response Using El Centro *1.0.

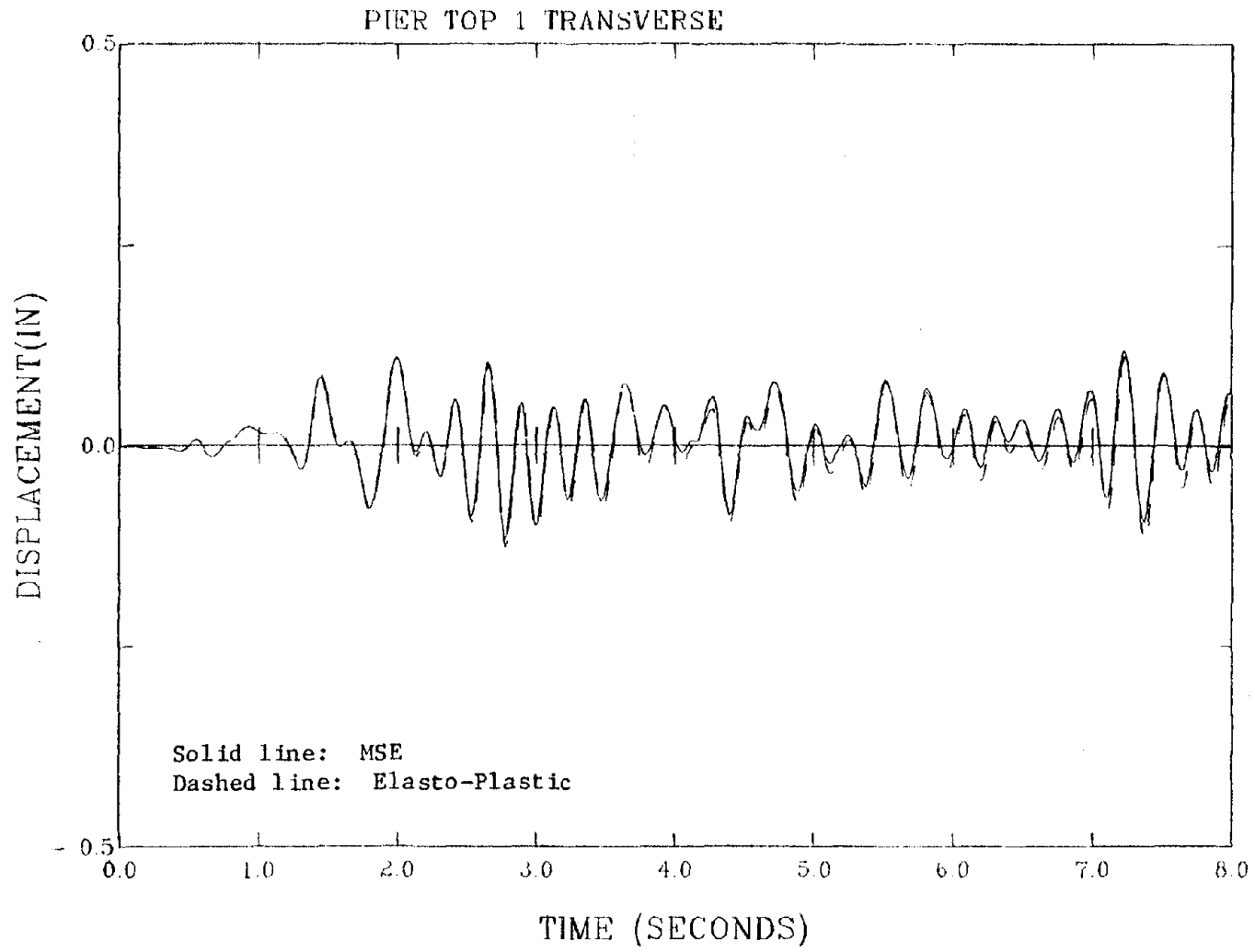


Fig. 6.32. Flamingo Road Overpass Model Response Using El Centro *1.0.

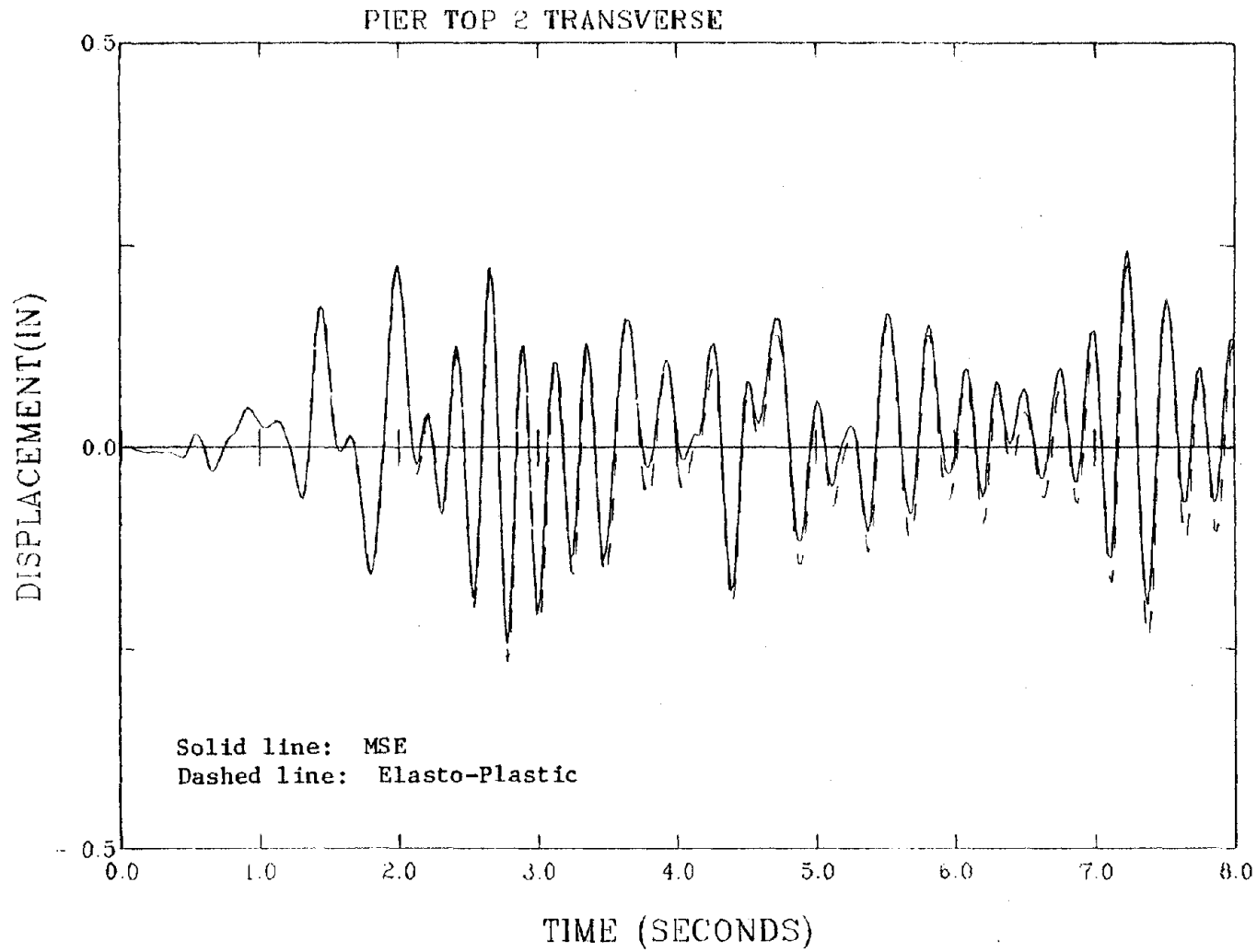


Fig. 6.33. Flamingo Road Overpass Model Response Using El Centro *1.0.

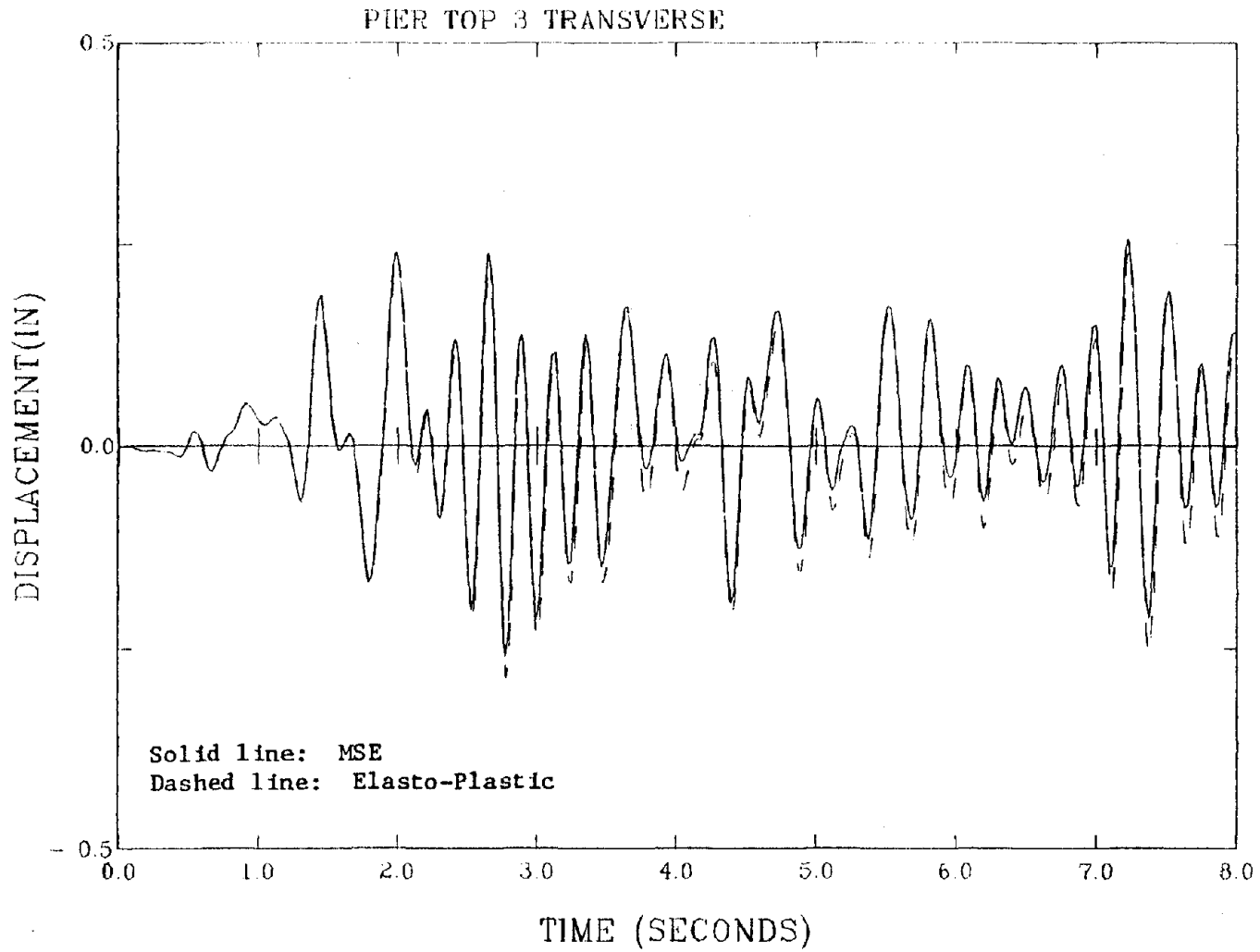


Fig. 6.34. Flamingo Road Overpass Model Response Using El Centro *1.0.

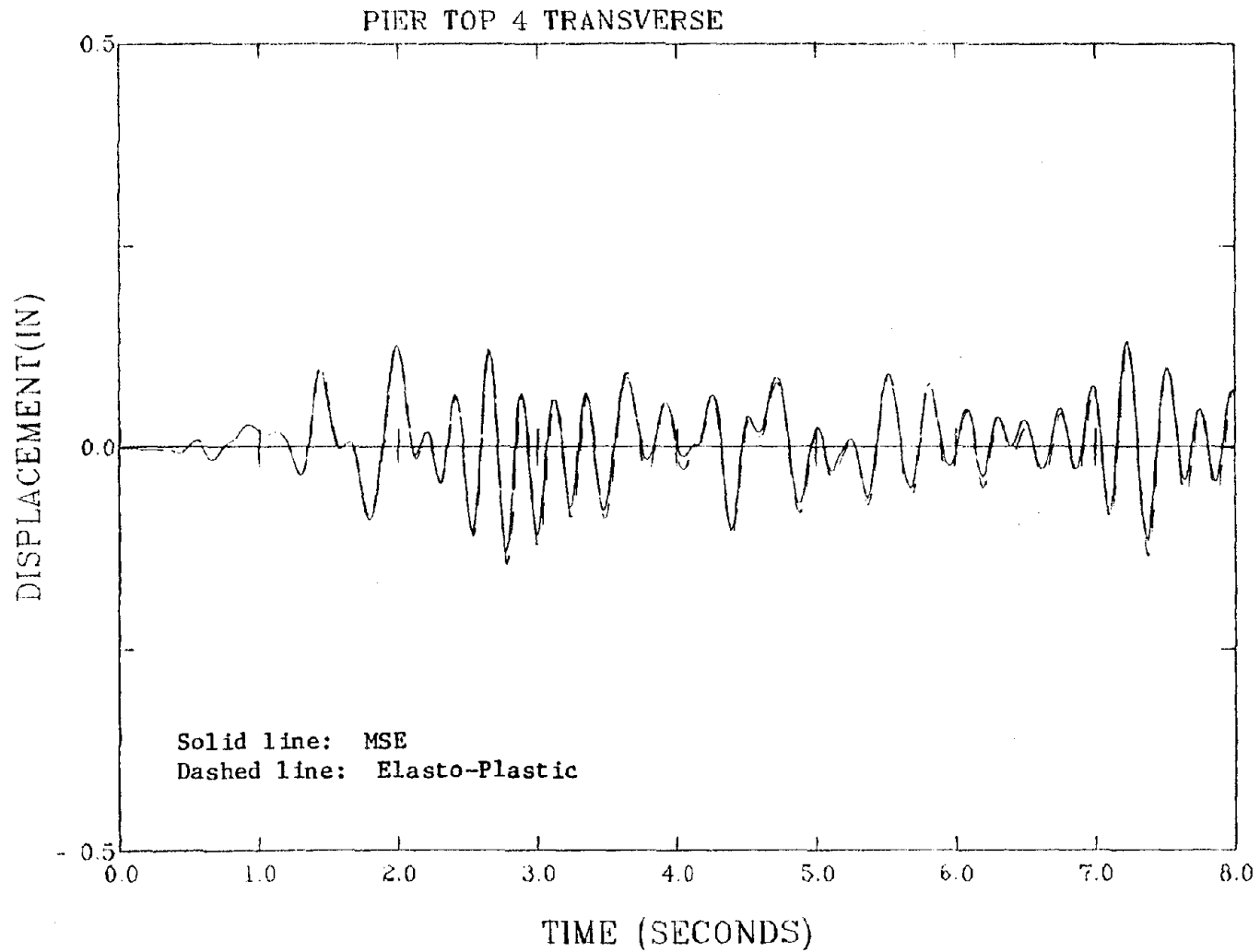


Fig. 6.35. Flamingo Road Overpass Model Response Using El Centro *1.0.

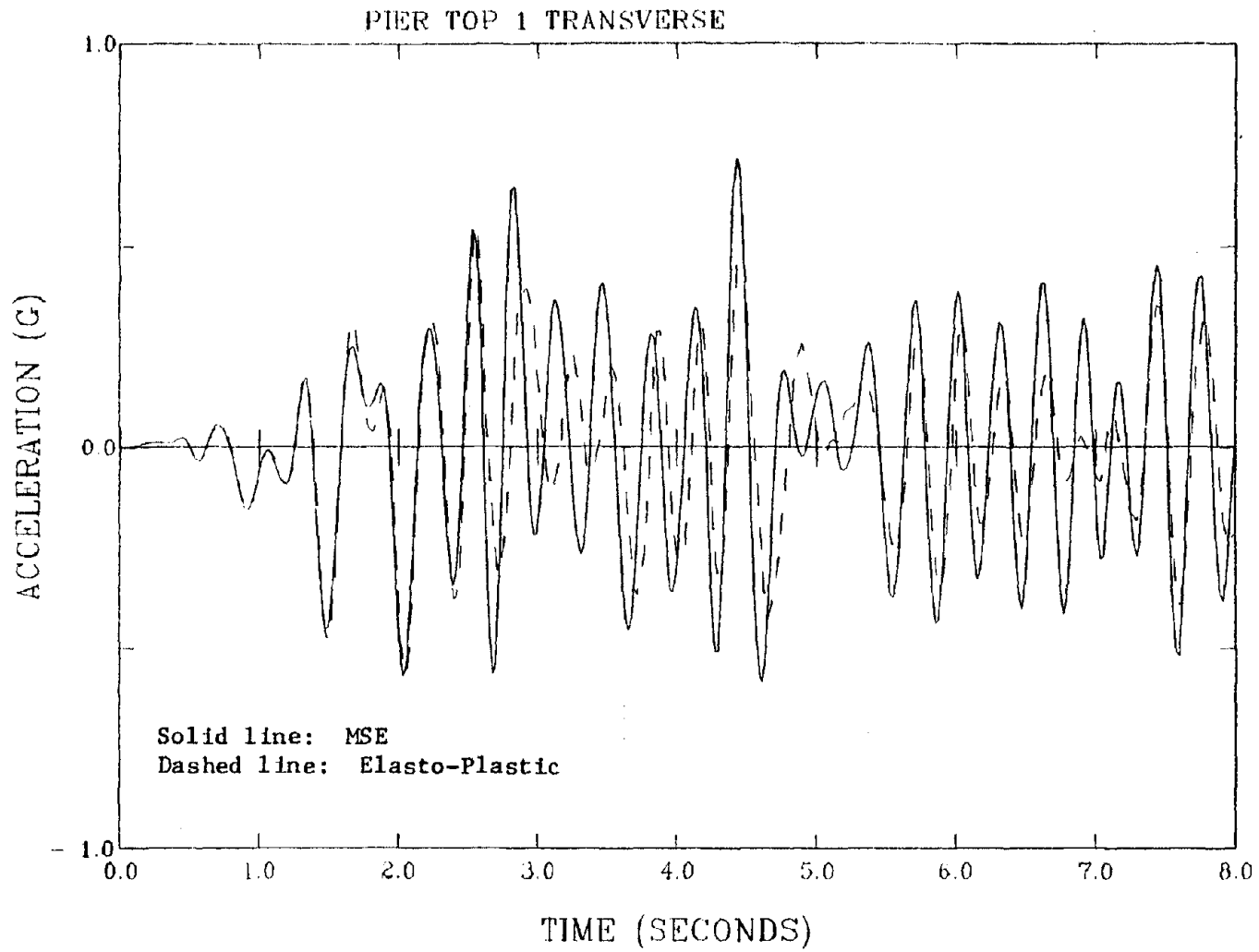


Fig. 6.36. Flamingo Road Overpass Model Response Using El Centro *1.5 (Unstable Elasto-Plastic Response).

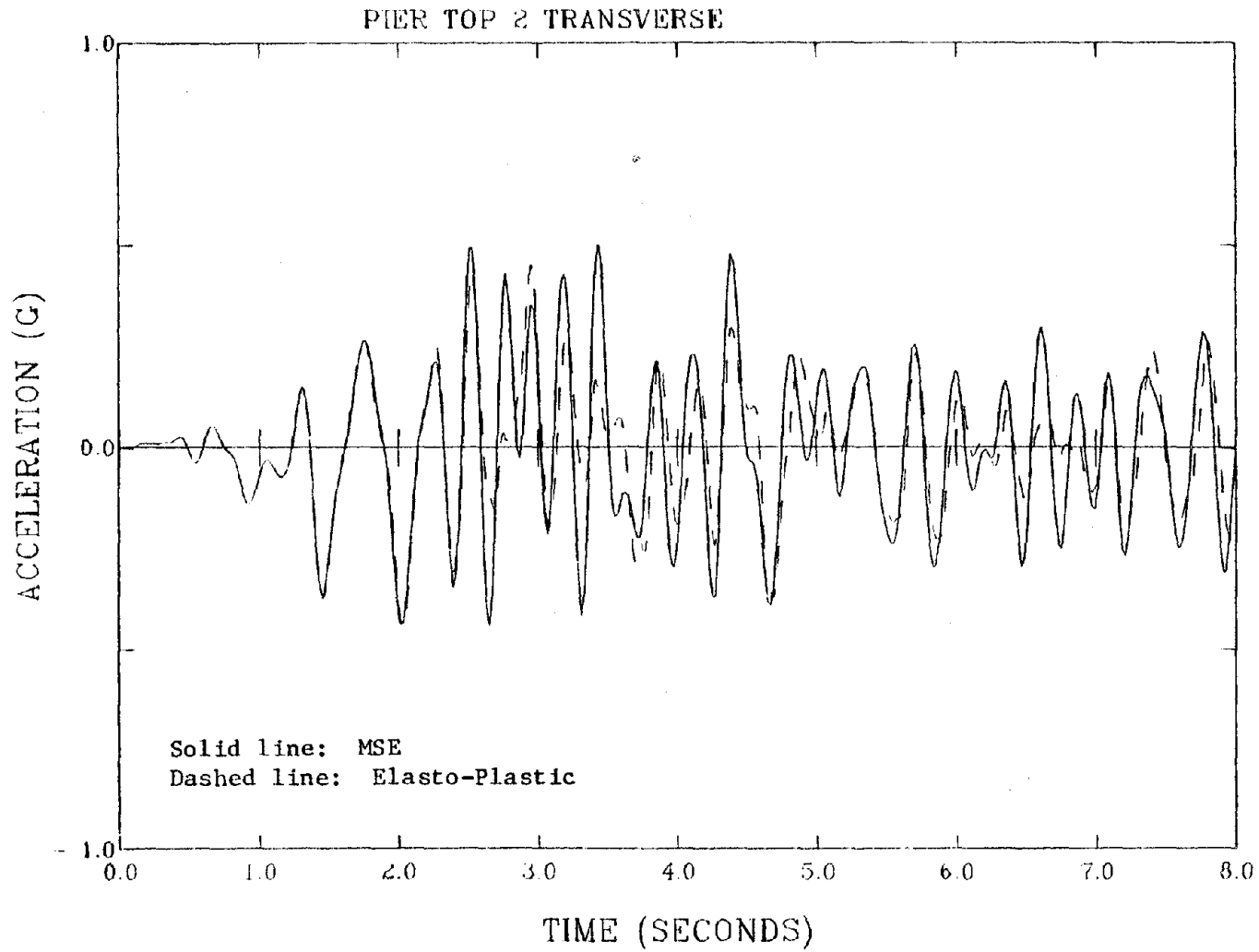


Fig. 6.37. Flamingo Road Overpass Model Response Using El Centro *1.5
(Unstable Elasto-Plastic Response).

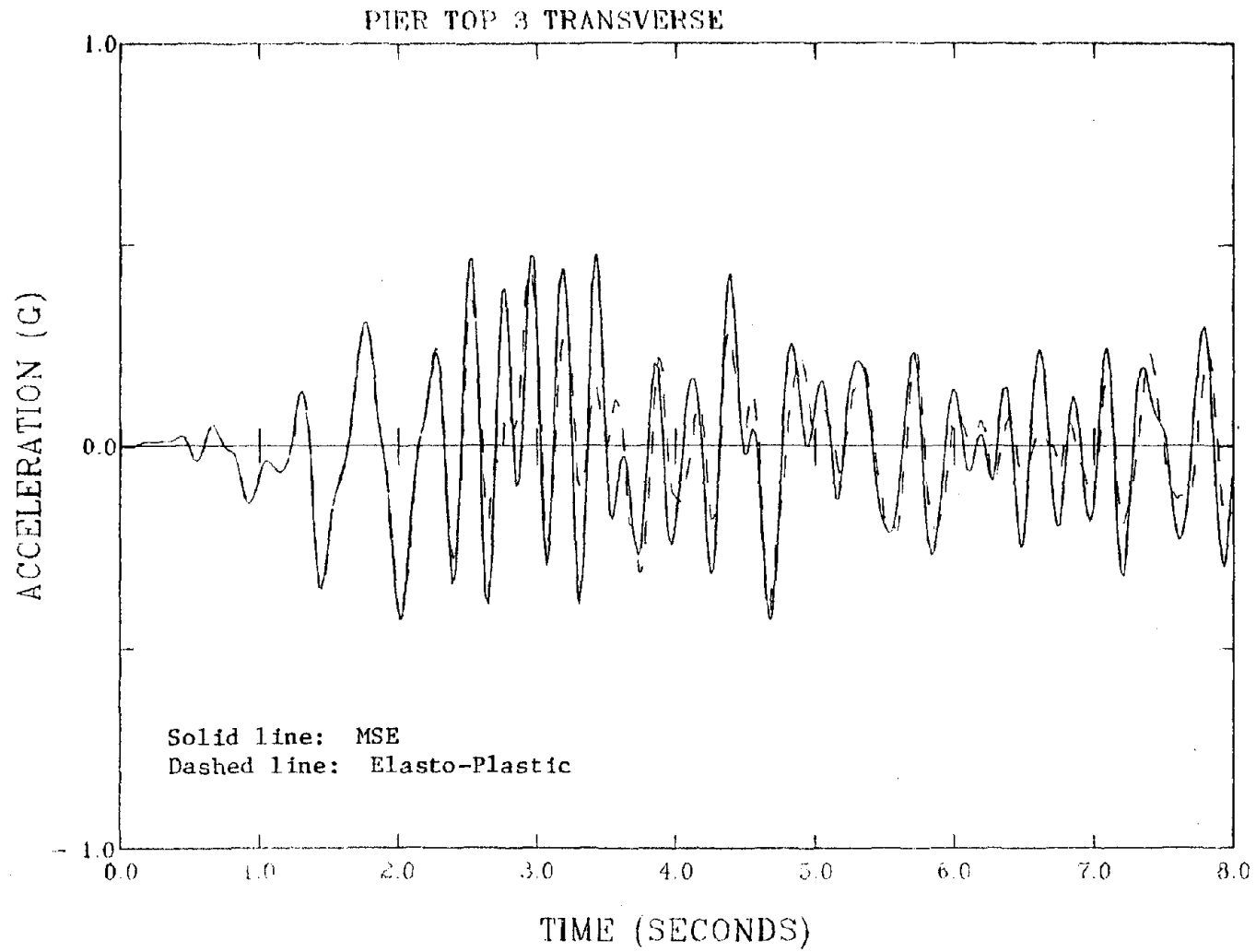


Fig. 6.38. Flamingo Road Overpass Model Response Using El Centro *1.5 (Unstable Elasto-Plastic Response).

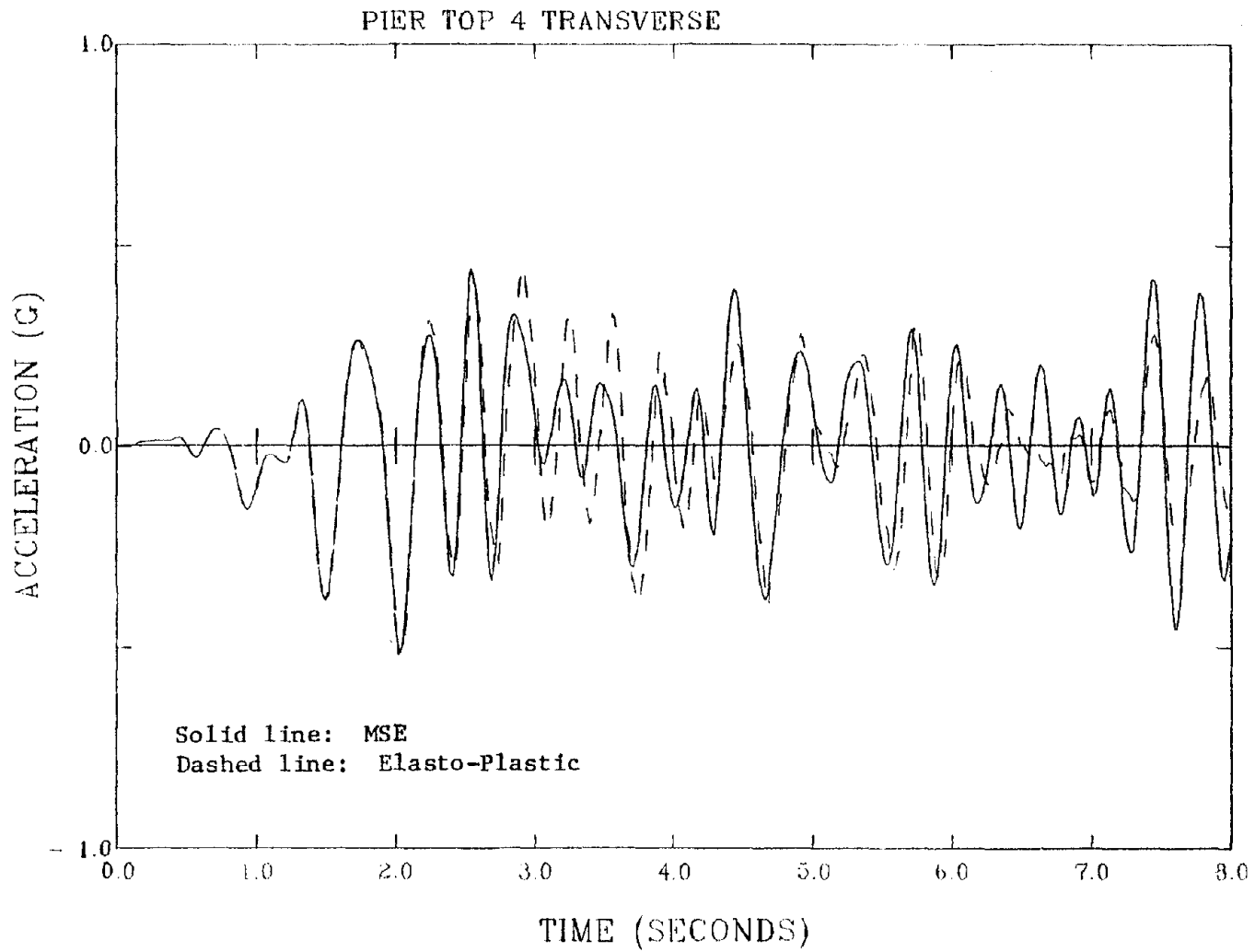


Fig. 6.39. Flamingo Road Overpass Model Response Using El Centro *1.5 (Unstable Elasto-Plastic Response).

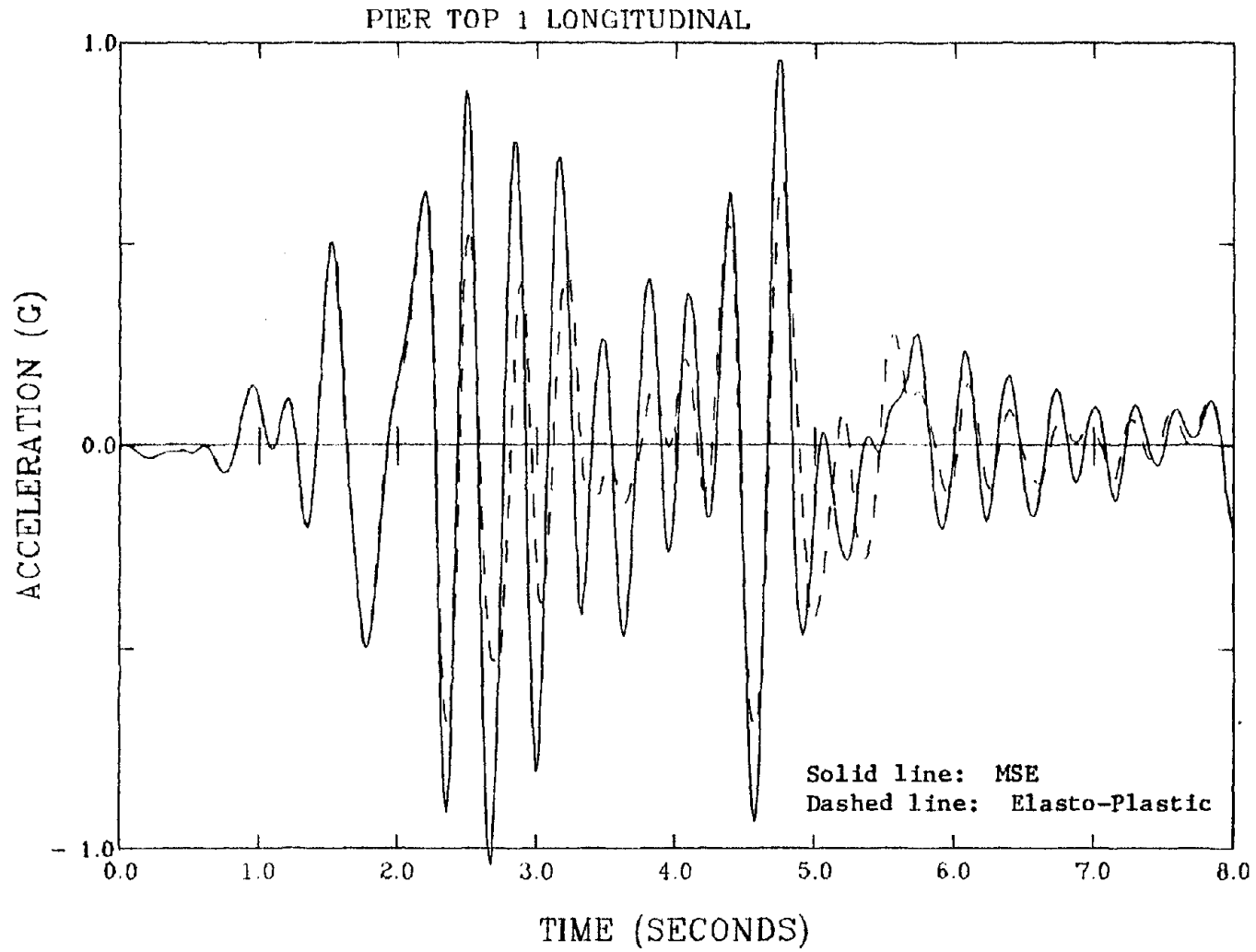


Fig. 6.40. Flamingo Road Overpass Model Response Using El Centro *1.5 (Unstable Elasto-Plastic Response).

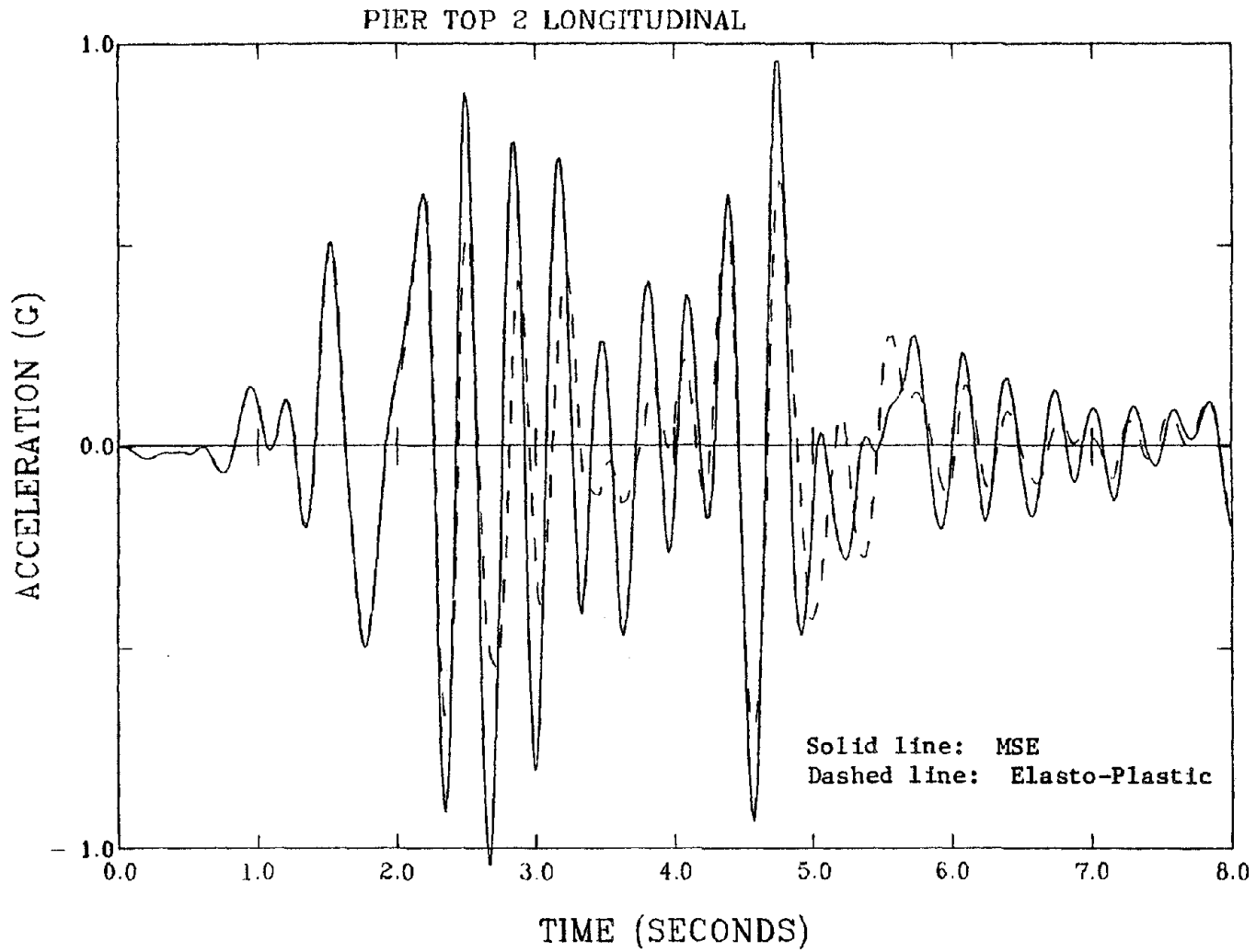


Fig. 6.41. Flamingo Road Overpass Model Response Using El Centro *1.5 (Unstable Elasto-Plastic Response).

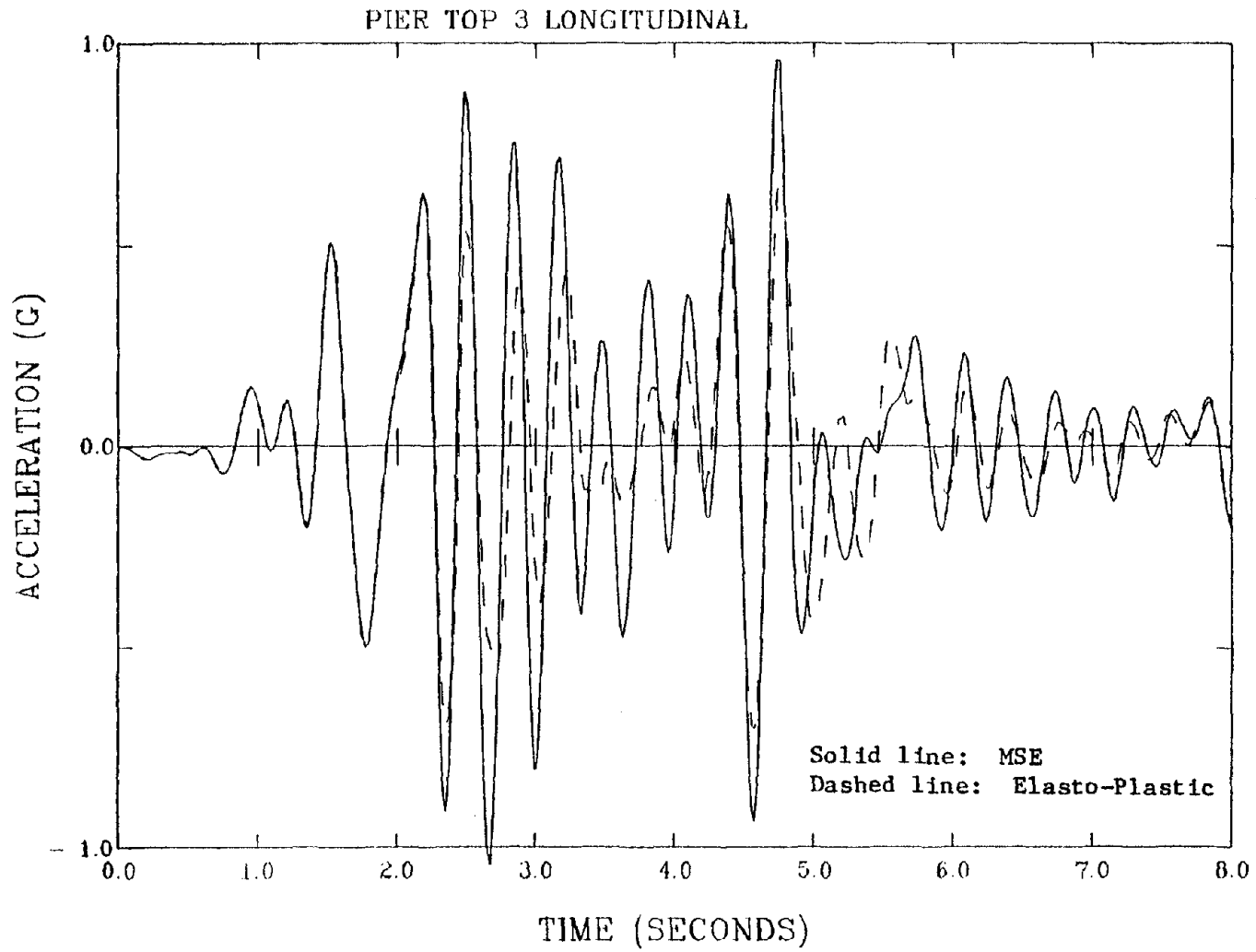


Fig. 6.42. Flamingo Road Overpass Model Response Using El Centro *1.5 (Unstable Elasto-Plastic Response).

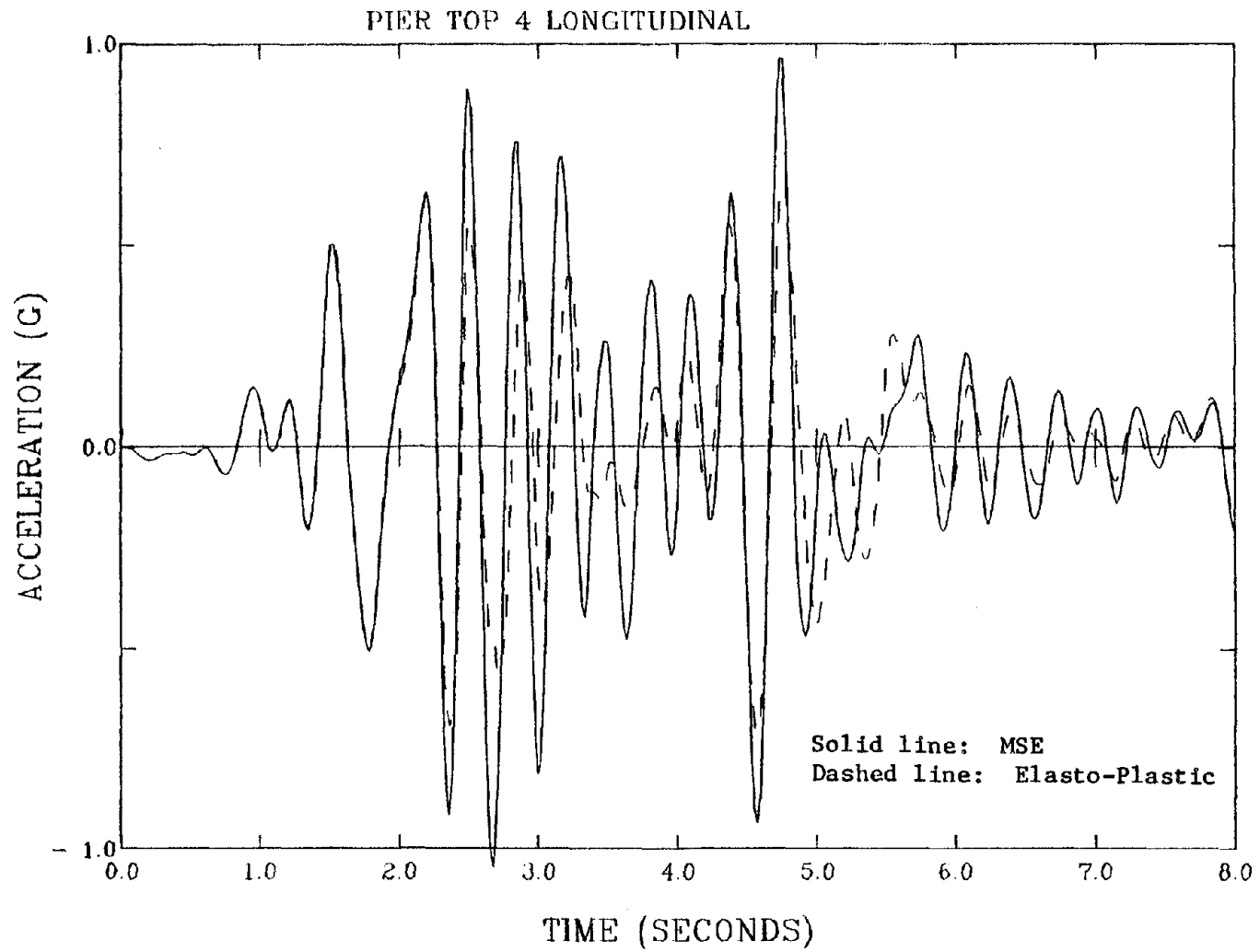


Fig. 6.43. Flamingo Road Overpass Model Response Using El Centro *1.5 (Unstable Elasto-Plastic Response).

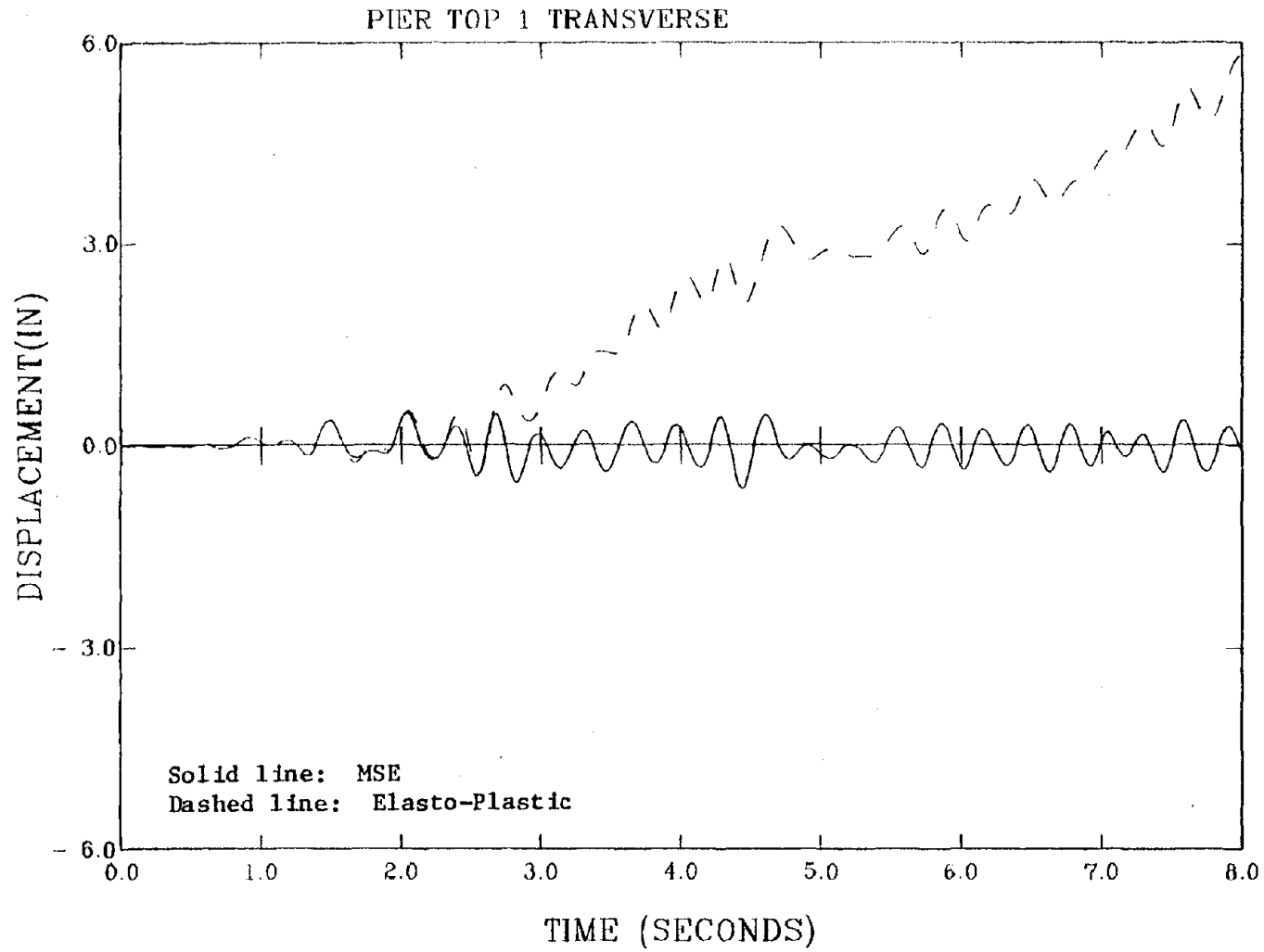


Fig. 6.44. Flamingo Road Overpass Model Response Using the El Centro *1.5 (Unstable Elasto-Plastic Response).

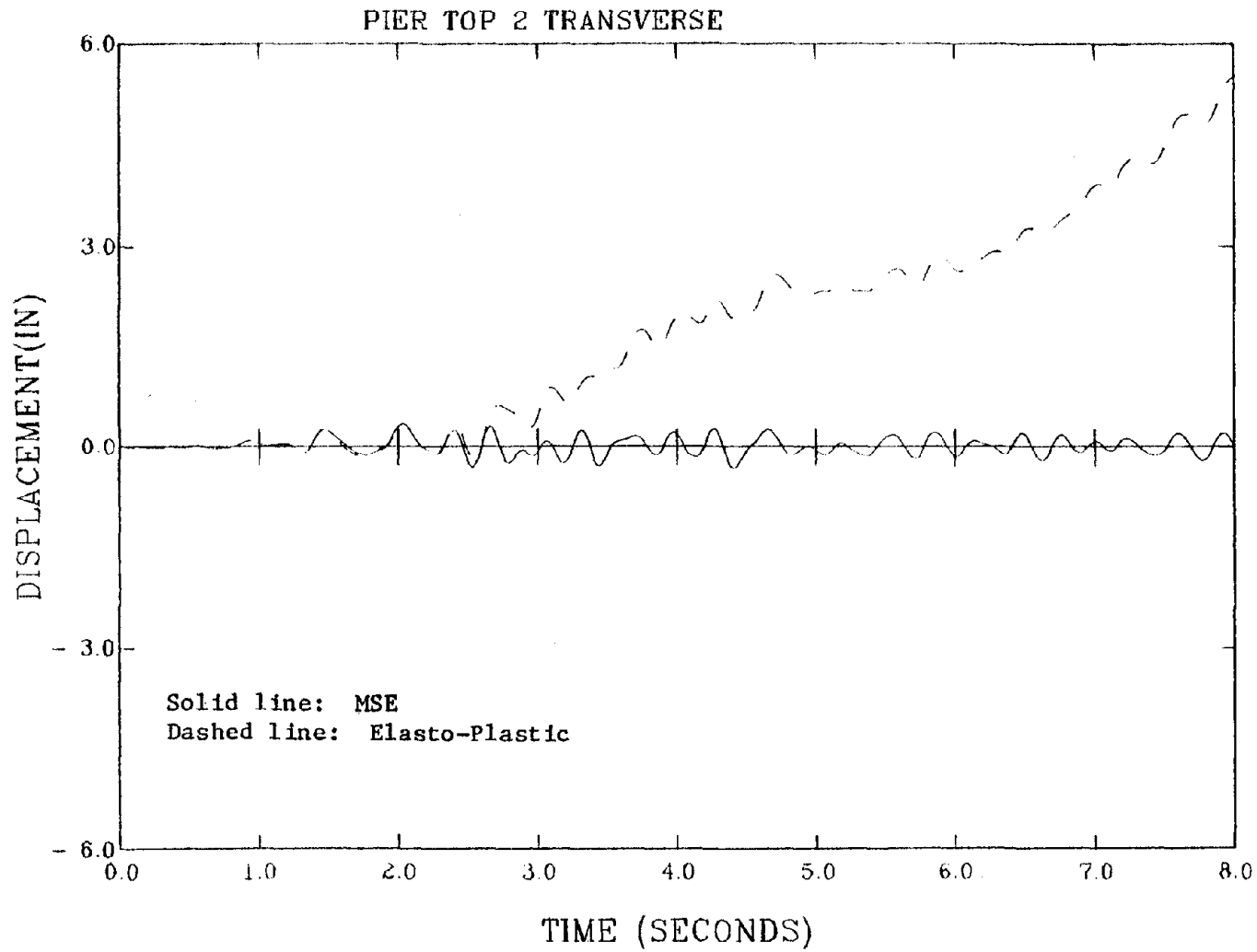


Fig. 6.45. Flamingo Road Overpass Model Response Using the El Centro *1.5 (Unstable Elasto-Plastic Response).

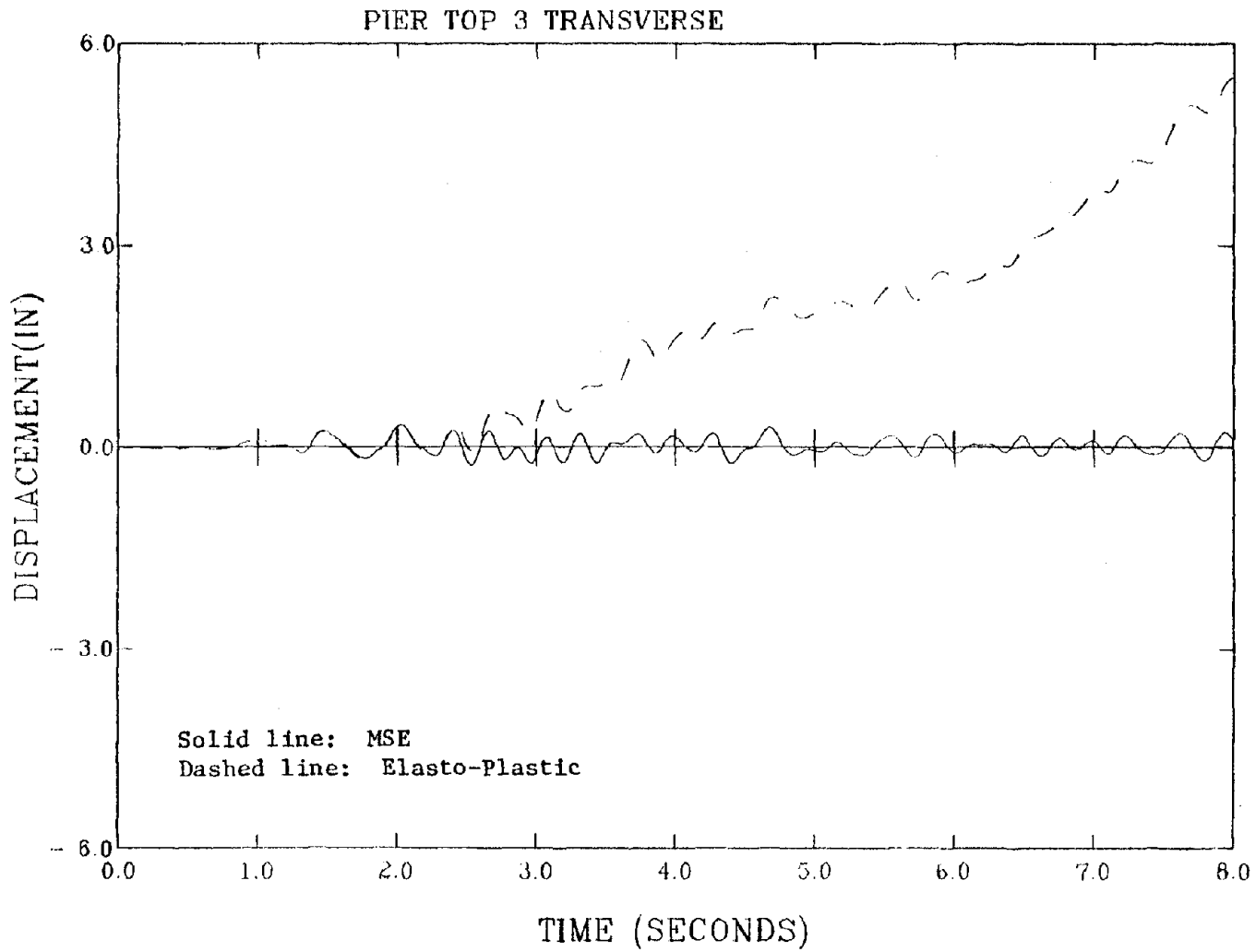


Fig. 6.46. Flamingo Road Overpass Model Response Using the El Centro *1.5 (Unstable Elasto-Plastic Response).

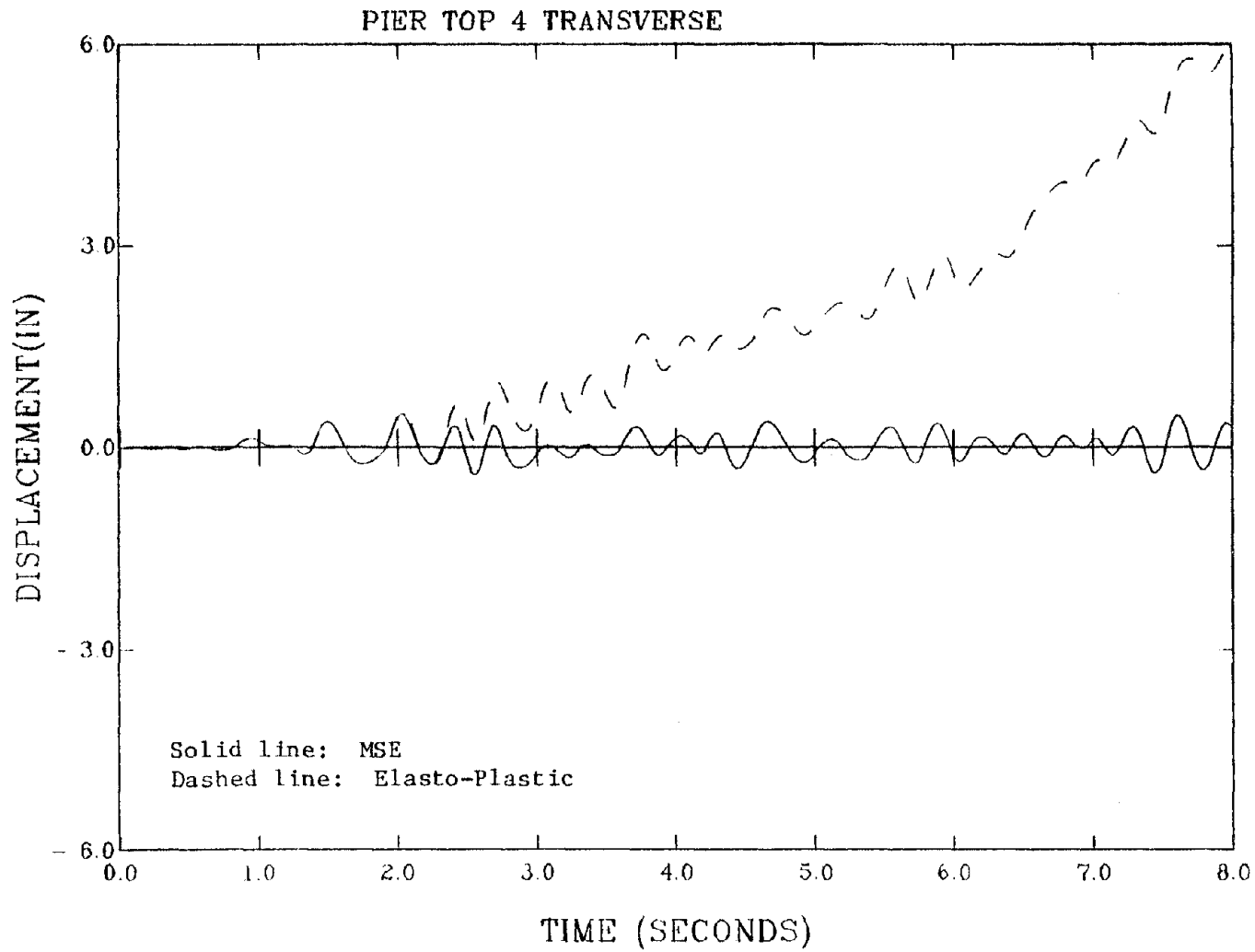


Fig. 6.47. Flamingo Road Overpass Model Response Using the El Centro *1.5 (Unstable Elasto-Plastic Response).

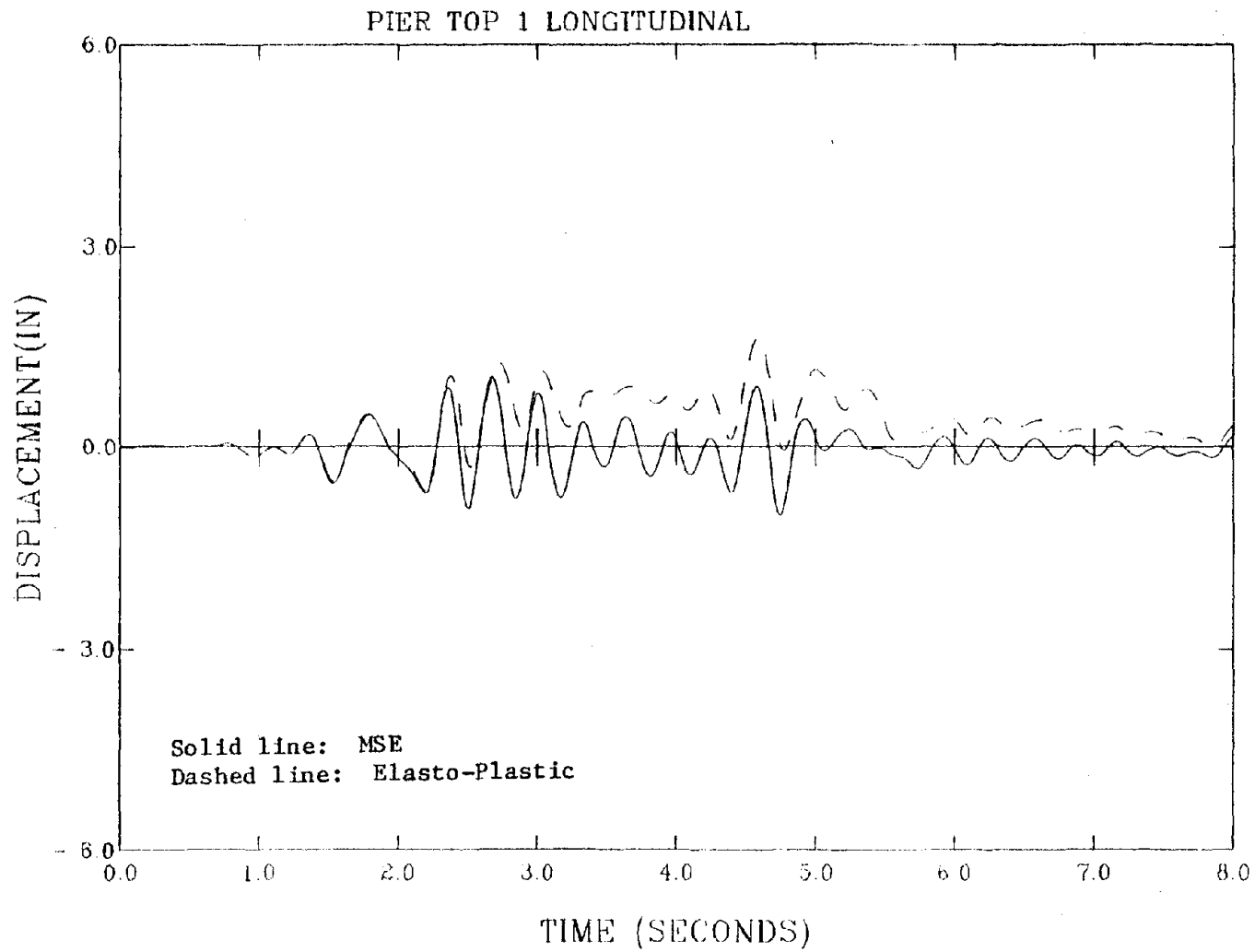


Fig. 6.48. Flamingo Road Overpass Model Response Using the El Centro *1.5 (Unstable Elasto-Plastic Response).

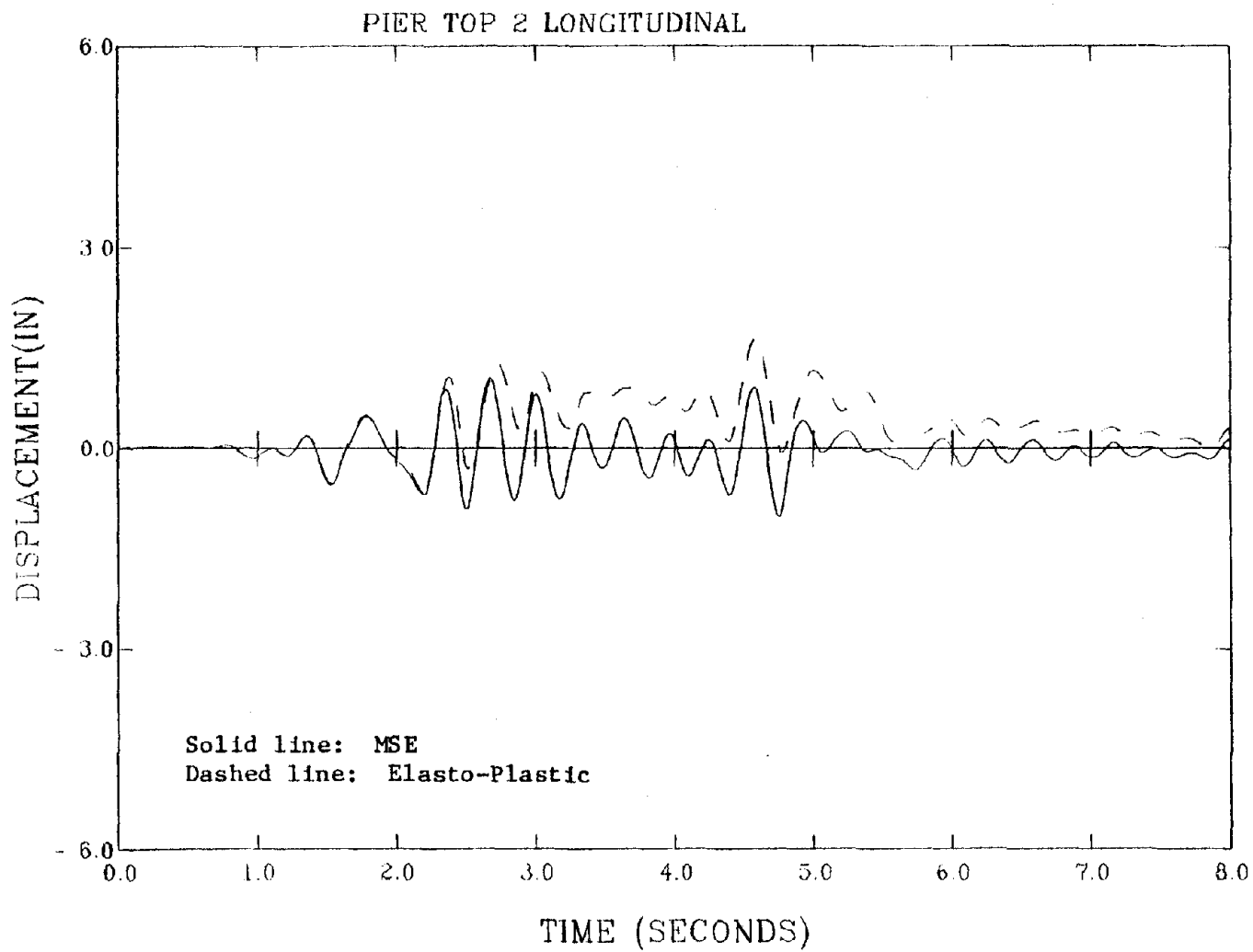


Fig. 6.49. Flamingo Road Overpass Model Response Using the El Centro *1.5 (Unstable Elasto-Plastic Response).

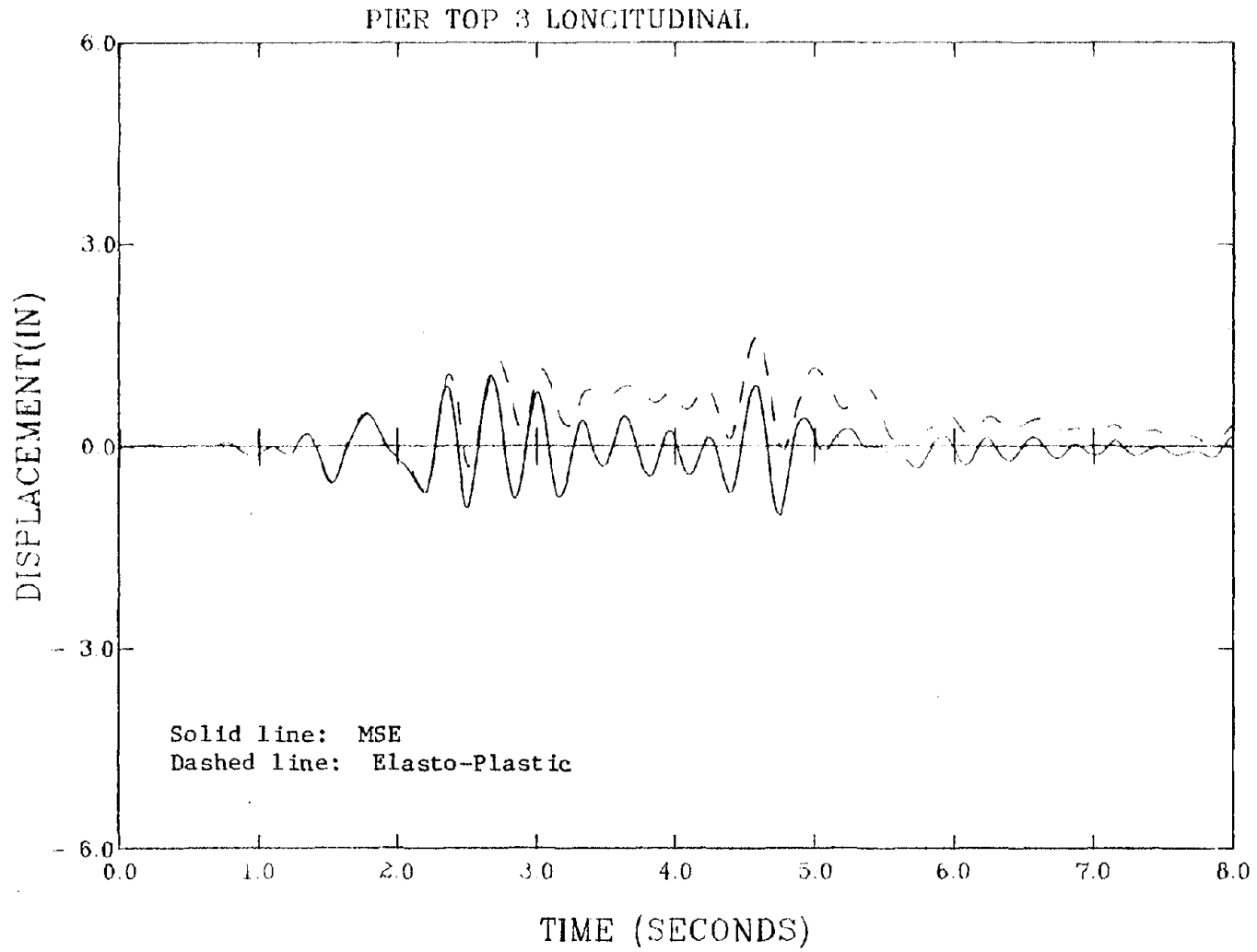


Fig. 6.50. Flamingo Road Overpass Model Response Using the El Centro *1.5 (Unstable Elasto-Plastic Response).

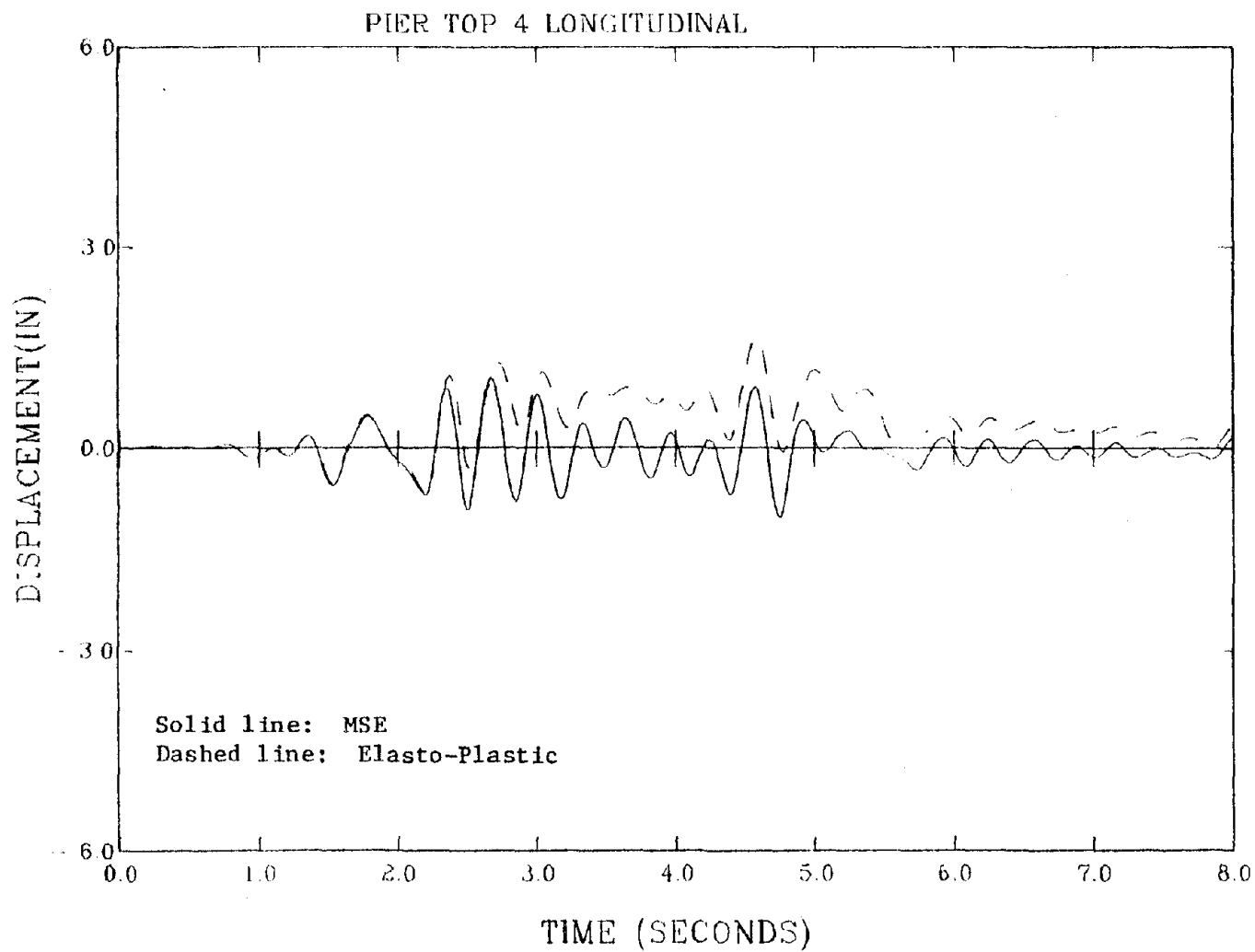


Fig. 6.51. Flamingo Road Overpass Model Response Using the El Centro *1.5 (Unstable Elasto-Plastic Response).

APPENDIX A

USER'S GUIDE FOR NEABS-86:

FIVE-SPRING BIAXIAL BENDING ELEMENT: TYPE 6

A. Control Data Card (14I5)

One card is required:

Columns	Variable Name	Comments
1- 5	MTYPE	MTYPE = 6 for this element
6-10	NBEAM	Number of elements
11-15	NUMETP	Number of cross section types
16-20	blank	
21-25	NUMMAT	Number of material property sets

B. Material Property Cards (I5, 2F10.0)

One card is required for each type (as many as NUMMAT specified above):

Columns	Variable Name	Comments
1- 5	N	Material property number
6-15	FC(N)	Compressive strength of concrete
16-25	FY(N)	Yield stress of steel rebar

C. Cross Section Property Cards I (I5, F10.0, 2F5.3)

One card is required for each type (as many as NUMETP specified above):

Columns	Variable Name	Comments
1- 5	N	Cross section property number
6-15	AGROSS(N)	Gross area of the cross section
16-20	BTO(N)	Stiffness degradation factor for tension
21-25	BT1(N)	Stiffness degradation factor for compression

D. Cross Section Properties Cards II (5F10.0, I5)

One card is required for each type (as many as NUMETP specified above):

Columns	Variable Name	Comments
1-10	PBAL	Average axial load at balanced moments
11-20	YMBAL	Balanced moment about the local y axis
21-30	ZMBAL	Balanced moment about the local z axis
31-40	SUMA	Total area of steel in the cross section
41-50	ULD	Development length for the rebar (note 1)
51-55	MATTP	Material property set for this section

Note 1: $ULD = (\text{area of bar}) * f_y / (n * \text{diameter of a bar} * u)$
where $u = 14 * (f'_c)^{0.5}$ (psi)

E. Element Data Cards (14I5)

One card is required for each element (as many as NBEAM specified above):

Columns	Variable Name	Comments
1- 5	INEL	Element identification number
6-10	INI	I-joint number (same as for a beam element)
11-15	INJ	J-joint number (same as for a beam element)
16-20	INK	K-joint number (same as for a beam element)
21-25	blank	
26-30	IMEL	Cross section property number

Notes: NSDIV and MAXIT must be set to zero.
I-joint and J-joint number cannot be the same point. They should be separated by 0.1 (any compatible units) in the axial direction.

APPENDIX B
NOTATIONS

A_b	area of a single rebar;
A_c	area of concrete represented by the spring;
A_{center}	area represented by the center concrete spring;
A_{corner}	area represented by a corner concrete spring;
A_{gross}	gross area of the cross section;
A_{st}	total area of steel in the cross section;
bt_0	degradation factor for tension ;
bt_1	degradation factor for compression;
d_b	diameter of a single rebar;
d_i	total current displacement in the i^{th} spring;
d_{max}	maximum displacement a spring has experienced;
d_{sx}	distance between the spring locations in the y direction;
d_{sy}	distance between the spring locations in the x direction;
d_y	yield displacement;
f'_c	specified compressive strength of concrete in psi;
f_i	total current force in the i^{th} spring;
f_R	force at the unloading point R;
f_{U_m}	force at U_m ;
f_y	specified yield stress of the rebar;
[K]	element stiffness matrix;
K_{cce}	initial elastic stiffness for the center spring;
K_{ce}	initial elastic stiffness for the corner springs;
k_i	stiffness at the i^{th} spring location;

K_{se} elastic stiffness of a steel spring;
 K_y post-yielding stiffness of a spring;
 l_d development length in inches;
LVL pointer to the next rule;
 M_{bi} balanced moment computed from flexural theory;
 M_x, M_y applied moments about the x and y axes, respectively;
 M_{ox}, M_{oy} yield moments about the x and y axes, respectively;
S1 $K_{se} * (d_y / d_{max})^{bt0}$;
S2 $(K_{se} + K_{ce}) (d_y / d_{max})^{bt1}$;
 P_b balance axial load for the section;
 P_{cy} yield level in the concrete spring;
 u bond stress in psi;
 U_m maximum displacement after yielding;
 Δ_p net axial displacement defined as the displacement
at the center of the section;
 θ_x and θ_y rotations about the x and y coordinate axes,
respectively.

APPENDIX C

LIST OF CCEER PUBLICATIONS

Report No.	Publication
CCEER-84-01	Saiidi, Mehdi and Renee a. Lawver, "User's Manual for LZAK-C64, A Computer Program to Implement the Q-Model on Commodore 64," Civil Engineering Department, Report No. CCEER-84-01, University of Nevada, Reno, January 1984.
CCEER-84-02	Douglas, Bruce M. and Toshio Iwasaki, "Proceedings of the First USA-Japan Bridge Engineering Workshop," held at the Public Works Research Institute, Tsukuba, Japan, Civil Engineering Department, Report No. CCEER-84-02, University of Nevada, Reno, April 1984.
CCEER-84-03	Saiidi, Mehdi, James D. Hart, and Bruce M. Douglas, "Inelastic Static and Dynamic Analysis of Short R/C Bridges Subjected to Lateral Loads," Civil Engineering Department, Report No. CCEER-84-03, University of Nevada, Reno, July 1984.
CCEER-85-01	Norris, Gary M. and Pirouze Abdollaholiaee, "Laterally Loaded Pile Response: Studies with the Strain Wedge Model," Civil Engineering Department, Report No. CCEER-85-01, University of Nevada, Reno, April, 1985.
CCEER-86-01	Ghusn, George E. and Mehdi Saiidi, "A Simple Hysteretic Element for Biaxial Bending of R/C Columns and Implementation in NEABS-86," Civil Engineering Department, Report No. CCEER-86-01, University of Nevada, Reno, July 1986.

